Advancing liquid MALDI Ion Source Designs and Applications in Modern Biological Mass Spectrometry

PhD in Chemistry

Department of Chemistry

Henriette Krenkel

October 2023

Declaration

I confirm that this is my own work and the use of all material from other sources has been properly and fully acknowledged.

Date Signed (Henriette Krenkel)

Contents

List of Figures

List of Tables

Abbreviations

α-CHCA	α-cyano-4-hydroxycinnamic acid
2,5-DHB	2,5-dihydroxybenzoic acid
ADC	analog-to-digital converter
ADE	acoustic droplet ejection
AMI	acoustic mist ionisation
AP	atmospheric pressure
AP-MALDI	atmospheric pressure matrix-assisted laser desorption/ionisation
CEM	chain ejection model
CID	collision-induced dissociation
CPCD	coupled chemical and physical dynamics model
CRM	charge residue model
CV	coefficient of variation
DC	direct current
DESI	desorption electrospray ionisation
DIA	data-independent acquisition
ESI	electrospray ionisation
FWHM	full width at half maximum
HTS	high-throughput screening
IEM	ion evaporation model
IR-MALDESI	infrared matrix-assisted laser desorption electrospray ionisation
ISD	inter-scan delay
LAP-MALDI	liquid atmospheric pressure matrix-assisted laser desorption/ionisation
LDTP-APCI	laser diode thermal desorption atmospheric pressure chemical ionisation
LS	lucky survivor model

LSM	liquid support matrix
MALDI	matrix-assisted laser desorption/ionisation
MS	mass spectrometry
MTP	microtiter plate
PRF	laser pulse repetition frequency
QToF	quadrupole time-of-flight
RF	radio frequency
TDC	time-to-digital converter
TIC	total ion count
ToF	time-of-flight
uHTS	ultra-high-throughput screening
WREnS	Waters Research Enabling Software

Abstract

Mass spectrometry (MS) is a sensitive and specific analytical method often used for biological samples and assays. Its widespread application for screening is restrained by the limited sample throughput compared to traditional photometric assay readouts. In this work, the suitability of mass spectrometry using liquid atmospheric pressure matrix-assisted laser desorption/ionisation (LAP-MALDI) as an ionisation technique for high speed MS analysis and screening of biochemical assays was investigated.

In a first step, a substrate and product of an enzymatic assay were detected at 5 samples/s without prior sample clean-up. More complex samples (milk) were analysed at 1 samples/s. After further improvements in hardware and software, the analysis of a second enzymatic assay was accelerated to 16 samples/s and peptide standards were analysed at 40 samples/s. This is faster than other MS-based methods reported in the literature and also highly competitive with photometric readouts.

Additionally, a systematic study of various components often used in biochemical screening assays and generally biological mass spectrometry on the ion signal of a peptide mixture was carried out. Although pronounced ion suppression was observed with some additives, compounds such as the surfactant octyl-β-D-glucopyranoside and the buffer tricine were found suitable with LAP-MALDI MS analysis.

In summary, LAP-MALDI allows for rapid MS sample analysis, the fast readout of biochemical assays and shows great potential for high-throughput screening. Possible improvements by enhanced automation are also discussed.

Acknowledgements

I would like to thank all the people who have shared their knowledge and experience, from conference attendees to contributors of StackOverflow. You spend your time helping others and there have been many occasions during my PhD when your advice has been incredibly useful.

I also would like to thank Roy, Mike and Yuba from our electrical and mechanical workshop. Some work is better done by professionals.

The devil's advocate, Rainer, certainly improved all work I produced. Sometimes it just takes a little distance (and a good portion of resilience) to see. You gave me the opportunity to work on the most interesting project I could have imagined and I learnt so many different things.

Thanks to my colleagues, especially Sophie, Evita and Ryan. It is unbelievable comforting to know one is not the only one in a seemingly endless tunnel.

My family and friends helped to see the life outside of the university and kept me going throughput the project.

Special thanks are due to my partner Paul who was my emotional and scientific backup, who believed in me, especially when I didn't.

Moreover, I would like to thank Micromass for the financial and scientific support throughout this project, especially Jeff, who got never tired of explaining and organising help.

Publications and conference contributions related to this work

Research articles

1. Title: Advancing Liquid Atmospheric Pressure Matrix-Assisted Laser Desorption/Ionization Mass Spectrometry Toward Ultrahigh-Throughput Analysis

   Citation: Henriette Krenkel, Evita Hartmane, Cristian Piras, Jeffery Brown, Michael Morris, and Rainer Cramer; Analytical Chemistry 2020, 92, 4, 2931-2936

2. Title: Ultrahigh-Throughput Sample Analysis Using Liquid Atmospheric Pressure Matrix-Assisted Laser Desorption/Ionization Mass Spectrometry

   Citation: Henriette Krenkel, Jeffery Brown, Keith Richardson, Emmy Hoyes, Michael Morris, and Rainer Cramer; Analytical Chemistry 2022, 94, 10, 4141-4145

3. Title: The use of salts, buffers and surfactants in LAP-MALDI MS

   Citation: Henriette Krenkel, Jeffery Brown, Michael Morris, and Rainer Cramer; International Journal of Mass Spectrometry 2023, 493, 117134

Conferences

1. Title: High-throughput assay and intact protein analysis by liquid AP-MALDI MS

   Citation: Henriette Krenkel; Evita Hartmane; Cristian Piras; Jeffery Brown; Michael Morris; Rainer Cramer; 68th Conference on Mass Spectrometry and Allied Topics, 31st May-4th June 2020, Online

2. Title: Ultra-high-throughput mass spectrometric analysis of peptides and enzymatic assays using LAP-MALDI

   Citation: Henriette Krenkel, Jefferey Brown, Keith Richardson, Mike Morris, Rainer Cramer, Analytical Research Forum 15th-16th June 2021

3. Title: A semi-automated workflow for ultra-high-speed, large-scale sample analysis using LAP-MALDI MS

   Citation: Henriette Krenkel, Jeffery Brown, Keith Richardson, Emmy Hoyes, Mike Morris, Rainer Cramer, 21st BMSS Annual Meeting, Sheffield 08th-09th September 2021

4. Title: LAP-MALDI MS for high-speed sample screening: from 5 to 40 samples/s

   Citation: Henriette Krenkel, Rainer Cramer - University of Reading, Jeffery Brown, Keith Richardson, Emmy Hoyes, Michael Morris; The British Mass Spectrometry Society Ambient Ionisation and Environment and Food Analysis Special Interest Group Meeting, 27th April 2022

5. Title: LAP-MALDI MS for ultra-high-speed analysis of enzyme assays: requirements, benefits, applications

   Citation: Henriette Krenkel, Jeffery Brown, Keith Richardson, Emmy Hoyes, Mike Morris, Rainer Cramer, 70th Conference on Mass Spectrometry and Allied Topics, Minneapolis, USA, 4th-9th June 2022

6. Title: Ion suppression by buffer compounds in LAP-MALDI MS

   Citation: Henriette Krenkel, Jeffery Brown, Mike Morris, Rainer Cramer, 42nd Annual Meeting of the British Mass Spectrometry Society, Manchester, UK,13-15th September 2022

1. Introduction

In the following sections, some fundamental principles required to understand the scope of this thesis are outlined. After the introduction of mass spectrometry for the analysis of biomolecules, in particular peptides, the mechanism of the creation of gas-phase ions and instrumentation to analyse and fragment those are summarised. Later, the field of high-throughput analysis and the benefits of using mass spectrometry in this area are presented.

1.1. Mass spectrometry for the analysis of biomolecules

Mass spectrometry (MS) determines the mass-to-charge ratio of gas-phase ions. First, liquid, solid or gas-phase samples are ionised. Then, ions are separated by their mass-to-charge ratio and finally detected. Within the mass spectrometer, both reactions and separations can be carried out to obtain specific information. MS is a valuable tool in a very wide field of applications from material science,[1] environmental studies[2] and space exploration[3] to clinical diagnostics.[4]

Living organisms are mainly constituted of water, small molecules and four classes of macromolecules: lipids, carbohydrates, oligonucleotides and peptides/proteins.[5] The latter compounds and their building blocks are the main targets for biological mass spectrometry.

MS can be used to detect the presence of those molecules, analyse their structure, help identify biological functions and determine their concentration in diverse biological samples. This versatility may be combined to yield temporal (metabolism) and spatial (MS imaging)[6] information about specific compounds.

Proteins account for $35\,\%$ to $60\,\%$ of the cells' dry weight.[7] Currently, there are about 80 peptide drugs commercialised which account for $5\,\%$ of the pharmaceutical market,
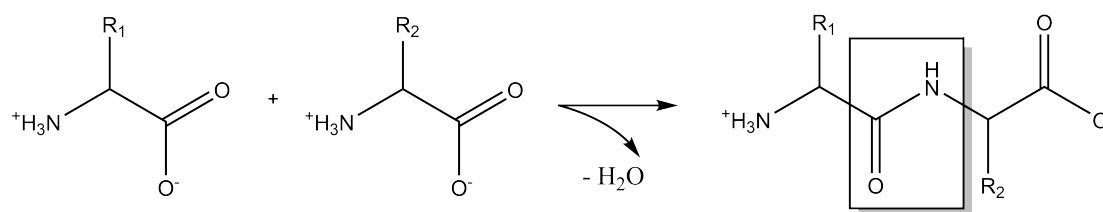
Figure 1.1.: Formation of a dipeptide from 2 amino acids. The peptide bond is highlighted.

the most prominent example being insulin.[8] Peptides and proteins are built by amino acids which are covalently linked through a peptide bond (see Figure 1.1). In contrast to proteins, peptides consist of fewer units and a simpler structure, although the exact boundary remains vague.[9] The ionisation of peptides mainly depends on the abundance of specific amino acids and the pH of the solution. At physiological pH of 7.4 many naturally occurring amino acids are charged. The ones carrying a net positive charge are readily detected in positive mode mass spectrometry. Initially, protons are located at the most basic sites of the peptides. Activation of those ions in the gas phase can lead to the migration of protons to different sites (mobile proton theory).[10,11]

1.2. Ionisation techniques

For the analysis of peptides and proteins most often ionisation techniques are chosen which result in intact molecular ions in the source region. These 'soft' ionisation techniques yield less fragments than 'hard' ionisation sources. The main difference between the two is the amount of internal energy acquired by the ions.[12] Internal energy is defined as the total energy of an ion above its ground state. The excitation can occur as electronic, vibrational and rotational excitation.[12] The more internal energy an ion has, the more likely fragmentation occurs. In soft ionisation techniques ions do not have high internal energies and hence are less likely to fragment. In the following sections, the two main soft ionisation techniques for the analysis of peptides, electrospray ionisation (ESI) and matrix-assisted laser desorption/ionisation (MALDI) will be introduced.

1.2.1. ESI

ESI is able to ionise molecules of a wide range of molecular weight (10 Da to MDa). This versatility combined with the lack of unintended fragmentation makes it the main

ionisation mode for biological MS. ESI can be used for the direct analysis of samples or be combined with an upfront chromatographic separation of a more complex mixture. In brief, a conductive capillary filled with the liquid sample is placed in front of the MS inlet and a high voltage is applied. The electric field results in the formation of a liquid cone at the tip of the capillary and a charge separation in the solution. Depending on the ionisation mode, cations or anions are enriched in the cone. When the forces of the applied field exceed the surface tension of the solution, a fine jet is ejected, and the charge repulsion of the ions in the liquid leads to the formation of droplets.[13] Evaporation of the solvent from the droplets is assisted by applying inert gases in the capillary region. With decreasing droplet size, the charge repulsion increases. When the forces exerted by the surface tension are exceeded by the Coulomb repulsion (Rayleigh limit), the droplet undergoes fission. This process of evaporation and fission is repeated several times with the respective progeny droplets (see Figure 1.2).

Ionisation occurs through the addition or loss of charge-carrying moieties if the analyte is not intrinsically charged. The amount and position of those charge carriers within the droplet influences the signal intensity of analyte ions. Molecular dynamics calculations have shown that the excess charge carriers will preferentially stay at the droplet surface if they have unpolar properties or in the inner droplet if they are small like protons and metal ions.[14] Even for those, the main charge of the droplet will reside on the surface as the ions in the inner droplet will induce orientational polarisation through the formation of solvation layers.[14]

The formation of analyte ions from charged droplets at a nanometre scale is still under discussion but is thought to depend on the type of analyte.[14] Different models have been proposed (see Figure 1.2) and will be briefly explained.

The ion evaporation model (IEM) is mainly suited for the ionisation of low molecular mass analytes. The electric field resulting from the charged nanodroplet ejects the analyte ion while still in connection to the droplet via a solvent bridge. The Coulomb repulsion between the analyte ion and the charged droplet favours ejection of a small analyte-solvent cluster, which loses its solvation shell subsequent to collisions with the background gas.[14] Recently, IEM has been discussed as a special pathway for protein ionisation if acidic solvents are used and the protein is not unfolding under these conditions.[15]

The charge residue model (CRM) describes ionisation for globular analytes, including folded proteins. As a first step, solvated protons and small ions are ejected from the
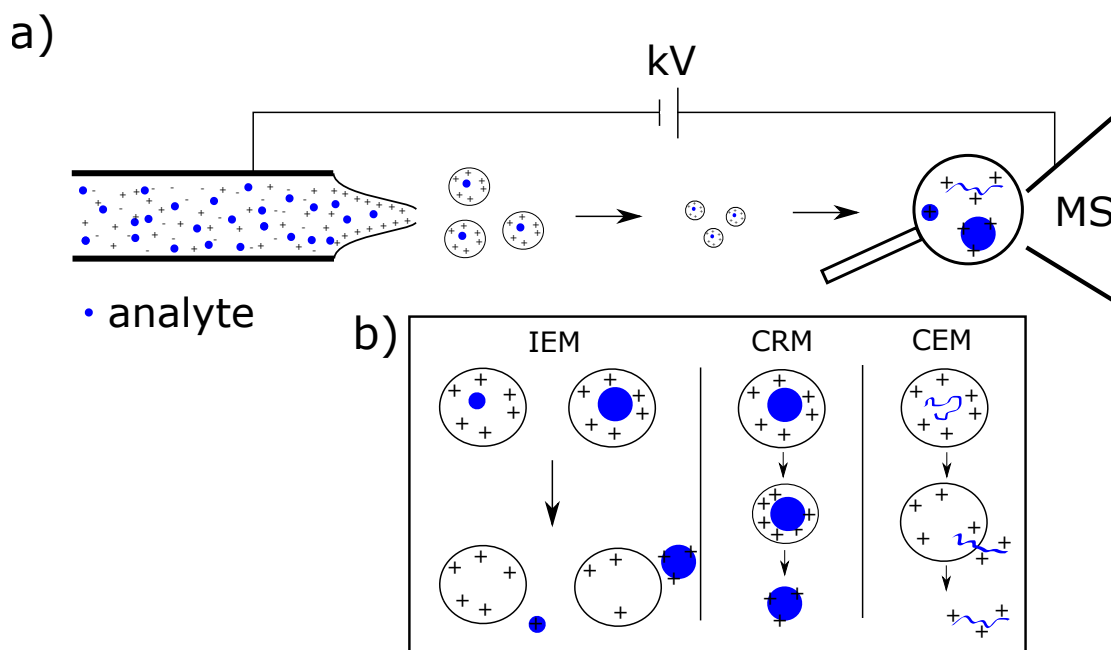
Figure 1.2.: Electrospray ionisation mechanisms in positive ionisation mode according to Aliyari and Kebarle.[13,15] a) The applied potential difference between liquid and mass spectrometer induces charge separation and droplet formation. b) Molecular mechanisms for the final formation of analyte ions. IEM - ion evaporation model, CRM - charge residue model and CEM - chain ejection model.

droplet according to the IEM. The droplet, only containing one analyte molecule, subsequently evaporates to dryness on a microsecond time frame, so a significant amount of analyte will remain in a droplet when reaching the vacuum inlet. The final charge of the analyte is hence independent of its charge state in solution,[14] but is determined by the molecular mass of the analyte.[13]

Naturally or artificially unfolded proteins are more likely to be ionised according to the chain ejection model (CEM). While unfolding the hydrophobic inner part of the molecule is turned towards the solvent, hence favouring migration to the droplet surface and sequential ejection similar to the ion evaporation model. In conclusion, unfolded proteins undergo another, faster ionisation process than folded proteins, yielding higher signal intensities.[14] Peptides will be ionised according to the IEM or CEM[16] depending on the initial droplet size of the spray.

1.2.2. MALDI

Matrix-assisted laser desorption/ionisation is a soft ionisation technique used in MS to create gas-phase analyte ions from liquid or solid samples. Franz Hillenkamp and Michael Karas first developed this method by adding small organic matrix molecules to help ionisation.[17]

The sample is mixed with a matrix and crystals are typically formed in a well-controlled process. The resulting crystalline MALDI sample is irradiated with laser light of a wavelength at which the matrix compound absorbs light. The MALDI sample is consequently ablated, and gas-phase matrix and analyte ions are created (see Figure 1.3).

Material ejection

The mechanisms of material ejection and analyte ionisation are interrelated[18] and still under discussion. The laser irradiates the sample at a given wavelength, pulse duration and pulse energy. This energy will be absorbed by chromophores of the matrix and dissipated through several pathways including excitation, heat conduction and phase-change.

The type and time frame of energy dissipation will influence the material ejection. In general, three types of material ejection can be distinguished: desorption of small molecules from the sample surface, ablation from the sample bulk in the thermal confinement and spallation of large relatively cold clusters caused by tensile stress (acoustic confinement). The type of occurring mechanism depends on experimental parameters, as higher fluence initiate bulk volume processes.[18] Experimental evidence for the mechanism present can be obtained by the velocity and size of emitted particles. Larger clusters from the bulk of the sample are usually ejected at lower velocities than small, desorbed particles from the sample surface as matter nearer to the surface reaches higher temperature.[18] Under typical MALDI conditions several processes can occur simultaneously, as under specific circumstances two distinct regions of particle velocities were found.[18,19]

The mechanism of material ejection can be deduced by the time scale of involved processes. The energy introduced into the sample can be spatially confined within the irradiated sample volume or dissipated into the bulk of the sample. Confinement times for stress and thermal regimes are:[20,21]

$$\tau_{stress} = \frac{\delta}{C_s} \tag{1.1}$$

$$\tau_{thermal} = \frac{\delta^2}{\alpha} = \delta^2 \frac{\rho C_p}{\lambda_t} \tag{1.2}$$

δ is the optical penetration depth of the laser light, C_s the speed of sound in the sample and α the thermal diffusivity which can be calculated from the density ρ, the heat capacity C_p and the thermal conductivity λ_t. The penetration depth δ is often defined as the path length at which the intensity of the incident light beam is attenuated to $1/e$ and can be calculated as the inverse value of the absorption coefficient. Due to the large excess of matrix molecules in MALDI samples, the penetration depth can be approximated using the absorption coefficient of the matrix compound. For typical UV-MALDI experiments the following conditions apply. At $337\,\mathrm{nm}$ the absorption coefficient for the matrix α-CHCA is $2.2 \cdot 10^5\,\mathrm{cm^{-1}}$.[22] Thus, most of the laser light will only penetrate the first $40\,\mathrm{nm}$. The thermal diffusivity was calculated to be around $1 \cdot 10^{-7}\,\mathrm{m^2\,s^{-1}}$,[23] although other estimates range from $1 \cdot 10^{-5}\,\mathrm{m^2\,s^{-1}}$ to $1 \cdot 10^{-6}\,\mathrm{m^2\,s^{-1}}$.[24] The resulting thermal confinement time is in the low ns range. With an estimated speed of sound of $2\,500\,\mathrm{m\,s^{-1}}$,[25] the stress confinement time is in the low ps range. Hence, for laser pulse durations τ_P of low nanoseconds, $\tau_{thermal} \gtrapprox \tau_P > \tau_{stress}$. This means that the energy brought into the sample by a single laser pulse cannot be dissipated quick enough by heat transfer (thermal confinement)[26] while stress-induced spallation is unlikely. As a result the sample overheats beyond surface evaporation and a phase explosion occurs.[25]

Material ejection processes are essential for the further development of the MALDI plume and the likelihood of reactions occurring within the plume. Imaging studies showed that MALDI ablation occurs at a nanosecond scale[27,28] and depends on the experimental conditions,[29] which is in good agreement with the theoretical finding described above. The initial plume expansion is influenced by the inertia of the ejected material as well as the energy brought into the sample. In the emerging plume, huge temperature and pressure gradients cause a redistribution of energy away from the centre of the plume.[18]

Ionisation mechanism

Apart from the release of particles from the bulk MALDI sample, the creation of molecular analyte ions is still under discussion. Several models for the underlying ionisation

mechanism have been proposed. The two most popular models are the lucky survivor model (LS), assuming that ions exist before ablation and energy input is required to release them, and the coupled chemical and physical dynamics model (CPCD), assuming ion formation in the gas-phase.[30] The LS proposes that analytes preserve their charge from being in solution, even after the analyte-matrix crystals have formed. The laser irradiation leads to charge separation in the sample and charged clusters are formed. An excess of charged matrix molecules in the cluster neutralises analyte counterions, leading to singly protonated or deprotonated analyte ions,[31] which can be detected in the mass spectrometer.

(a) Lucky survivor model

(b) Coupled chemical and physical dynamics model
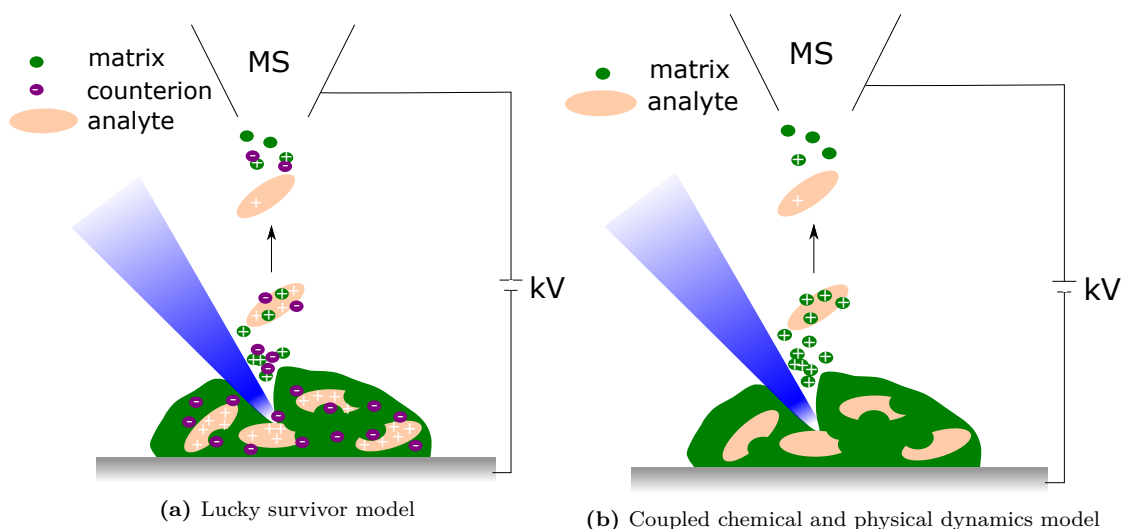
Figure 1.3.: Matrix-assisted laser desorption/ionisation mechanism in the positive ionisation mode. The laser penetrates the sample and a dense plume of material is ejected. Subsequent in-plume reactions create analyte ions which are detected by mass spectrometry. a) In the lucky survivor model analyte ions are ejected from the sample and ions not neutralised by gas-phase reactions are detected. b) In the coupled chemical and physical dynamics model neutral analyte molecules are ejected and ionised by in-plume reactions with charged matrix ions.

In contrast, the CPCD assumes a gas-phase ionisation in a two-step process. First, matrix molecules are ionised by the laser irradiation and in a second step, ion-molecule interactions form analyte ions.[30] However, the formation of matrix ions is not occurring through direct photo-ionisation by the laser as the photon energy is not sufficient.

In UV-MALDI, often employing a nitrogen laser of 337 nm, an energy of $5.89 \cdot 10^{-19}$ J per photon is released ($355\,\mathrm{kJ\,mol^{-1}}$). α-CHCA has an ionisation energy of $1.36 \cdot 10^{-18}$ J ($820\,\mathrm{kJ\,mol^{-1}}$).[32] Therefore, multiple photons, in this case three, would be required to photoionise the matrix compound. Hence, the energy of a single photon is not suffi-

cient.[30]

A widely accepted theory of accumulating the photon energies is the creation of many excited matrix molecules[25] due to photon absorption. Their density favours subsequent energy pooling (see Figure 1.4). Matrix molecules reach the first electronic excited state due to photon absorption. Then two excited states pool, so that one falls back into the ground state whereas the other reaches a higher excited state. When an electron in the higher excited state is then pooled with another one in the first electronic excited state, enough energy is provided to abstract one electron and ionise the molecule.[30]
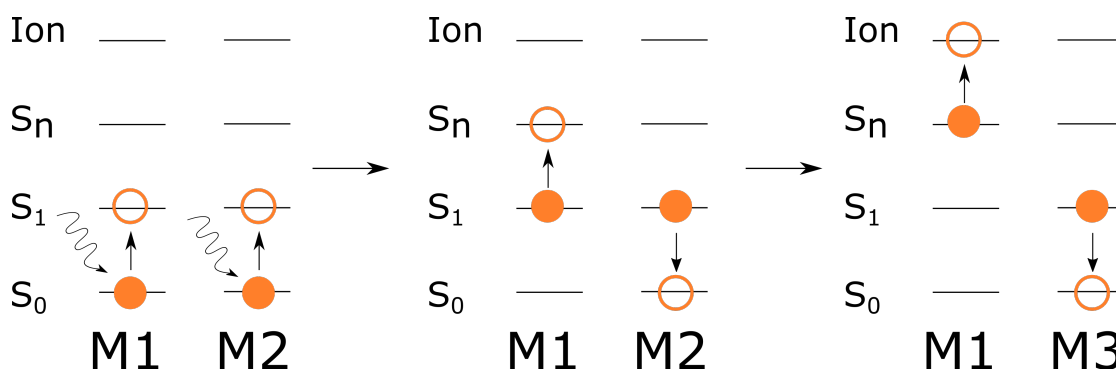
Figure 1.4.: Energy concentration in matrix-assisted laser desorption/ionisation according to Knochenmuss.[30] First, several matrix molecules (M1, M2, M3) are excited by the laser irradiation. Then, energy pooling brings one matrix molecule into a higher excited state and finally primary ionisation of the matrix molecule occurs after a second pooling with another excited molecule.

After creating matrix ions, the CPCD model predicts charge transfer reactions as a second step to ionise analyte molecules. Directly after phase transition, the plume is still dense, so reactions between ions as well as between ions and neutrals are likely. After electron transfer, proton transfer can occur in the positive ion mode.[30] This is especially likely for matrices with acidic functional groups and low proton affinities.[30] For some matrices more complex secondary reactions have been proposed.[30]

Studies have been carried out to elucidate which of the ionisation mechanisms actually take place. Jaskolla and Karas used deuterated matrices to differentiate between pre-formed ions (Lucky Survivor model) and ions formed in the gas phase (CPCD model).[31] Analyte ions which existed before mixing with the matrix (LS) will be protonated, as special precautions have been taken to minimise exchange with deuterium, and ions created through interactions with matrix (CPCD) will be deuterated. For medium basic analytes, deuterated and protonated ions were confirmed. This is in accordance with

the fact that only some analyte molecules are charged before mixing with matrix. Furthermore, this indicates the simultaneous existence of both ionisation pathways.[31] The prevalence of either mechanism depends on several parameters, including protonated-to-neutral analyte ratio, and proton affinity of matrix and analyte. With higher laser fluence, both pathways are enhanced, as more preformed ions get ablated, and more matrix ions are created that can react with neutral analyte molecules. Nevertheless, the signal enhancement is more pronounced for ions created in the gas-phase.[31] The efficiency of the LS ionisation mechanism depends on the ability of charge stabilisation of the preformed analyte ions, as better stabilised ions have a higher probability to survive. Therefore, especially large and basic analytes preferentially undergo Lucky Survivor ionisation.[31] In contrast, deprotonated analyte ions are most probably not created according to the Lucky Survivor mechanism.[31]

1.2.3. LAP-MALDI

Liquid matrix-assisted laser desorption/ionisation

Originally, MALDI was developed for use with solid matrices, where analyte and matrix co-crystallise. In solid MALDI, the analyte distribution is generally heterogeneous among and within matrix crystals.[33] Chemically different domains can be found, yielding different analyte ions explaining the often encountered 'hot-spot' phenomenon.[34] Although progress was made by developing new solid MALDI matrices and sample preparation procedures, the main disadvantages such as short sample lifetime and low reproducibility, both in terms of sample-to-sample and laser shot-to-shot, remained as a result of the process of co-crystallisation.[35] Furthermore, not all analytes are suited for solid-state deposition, as they might impede crystallisation or degrade. For instance, unpurified protein digests are less suitable for solid-state MALDI[36] and labile protein complexes are thought to be altered due to the phase transition.[37]

To overcome these drawbacks, liquid sample preparation techniques were developed. Liquid samples show a more even distribution across the sample and is more similar for different analytes.[38] The challenge of reproducibility is addressed by liquid MALDI sample droplets as they offer a self-renewing surface.[35,39] Liquid MALDI samples are especially suited for pH-sensitive analytes and those impeding the crystallisation of solid MALDI samples.[36]

Three main types of liquid matrices have been developed: ionic liquids,[38] liquid support matrices (LSMs)[40] and particle suspensions.[41,42] LSMs offer multiple advantages[38] and will be used throughout this project. They typically consist of a solvent to solubilise analyte and chromophore,[35] a viscous support to increase sample lifetime and help solubilisation as well as a chromophore for laser energy absorption.[39] Many substances for all three components as well as different mixing ratios have been tested throughout the years[40,43] and need to be chosen according to the analyte class of interest. Apart from the matrix preparation, the performance of the method depends on the chosen target plate (metallic support), namely the surface roughness.[38]

Atmospheric pressure matrix-assisted laser desorption/ionisation

Traditionally, MALDI is used under vacuum conditions, but medium or atmospheric pressure sources have been developed.[44–47] Although the sensitivity at atmospheric pressure (AP) is generally lower compared to vacuum conditions,[48] several advantages counterbalance and outweigh this drawback. Firstly, atmospheric pressure matrix-assisted laser desorption/ionisation (AP-MALDI) can result in complementary information,[6] presumably due the increased collisional cooling under AP. Secondly, AP-MALDI is cost-effective and the sample-throughput can be increased as no pumping of the sample chamber is required. In terms of operating conditions, AP-MALDI differs slightly from MALDI under vacuum conditions, as for instance the laser threshold energy is found to be higher compared to low-pressure MALDI.[47] Moskovets et al. suggested, that the enhanced collisional cooling prevents cluster dissociation and hence limits the release of analyte ions. Therefore, an enforced heating of the plume is needed.[47]

Liquid atmospheric pressure matrix-assisted laser desorption/ionisation

LAP-MALDI was born when predominantly multiply charged analyte ions were obtained.[49] This is especially advantageous as most mass analysers are not able to efficiently transmit ions with a high mass-to-charge ratio and multiply charged ions are often a prerequisite for carrying out fragmentation experiments. The ionisation mechanism for liquid AP-MALDI differs from the conventional solid and in-vacuo type. Although low intensity doubly and triply charges peptides were recently shown with solid state MALDI,[50] in liquid AP-MALDI multiply charged ions are preferentially created[49] when used with a heated transfer tube. In one study, the best yields for multiply charged ions

were accomplished at wavelengths different from the maximum absorption of the matrix and good yields were achieved without chromophores.[51] Therefore, it was suggested that the laser only ejects sample material whereas the ionisation takes place in a heated capillary through an ESI-like evaporative process.[51]

1.3. QToF instrumentation

1.3.1. The quadrupole

Quadrupoles are ion guides which can also be used as mass filters to select ions according to their m/z ratio. This is achieved by guiding selected ions through the device into the next section of the mass spectrometer, while ions with other properties (m/z ratio) will not be transmitted.

The simplest design of a quadrupole consists of 4 parallel cylinders. An electric field is created by applying a direct current (DC) and radio frequency (RF). Opposite rods are electrically connected, so neighbouring electrodes are on opposite potential (see Figure 1.5). The potential applied to the electrodes ϕ_0 at a given time t is derived from the potential of the DC U and the amplitude V and frequency ν of the RF (see Equation 1.3).[52] For every m/z ratio, transmission is achieved for a set of DC and RF values.[52]

$$\phi_0 = \pm(U - V cos(2\pi\nu t)) \tag{1.3}$$
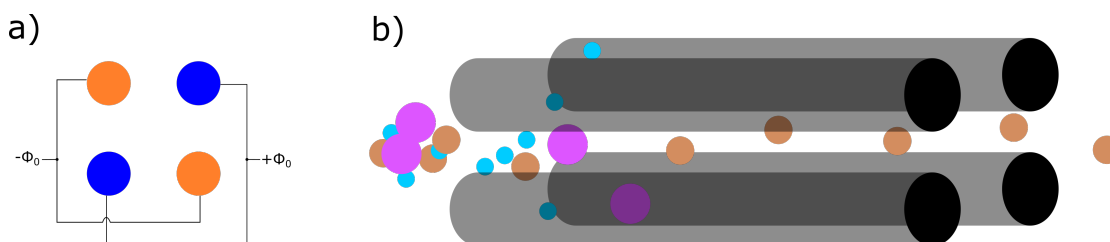
Figure 1.5.: Schematic representation of the quadrupole. a) Opposite rods are connected. Neighbouring rods exhibit opposite potential ϕ_0. b) Ions are filtered according to their m/z value.

Three main operational modes for a quadrupole can be distinguished: broadband transmission, scanning and fixed ion selection. In broadband transmission, the quadrupole is used as an ion guide to transmit and focus ions. This is achieved by disabling the

DC and setting a fixed RF value. The lower the RF amplitude the lower the minimal transmitted m/z. Theoretically, all ions with higher m/z ratios will have stable trajectories through the quadrupole. In practice, ions with a considerably higher m/z ratio will not be transmitted efficiently. This is due to a lack of focussing into the centre of the ion guide. To get a good transmission for a wide range of ions, RF settings need to be changed during the experiment.[52]

In scanning mode, the DC and RF settings are changed throughout the experiment to stabilise the trajectories of different m/z values one after each other. Ions will be filtered efficiently. However, the sensitivity is lower compared to the RF-only mode as ions of a higher or lower m/z ratio than the selected filter window will be lost during the scanning.

The last main mode of operation is setting the quadrupole to transmit only one specific m/z value. This allows very good sensitivity (signal-to-noise ratio) for the ion of interest and enables subsequent fragmentation experiments.[52]

Quadrupoles are often combined with other mass analysers in high-performing mass spectrometers. Combining three quadrupoles in series, so called triple quadrupole instruments, allows for versatile fragmentation experiments often used in small molecule quantitation. The second common tandem instrument is a QToF where the quadrupole is coupled with a time-of-flight (ToF) analyser. This hybrid instrument is used in this work and will be described in the next sections.

1.3.2. Time-of-Flight

In the ToF mass analyser, ions are accelerated in an electric field and then enter a field-free region. Ions with a higher velocity will reach the detector first. The acceleration of ions in the electric field depends on the applied potential difference U and their charge z (see Equation 1.4). This potential energy E_{pot} is converted into kinetic energy E_{kin}. The ion velocity v in the field-free analyser region is constant and can be derived from the length of the flight tube d and the time t needed to traverse the analyser (see Equation 1.5). Hence, the arrival time of the ions at the detector is dependent on the mass and charge (see Equation 1.6). Longer flight paths will lead to higher mass resolution, but come at an expense of sensitivity, as more ions will be lost on their way.

$$E_{pot} = E_{kin}$$

$$zU = \frac{1}{2}mv^2 \tag{1.4}$$

$$v = \frac{d}{t} \tag{1.5}$$

$$t = \frac{d}{\sqrt{2U}}\sqrt{\frac{m}{z}} \tag{1.6}$$

The dependency of mass resolution on the flight time highlights an issue with ToF analysers. The flight time depends on the kinetic energy of the ion which is mainly acquired from the potential difference used for acceleration. However, ions having the same m/z ratio might not have the same kinetic energy if their initial energies (for example from the source region) are different.[52] In this case they will arrive at the detector at different times. To counterbalance this effect, reflectron instruments were invented (see Figure 1.6). By placing a series of electrodes between the entrance to the flight tube and the detector, the motion of ions is reversed. This ion mirror is typically built of a series of grid electrodes although newer instruments use grid-less electrodes. Ions with higher kinetic energies will move deeper into the reflectron, while those with less kinetic energy are deflected earlier. As a result, the differences in flight time due to the initial kinetic energy distribution of the ions is minimised. A beneficial side effect of reflectron instruments is the possibility to build small footprint flight tubes with long flight paths, allowing for higher mass resolution.

ToF instruments are designed in two main configurations depending on the ionisation source. In the axial design, ions originating from the source of the mass spectrometer enter the ToF flight tube directly, staying on their axis. In orthogonal designs (see Figure 1.6), the flight tube is at 90° to the ion beam path. A pusher is used to deflect ions into the flight tube. This design allows the use of ToF analysers with continuous beam ion sources, such as ESI[52] and circumvents peak broadening caused by the initial velocity distribution of ions from the source region.

1.3.3. Tandem mass spectrometry

Tandem mass spectrometry uses several stages of mass analysis or filtering/separation combined with a reaction of the ion.[52] A wide range of reactions and mass analyses
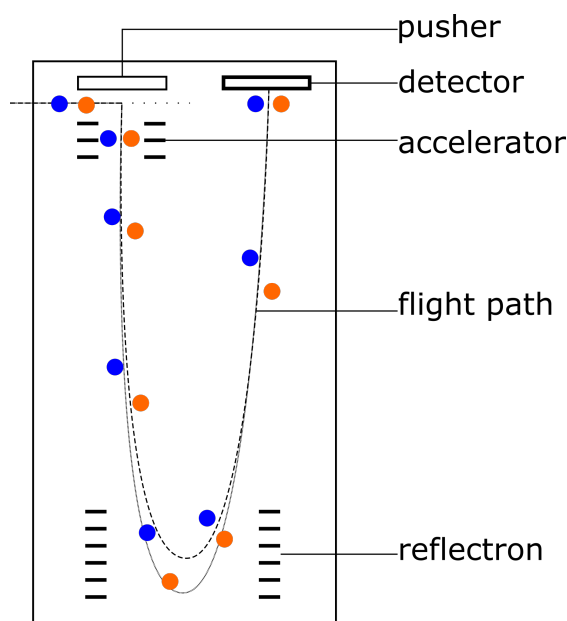
Figure 1.6.: Schematic representation of an orthogonal time-of-flight with reflectron. Flight paths for two ions with the same m/z ratio and different kinetic energies are shown (adapted from Hoffmann and Stroobant[52]).

exist which provide access to different types of information. In QToF instruments, the quadrupole acts as the first mass analyser, selecting a specific m/z ion or scanning over a range of values. The ToF analyser separates all transmitted ions as described above. In between the two mass analysers, different reactions can occur. Here, only the collision-induced dissociation (CID) relevant for this work will be described.

If ions are created using 'soft' ionisation techniques, ideally only a few low abundant fragments will be formed. To obtain structural information about the analyte, fragmentation can be induced by increasing the internal energy of the ion after the source region (secondary excitation).[12] In CID, ions are accelerated in an electric field and collide with a neutral gas.[12] A fraction of the kinetic energy of the collision partners can be transformed into internal energy of the analyte ion and hence induce fragmentation. The efficiency of this conversion depends on the mass of the gas and the analyte, so that higher efficiencies are reached for high-mass inert gases like Ar and lower mass analytes.[53] Fragmentation occurs if the internal energy is higher than the threshold dissociation energy[54] and occurs within the time-scale of the mass spectrometric experiment.

1.4. High-throughput analysis in drug discovery

Two main application areas of high-throughput analysis have emerged in drug discovery: optimising chemical synthesis[55–59] (high throughput experimentation) and identifying potent drug candidates (high throughput screening).[60–64] The latter will be described in more detail below.

1.4.1. Drug discovery

The discovery and development of new therapeutic drugs is a long and costly process with no guarantee of success. Different strategies are used to identify chemical structures, so called leads, which show enough promising properties to advance into medicinal optimisation and eventually into preclinical and clinical trials.[65] HTS is the main lead generation technique if the drug candidate is not derived from a known structure[66].[65] It has been successfully used for a variety of drug targets (e.g. enzymes, receptors, ion channels) and therapeutic areas (including oncology, immunology, infectious diseases, neuroscience).[65]

A typical workflow of an HTS-based drug discovery campaign is shown in Figure 1.7. First, a target for a given disease must be identified and assays to test drug candidates are developed and validated. Then, large compound libraries are screened against the target to detect active compounds. These hits are further analysed and the identified lead compounds are modified to optimise their properties. After preclinical trials, the drug development starts with a series of clinical trials and if successful, the regulatory approval and marketing. Typically, this process starts with over 100.000 potential compounds from which if it all only a couple reach clinical trials[67] and approximately 1 out of 10 clinical trials are completed successfully.[67] Due to the resources needed, care is taken to identify or dismiss drug candidates as soon as possible in the process.

HTS is based on two main types of assays: biochemical and cell-based assays. Biochemical assays are direct assays of the isolated and purified drug target. Hits will be identified through their direct interaction with the target and hence are specific.[68] Biochemical assays only contain compounds necessary for the direct interaction of drug candidate and target. On one hand, these assays are less representative to mimic the complex physiological environment of the later application, and the identified hits are
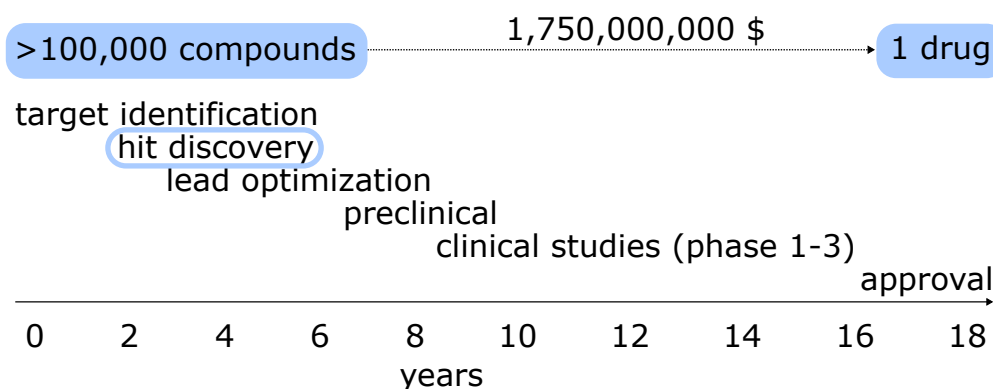
Figure 1.7.: Drug discovery and development steps (adapted from Blass[67]). High-throughput screening is employed in hit discovery.

likely to prove unsuitable at later stages of the process. On the other hand, these assays are easier to perform and miniaturise[68] and cause less interference.

If the molecular target of a disease is not known, not accessible in biochemical assays or only exists under physiological conditions,[69] assays involving whole cells (cell-based assays) are needed. Their representation of the drug environment is more realistic but due to the complex matrix the assay readout is not necessarily target-specific. Cell-based assays probe the modifications of complex pathways.[68] As a result, one assay can identify different modes of action of drugs and may explore new targets and drugs which would not have been identified using targeted assays. Cell-based assays not only screen for activity but also whether a drug candidate is able to penetrate the cell membrane or is toxic. These additional criteria facilitate downstream drug development but might exclude potential drugs which are highly active and could be optimised by medicinal chemists. Although cell-based assays have gained increasing interest[70] both assay types are nearly equally employed[70,71] or are used simultaneously.

Assay development and validation are critical for the identification of active drug candidates. Their performance can be described by various parameters[72] of which most rely on control samples. Special care needs to be taken to choose these controls so they reflect the sample behaviour. Insufficient number, positioning or treatment[73] of controls can lead to a wrong estimation of assay performance and hence impede all downstream analyses.

Biochemical assays for HTS probe a variety of targets.[74] With 28.5 %, enzymes are the second largest class of human drug targets after receptors.[74] As enzymes accelerate

biochemical reactions, they are ubiquitous in cellular processes. HTS assays often analyse enzymatic activity by measuring the precursor (substrate) or product of the catalysed reaction or the bound enzyme complex.[75]

1.4.2. Screening techniques for biochemical assays

Modern compound libraries consist of more than one million substances (see Table 1.1) and special care is taken to curate them.[76] These libraries are unique with similarities between different companies of less than or close to 5 %.[77–79] As a result, pharmaceutical companies started to share their compound libraries[80] to increase success rates which leads to even larger numbers of samples.

Due to the size of screening campaigns, readout methods need to produce results within a reasonable time frame. However, the more accurate this initial step is, the less secondary tests are necessary which speeds up the process and reduces costs. HTS techniques need to be found with a compromise between data quality and time of analysis (see Figure 1.8).

The definition of high throughput is vague but can be described as allowing the analysis of 10 000 s to 100 000 s of samples per day.[72,85] To further differentiate within this broad term, ultra-high-throughput screening (uHTS) was introduced to describe the analysis of more than 100,000 samples per day typically using miniaturised setups.[86]

Among the multitude of assay readout techniques available, photometric methods are widely employed and provide high throughput. Besides absorbance measurements, most photometric readouts rely on the emission of light (luminescence), which is caused by

Table 1.1.: Size of small molecule compound libraries for HTS.

Company/Entity	Number of compounds	Reference
European Lead Factory	500,000	[81]
Novartis	1,500,000	[76]
Bayer Schering Pharma AG	3,000,000	[78]
Bayer Pharma AG	2,750,000	[79]
AstraZeneca	1,410,000	[79]
Pfizer	3,320,680	[82]
Roche/Genentech	2,000,000	[65]
GSK	> 2,000,000	[83]
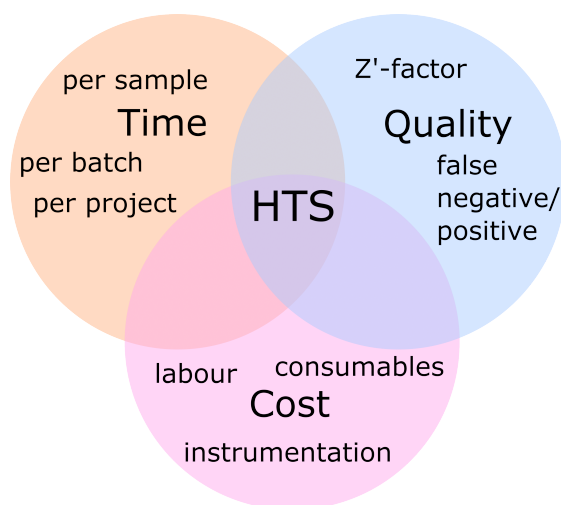
Figure 1.8.: "Magic triangle" of high-throughput screening.[84] A successful method provides a good compromise between analysis speed, quality of results and resources needed.
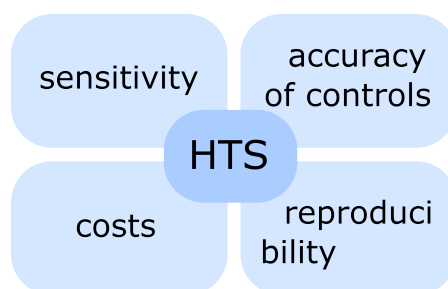
Figure 1.9.: High-throughput screening assays should be optimised for their sensitivity, reproducibility, meaningfulness of controls and costs.[72]

(bio)chemical reactions, radioactivity or irradiation with light (see Figure 1.10). Photometric techniques can be used to directly detect a change in the assay[75] either with or without using labels or indirectly by coupling the target reaction with a secondary one which is used for detection. Due to the lack of natural chromophores and interference, direct readouts are rare and coupling reactions or labels are most often used.[72]

Label-based readouts and indirect methods using coupling reactions are more prone to produce false positive or negative results. Assay interferences can lead to a huge number of false positive screening results, meaning the number of hits is large but the number of compounds actually active against the target is small (0.01-0.1% of library).[87] False results can be caused by interference with the detection (for example by fluorescence-quenching compounds), the biology of the target (by non-specific binding or aggregation) or the coupling reaction.[87] Certain molecular classes frequently lead to false positive

results and have been banned from compound libraries to minimise those.[88] In contrast, missed hits may exclude potent drug candidates from early on in the discovery process. The false-negative rate of a screening campaign can be between 15 % and 25 %.[89] Due to the number and types of possible interferences with the assay and detection, careful consideration of the setup is necessary.[90] After identification of hits in the primary screen orthogonal assays are carried out to reduce the number of false positives and reduce the number of compounds transferred to the next stage of drug development.
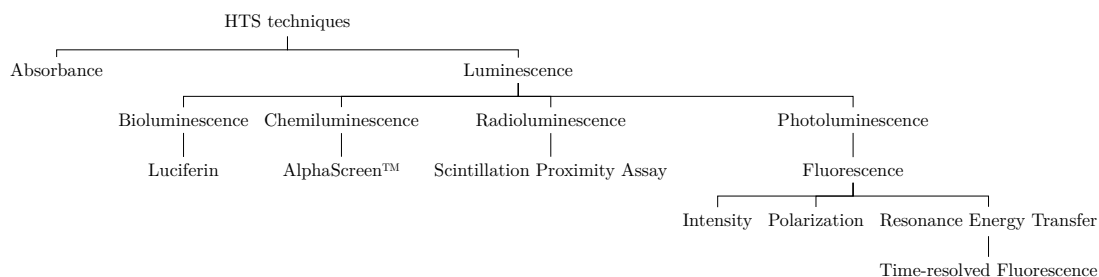
Figure 1.10.: Classification of typical optical readout methods used in high-throughput screening of biochemical assays.

MS-based techniques

HTS using MS has been developed to overcome some of the drawbacks of optical detection methods.[64] MS is seen as a sensitive and specific method allowing the direct detection of several important drug targets.[64] Photometric and MS-based assay readouts show similar robustness.[91] However, the correlation of results between the two readouts is acceptable ($R^2 = 0.54$[92] and $R^2 = 0.44$[93]), with some hits only being identified with either method. It should also be noted that the inter-day reproducibility in the first study was only at $R^2 = 0.64$.[92] In another comparative study, only 20 % of hits were detected with both methods and each readout detected unique hits which included true and false positives.[94] Hits identified by both methods were generally more potent.[94] Additionally, MS-based detection methods can reduce the costs of consumables and specific reagents (such as antibodies).[92]

As a result of to its label-free nature, MS-based methods avoid time- and resource-consuming use of radioactive or fluorescent labels and also assay interference from these labels. Common causes of assay interference in optical and mass spectrometric readouts are presented in table 1.2. Interferences caused by the biological assay itself are present in both types of detection. However, false readouts arising from the optical properties of the

Table 1.2.: Common causes of interference in optical and mass spectrometric HTS assays.[64] Causes for which remediation strategies are commonly employed are denoted in brackets.

Interference	Mass Spectrometry	Optical Methods
Compounds which are light-scattering /fluorescent/absorbent/fluorescent-quenching		X
Inhibition of coupled reaction		X
Altered behaviour due to label		X
Detergent-like compounds	X	X
Aggregation	(X)	(X)
Redox cycling compounds	X	X
Isobaric compounds	X	
Ion suppression	(X)	

screened compounds are also avoided in mass spectrometric techniques. In contrast, mass spectrometry is susceptible to ion suppression and the possible presence of compounds with the same m/z (isobaric). Isobaric compounds can lead to false-positive and false-negative results if they are interfering with the precursor, internal standard or product. For a screening campaign with over 1 million compounds isobaric interference with the internal standard appeared at 0.5% of the hits.[95] To counterbalance, a different internal standard can be chosen or the samples are analysed using tandem mass spectrometry as fragments will be different.[95] Isobaric interference with the product was estimated to yield additional 4 hits without using tandem MS.[95] Different ionisation efficiencies can impact qualitative and quantitative results by reducing or enhancing a specific ion signal. This effect can be counterbalanced by the use of an internal standard[92] that is in many cases an isotopologue of or otherwise physico-chemically close to the readout compound.

Historically, MS techniques were used to confirm hits found by photometric primary screens[96] as they did not provide the required throughput. Some progress has been made using ESI by multiplexing[97] and introducing the RapidFire system which allows the analysis of 0.4 samples per s.[98] However the statement still holds true, especially with upfront chromatographic separation. As a result, other ionisation techniques with minimal sample preparation have been put forward for HTS. The main ionisation techniques used for HTS of enzymatic reactions in biochemical assays are infrared matrix-assisted laser desorption electrospray ionisation (IR-MALDESI), MALDI, desorption electrospray ionisation (DESI), acoustic mist ionisation (AMI) and acoustic droplet ejection (ADE), which will be briefly described below.

Laser-based techniques offer contact-less sampling. They can be used for sample desorption and combined with a variety of ionisation methods.[99] Laser diode thermal desorption atmospheric pressure chemical ionisation (LDTP-APCI) uses an infrared laser to desorb analytes and a corona discharge for ionisation. With less than 0.5 samples/s for enzymatic assays[100] the throughput is below the often cited threshold of 1 sample/s. Similarly, IR-MALDESI employs a pulsed infrared laser to desorb (mainly neutral) particles from a liquid sample. The neutrals are caught by an orthogonally mounted electrospray and charged particles are transported into an extended heated inlet tube of the mass spectrometer[63] (see Figure 1.11). No additional matrix is needed as the laser excites the vibrational modes of the O-H bond in water.[101,102] Compared to UV lasers, wavelengths in the IR have a deeper penetration depth into the sample (see section 1.2.2) and lead to the desorption of larger amounts of material.[101] Samples can be directly analysed from 384-microtiter plates (MTPs).[103] Biochemical assays using lipids, metabolites and small peptides were shown at 0.5 samples/s.[63] More recently, 5 samples/s were shown for a large-scale screening campaign and 22 samples/s[103] for standards which is the highest throughput reported so far for any MS-based method (see Table 1.3) – apart from the LAP-MALDI method reported here. Furthermore, IR-MALDESI can be used for direct kinetic measurements of enzymatic assays due to its non-destructive nature,[63] meaning that the same sample can be analysed several times while the enzyme remains active.

Conventional MALDI is one of only a few commercially available techniques for MS-based HTS. MALDI has been successfully used to analyse a wide range of enzymatic assays[64] at 0.5-0.8 samples/s using 1536-well MTP.[104] MALDI signals are affected by commonly used buffers[105,106] and MALDI-compatible assays need to be developed. Boehringer-Ingelheim recently showed a fully automated sample preparation and analysis system for biochemical assays using 1536-well MTP for analysis.[92] This allows analysis times of 2.5 samples/s. However, the preparation of the target plates and an on-target washing step took another 0.7 s per sample but significantly improved data quality and eventually allowed the analysis using certain buffer compounds. MALDI has been used for large-scale screening campaigns with over 1 million compounds. Data quality remained acceptable without the need for intermediate cleaning of the MS inlet.[92] The coefficient of variation (CV) between control wells remained below 4 % throughout the 20-day campaign.[95] One apparent drawback of conventional MALDI is the use of vacuum ion sources. The exchange of MALDI sample plates requires about 5 min[107] additional time to reinstate the vacuum for analysis. MALDI has been shown with even greater miniaturisation compared to other ionisation techniques as 6144-well formats were used which

required only 25 nL per sample.[107] Smaller volumes resulted in lower assay quality due to the liquid dispensing.[107] Hence, the improvements in liquid handling will likely further improve speed and quality. Running costs are estimated to be around 0.02 - 0.03 GBP/well.[107]

In DESI an electrospray is directed at the liquid sample and analyte ions are desorbed and transported to the MS inlet[115](see Figure 1.11). Comparable to ESI, DESI is widely used in biological MS.[116] Recently, a fully automated system from sample preparation to data processing has been developed.[57] Inter-day repeatability studies revealed that 6 % of monitored reactions showed inconsistent results which were mainly attributed to sample preparation/spotting and solvent delivery.[57] Semi-automated MS/MS data acquisition is possible from duplicate samples for which three different collision energies are analysed in 18 s per sample.[57]

In AMI a high voltage is applied just above the liquid sample which induces charge separation. An acoustic wave applied from below the sample well ejects charged droplets which are desolvated in a heated inlet tube that extends from the MS inlet.[112] Comparable to MALDI, AMI cannot directly run conventional HTS assays due to ionisation suppression but buffers need to be optimised.[94] Kinetic studies carried out using AMI are comparable to ESI and photometric readouts (scintillation).[94] Within a 44,000 compound screening campaign 6 % of the samples were rejected due to unsatisfying quality.[94] AMI costs about 0.009 USD/well with the possibility to reduce costs to 0.0045 USD/well by reducing assay volumes and even further if using a 1536-well MTP. To compare, a similar scintillation assay costs 0.029 USD/well.[94] AMI was used to perform a screen with more than 2,750,000 samples, analysing 100,000 samples per day.[113] Only minimal cleaning (wiping the high voltage cone used to charge the liquid) every 2-3 days was necessary.[113]

ADE uses acoustic waves to create sample droplets similar to AMI. Two major differences should be noted. Firstly, the droplets ejected in ADE are in the nL range, whereas for AMI fL droplets are created.[117] Secondly, no high voltage is used in the desorption stage so that mainly neutrals are ejected from the sample. After acoustic ejection, sample droplets reach the open-port interface which consists of two concentric capillaries.[118] Solvent is injected through the outer one and mixed with the ejected sample droplets. This diluted sample is aspirated into the inner capillary and subjected to a conventional electrospray process[119] (see Figure 1.11). For standard substances a speed of 6 samples/s was achieved, although some overlap between neighbouring peaks was

Table 1.3.: Summary of HTS techniques for biochemical enzyme assays using MS with a sample throughput of more than 1 sample/s.

Method	Instrument	Throughput in samples/s	Plate format	Kinetic studies
IR-MALDESI	FT-ICR,[101] Orbitrap,[63] QToF[108]	5 (assay), 22 (standards)[103]	384[103]	continuous[63]
MALDI	ToF	2.5[92]	1536,[95] 6144[107]	discontinuous*
DESI	QToF,[109] Orbitrap[57]	1[109,110]	1536,[110] 6144[109]	discontinuous*+[109,111]
AMI	Q,[112] QToF[94]	1,[94] 2-3[113]	384[94]	continuous[94]
ADE	QQQ,[60] ToF[114]	0.74,[60] 1.2[62]	1536[60]	continuous[114]

* Discontinuous sampling by preparing one sample per timepoint and quenching the reaction.

+ Continuous analysis is possible but not at high speed.

observed.[120] Good reproducibility was shown as the relative standard deviation of peak areas for two low molecular weight analytes was below 10 % from a 384-well MTP.[120] The acoustic sample ejection failed in 0.3 %[120] and 0.1 %[62] of the samples and standards were added to detect these events. Although it is claimed that the dilution of the sample by a factor of 200 to 1000 by the sampling method reduces buffer effects,[117] significant impact of the signal was observed for several buffer components.[60,120] Furthermore, the conditions for the acoustic ejection and the solvent system need to be optimised for peak shape.[60,62,120] Recently, large-scale screening involving 32,000 compounds was performed at 0.74 samples/s.[60] Direct comparison with a parallel MALDI readout showed 85 % common hits.[62] Besides MALDI, ADE is the second commercially available HTS platform using MS. Based on this, an automated system from assay preparation to MS readout was established.[62] For larger screening campaigns, a washing step of the inlet was necessary to maintain performance over 65,000 consecutive samples. This additional step did not lower throughput as it is performed during plate handling times.[62] To extend the field of application, it has been shown that samples can be directly analysed from phase-separated extraction plates at 0.3 samples/s with a CV of <6 %.[61]
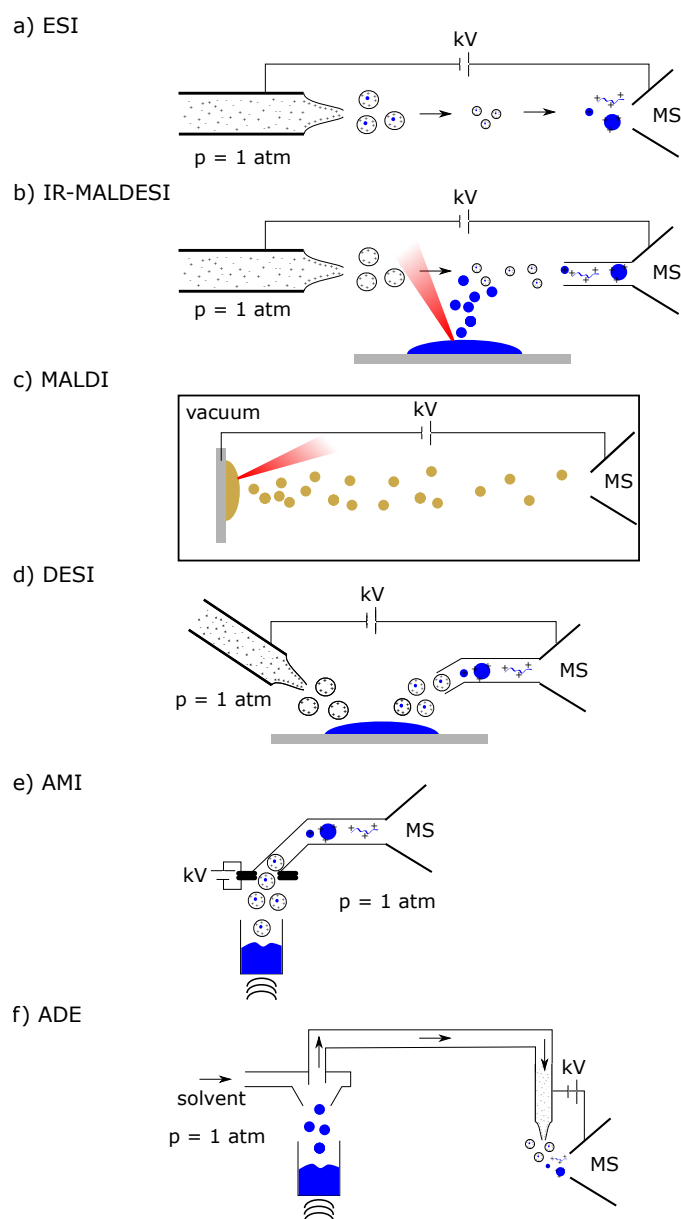
Figure 1.11.: Schematic representation of the main ionisation sources used for mass spectrometry-based high-throughput screening: a) electrospray ionisation, b) infrared matrix-assisted laser desorption electrospray ionisation, c) matrix-assisted laser desorption/ionisation, d) desorption electrospray ionisation e) acoustic mist ionisation and f) acoustic droplet ejection. Conventional MALDI stands out as it analyses solid samples under vacuum conditions whereas the other sources operate under atmospheric pressure using liquid samples. Note, the final stage of ion formation is enlarged.

1.5. Project description

LAP-MALDI is an ambient ionisation technique which offers a good signal stability and the capability of generating multiply charged ions. In conjunction with a quadrupole time-of-flight (QToF) mass spectrometer, the technique was used to explore its applicability for HTS.

In the following sections, two peer-reviewed research articles are presented which were produced during the course of this PhD project. The first article describes the proof-of-principle of LAP-MALDI MS used for HTS. Based upon this, the second article presents an improved setup to further increase the analysis speed (see section 2.3). More insights into these changes are given in subsections 2.3.1 to 2.3.4.

To facilitate the future usage of LAP-MALDI for (large scale) analysis of biological samples, the influence of compounds often encountered in biochemical assays was systematically investigated and the corresponding manuscript is included in section 2.4.

Finally, an overall discussion and points for future research are presented.

2. Results and Discussion

2.1. Context of articles

The following sections highlight the results obtained throughout the course of this work and the resulting peer-reviewed articles. During the course of this PhD, the field of HTS using mass spectrometry evolved quickly. The timeline in Figure 2.1 puts the work presented here in the temporal context with similar techniques.
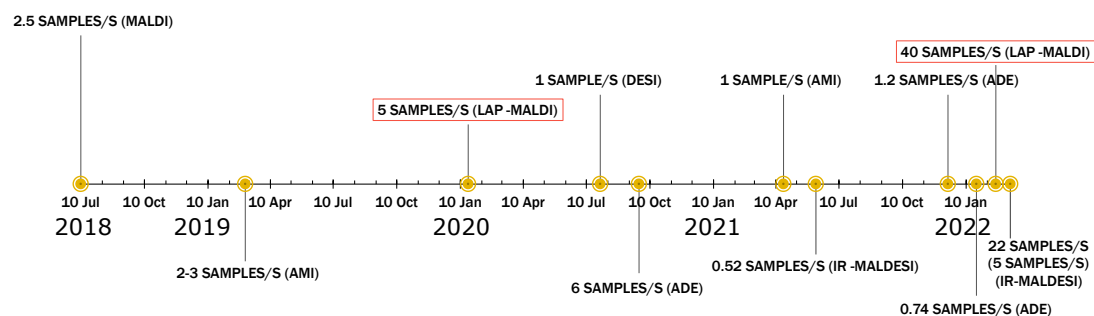
Figure 2.1.: Timeline of articles published on HTS of biochemical assays using MS. Work presented as part of this dissertation is highlighted in red.

2.2. High-speed sample analysis using LAP-MALDI MS (Article 1)

The following technical note presents for the first time the use of LAP-MALDI for fast analysis of biomolecules. In less than 1 s standard substances and milk extracts were analysed with the goal to accelerate (veterinary) diagnostics.

analytical chemistry

Technical Note

Advancing Liquid Atmospheric Pressure Matrix-Assisted Laser Desorption/Ionization Mass Spectrometry Toward Ultrahigh-Throughput Analysis

Henriette Krenkel, Evita Hartmane, Cristian Piras, Jeffery Brown, Michael Morris, and Rainer Cramer*

Cite This: *Anal. Chem.* 2020, 92, 2931−2936

Read Online

ACCESS | Metrics & More | Article Recommendations

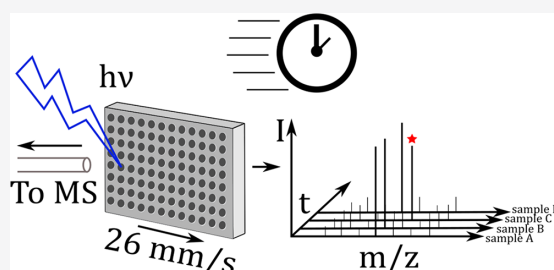**ABSTRACT:** Label-free high-throughput screening using mass spectrometry has the potential to provide rapid large-scale sample analysis at a speed of more than one sample per second. Such speed is important for compound library, assay and future clinical screening of millions of samples within a reasonable time frame. Herein, we present a liquid atmospheric pressure matrix-assisted laser desorption/ionization (AP-MALDI) setup for high-throughput large-scale sample analysis (>5 samples per second) for three substance classes (peptides, antibiotics, and lipids). Liquid support matrices (LSM) were used for the analysis of standard substances as well as complex biological fluids (milk). Throughput and analytical robustness were mainly dependent on the complexity of the sample composition and the current limitations of the commercial hardware. However, the ultimate limits of liquid AP-MALDI in sample throughput can be conservatively estimated to be beyond 10−20 samples per second. This level of analytical speed is highly competitive compared with other label-free MS methods, including electrospray ionization and solid state MALDI, as well as MS methods using multiplexing by labeling, which in principle can also be used in combination with liquid AP-MALDI MS.

L abel-free high-throughput screening (HTS) of large sample sets using mass spectrometry (MS) has gained increased attention in recent years.[1−5] Especially, the reduced numbers of false positive or negative results is a particular advantage in contrast to the non-MS label-based screening approaches such as fluorescence-based assays.[6,7] The latter also require elaborate sample preparations using costly labels such as dyes.

So far the main focus for mass spectrometric HTS has been on electrospray ionization (ESI)[8] and solid-state matrix-assisted laser desorption/ionization (MALDI)[9] as ionization techniques, and a critical review has been published recently.[10]

ESI is a versatile and well-studied platform for the ionization of a broad range of pharmaceutically interesting compounds.[11−16] However, a major drawback of ESI is a lack of speed in the supply of samples, which is a prerequisite for HTS applications. The fastest commercially available system using ESI is the Agilent RapidFire for which a maximum throughput of 2.5 s per sample was reported without using the supplied solid-phase extraction.[17]

Solid-state MALDI achieved an analytical speed of up to 2.5 samples per second (0.4 s per sample) for certain analytes using the Bruker RapifleX Pharma Pulse.[9] However, the time for spotting and the actual biochemical assay were considerably longer. Acoustic Mist Ionization (AMI) and Desorption

Electrospray Ionization (DESI) yielded comparable throughput with 0.45 s[18] and 0.4 s[19] per sample, respectively.

For the different MS ionization methods, biochemical matrices or necessary assay components can be challenging due to their imparted ion signal suppression,[18] impeding crystallization in the case of MALDI or being generally incompatible with the necessary requirements regarding the sample environment or mass spectrometry (nonvolatile salts). However, the suitability of commonly used buffers for MS analysis was investigated[20] and it was shown that label-based non-MS assays can be readily adapted for MALDI MS analysis.[2] The implementation of an additional MALDI spot washing step offers the possibility to reduce buffer concentrations and hence make more assays accessible for analysis with MALDI MS.[9]

Liquid atmospheric pressure (AP) MALDI combines the advantages of both the analysis speed of conventional solid-state MALDI under AP and the versatility of ESI. Different

types of biomolecules[21−23] can be analyzed over a wide range of pH values[24] and in a complex biological matrix,[25] illustrating the general suitability of liquid AP-MALDI for biochemical screening assays. Additionally, the predominant formation of multiply charged analyte ions offers the possibility for further target characterization by highly informative MS/MS.[26]

■ EXPERIMENTAL SECTION

AP-MALDI MS. A detailed description of the in-house developed AP-MALDI setup can be found in a previous publication.[27] Briefly, a heated transfer tube (1 mm internal diameter, 6 cm length) was placed at the inlet of a Synapt G2-Si HDMS instrument (Waters, Wilmslow, U.K.). Ions were generated using a pulsed 337 nm nitrogen laser (3 ns pulse duration; 30 Hz pulse repetition rate) and extracted from a target plate across a gap of approximately 3 mm to the ion transfer tube with a potential difference of 3.5 kV. A counter N_2 gas flow of 180 L/h was applied to the ion transfer tube. Target plate movement was achieved using a Waters Research Enabled Software (WREnS)-controlled xy-stage and its start was synchronized with the start of the MS data acquisition. Data acquisition was set to TOF, sensitivity and positive ion mode with an m/z range of 100−2000. Manual calibration was performed by AP-LDI using sodium iodide and an acquisition time of 3 min with an m/z range of 100−2000 using Intellistart (MassLynx; Waters).

Materials. Ethylene glycol, propylene glycol, glycerol, water, tris base (trizma), acetonitrile (MeCN), trifluoroactic acid (TFA), bradykinin, α-cyano-4-hydroxycinnamic acid (CHCA), 2,5-dihydroxybenzoic acid (DHB), ampicillin sodium salt (AMP), and penicillinase from *Bacillus cereus* were purchased from Sigma-Aldrich (Gillingham, U.K.).

Solid MALDI Sample Preparation. Solid MALDI samples were prepared by mixing matrix solution with analyte solution at a ratio of 1:1 (v/v), spotting 1 μL of the mixture onto the target plate and leaving it to dry at room temperature. The CHCA matrix solution was prepared by dissolving CHCA in 0.1% TFA/MeCN (50:50; v/v) to yield a final concentration of 10 mg/mL. Similarly, a 20 mg/mL DHB matrix solution was prepared in 0.1% TFA/MeCN (70:30; v/ v).

Liquid MALDI Sample Preparation. Liquid MALDI samples were prepared by mixing a liquid support matrix (LSM) with analyte solution at a ratio of 1:1 (v/v). The LSM consisted of a CHCA solution (5−30 mg/mL, 50:50 or 70:30 H_2O/MeCN; v/v) with ethylene or propylene glycol added equal to 60−70% of the solution volume. For milk lipid extracts glycerol-based LSM was used to enhance droplet stability.

For the lactamase assay, an aqueous solution of AMP was prepared at a concentration of 50 μg/mL. The penicillinase was dissolved in 0.1 M tris buffer around pH 8 to a final concentration of 1800−3600 units/mL. Tris buffer or enzyme solution were respectively added to AMP and incubated in a block heater for 2 h at 35 °C.

Milk for lipid analysis was obtained from the dairy cow herd at the Centre for Dairy Research (CEDAR) at the University of Reading (UoR). A total of 100 milk samples were collected from 100 healthy cows through a Dairymaster 50 rotary parlor (Dairymaster Ltd., Bromsgrove, U.K.). All milk samples were pooled and stored in 2 mL cryotubes at −80 °C.

Prior to the analysis, one cryotube of milk was defrosted at room temperature for 5 min and 50 μL of pooled milk was aliquoted in 1.5 mL tubes. The aliquots (50 μL) were mixed with 450 μL of hexane/isopropanol (3:2; v/v) and vortexed for 5 s. No centrifugation was required, and the supernatant (lipids fraction) was directly used as analyte solution for analysis.

■ RESULTS AND DISCUSSION

Subsecond sample analyses require data acquisition with significantly faster scan rates in order to obtain an adequate number of sampling points. This is critical for accurate recording of each sample's ion signal as well as the separation of individual subsequent samples in high-throughput applications. Thus, using the liquid AP-MALDI source, analyses were carried out in TOF mode without ion mobility measurement. The MS scan time was set between 0.1 and 0.03 s and the interscan delay time to its shortest value (0.01 s), which resulted in an actual interscan delay time of 50 ms due to data transfer restrictions and automated software-driven delay time adjustment.

Bradykinin was selected as a peptidic analyte standard for the proof of principle of high-throughput analysis using liquid AP-MALDI MS. A commercial 96-well MALDI sample plate (Waters) was manually spotted with a mixture of the LSM and analyte. Figure 1 shows the results that can be obtained by
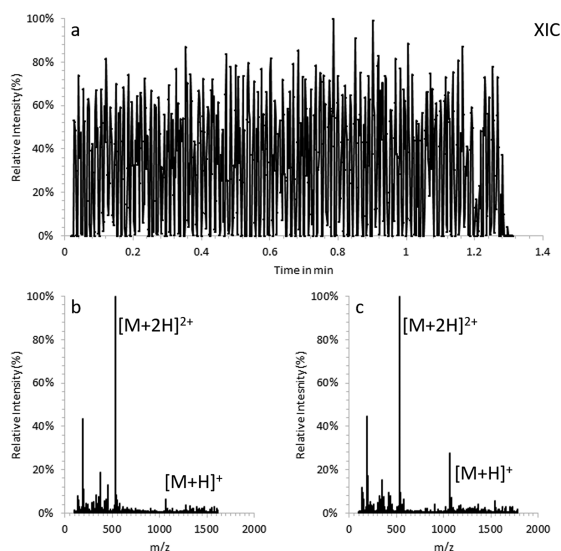
Figure 1. (a) Liquid AP-MALDI extracted ion chromatogram (m/z 530.79) of 96 sample wells with bradykinin as analyte (1 μL total sample volume spotted, 25 pmol analyte on target) at 5 mm/s stage movement speed. (b) Mass spectrum of all scans acquired for the first sample. (c) Mass spectrum of all scans acquired for the last sample.

moving the plate at a speed of approximately 5 mm/s. At this speed 96 samples spotted in 8 rows were analyzed in approximately 76 s, that is, 1.3 samples per second. As the plate moved at a constant speed across each row, the MALDI samples were irradiated by the laser only for a fraction of the time. In addition, as the laser pulse repetition rate was not synchronized with the sample presentation rate, the laser randomly irradiated different areas of the sample droplets, arguably leading to some fluctuation in sample-to-sample ion signal intensities due to the dome shape of the sample droplets and the laser beam's angle of incidence on the MALDI sample
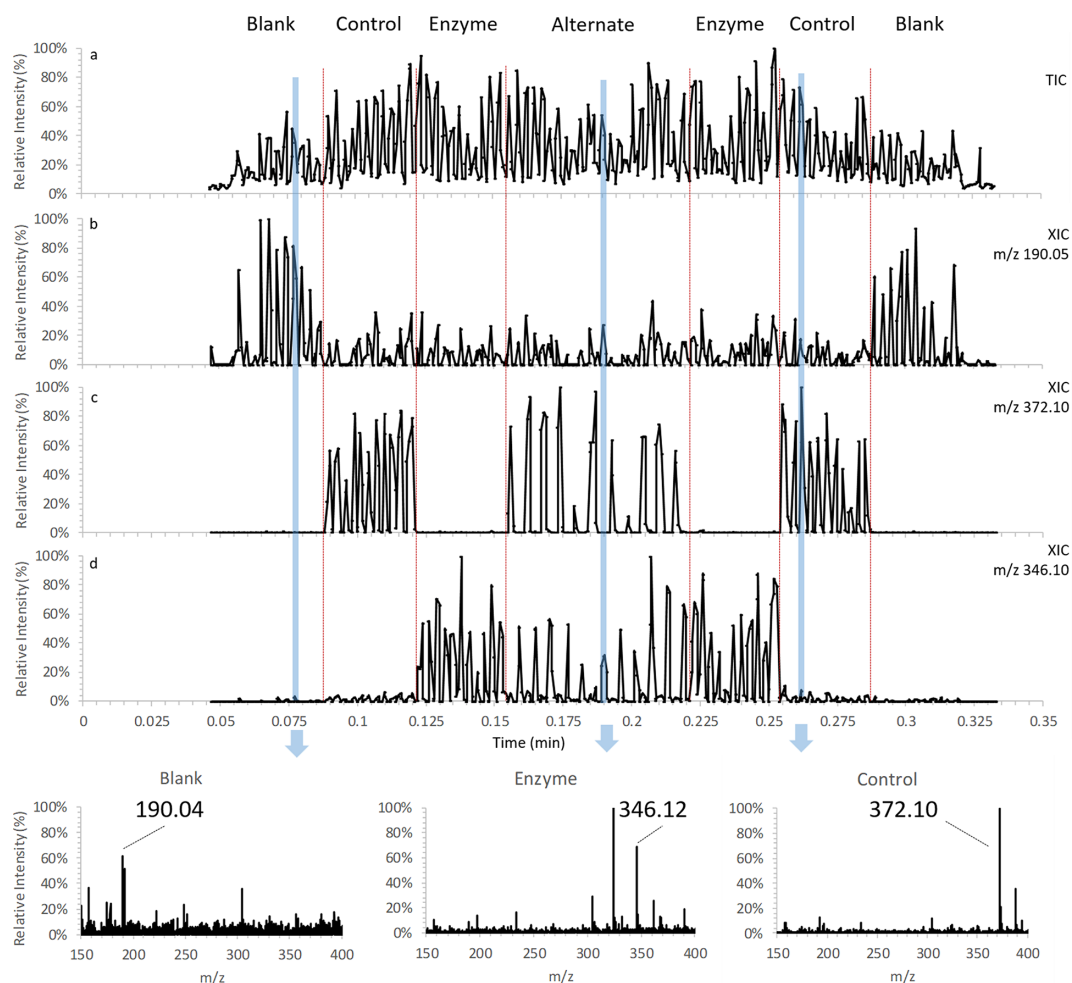
Figure 2. Liquid AP-MALDI MS ion chromatograms of 88 samples consisting of LSM with water only ("blank"), LSM with ampicillin incubated with penicillinase (64.1 amol on target; "enzyme") and without penicillinase ("control") acquired at 0.18 s/sample (26 mm/s) speed. Some of the "enzyme" and "control" samples were alternatingly spotted in the two middle rows of the sample plate ("alternate"). (a) Total ion chromatogram and extracted ion chromatogram of (b) protonated CHCA, (c) sodiated intact ampicillin, and (d) sodiated decarboxylated hydrolyzed ampicillin. (e) Mass spectra of all scans for each respective sample as indicated in the chromatograms (m/z 190.04 protonated CHCA, m/z 346.12 sodiated decarboxylated hydrolyzed ampicillin, m/z 372.10 sodiated intact ampicillin).

plate of approximately 60°. Additionally, the effect of deceleration and acceleration of the stage at the turning points caused some peak broadening at these positions. Yet, all sample spots yielded intense analyte ion signals with low sample-to-sample variation and subsequent samples were easily distinguished. It should be noted here that liquid MALDI can produce "ESI-like" multiply charged ions and therefore the base peak in the MALDI sample spectra is in all cases the doubly protonated bradykinin ion signal (see Figure 1b,c).

As the next step, a slightly faster stage for the MALDI plate was installed and a simple biochemical assay to detect lactamase activity was chosen to demonstrate the potential of liquid AP-MALDI MS for screening assays. The β-lactam antibiotic ampicillin was incubated for 2 h with penicillinase in the appropriate buffer as well as with buffer only (control). A target plate was then spotted with MALDI samples consisting

of LSM with water as analyte solution (blank), LSM with ampicillin in buffer only (control), and LSM with lactamase-treated ampicillin in buffer. Because of the geometrical constraints of the setup with the new stage (due to the larger footprint of the new stage and space restrictions of the current setup), only 11 of the 12 columns could be used and a total of 88 MALDI samples were spotted and irradiated. Figure 2 displays the total ion chromatogram (TIC) and selected extracted ion chromatograms (XICs) obtained from analyzing all 88 samples with a stage movement speed of 26 mm/s.

The XIC for CHCA (m/z 190.05; Figure 2b) shows 11 peaks at higher intensity for the spots where matrix was only spotted with water (blank). The sodiated ampicillin ion signal at m/z 372.1 was only detected when the MALDI samples with ampicillin but without lactamase were irradiated (Figure 2c). Strong ion signals at m/z 346 were only detected from the

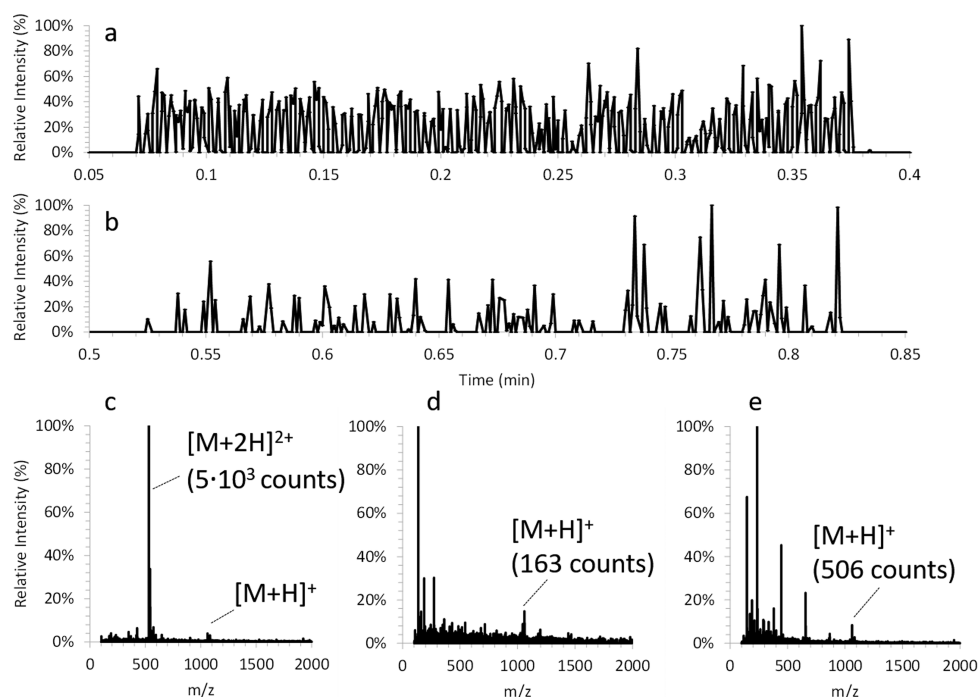**Figure 3.** (a) Liquid AP-MALDI extracted ion chromatogram of 88 sample wells (1 μL total sample volume spotted, 25 pmol analyte on target) at 26 mm/s stage movement speed for doubly charged bradykinin. (b) Solid AP-MALDI extracted ion chromatogram of 88 sample wells (1 μL total sample volume spotted, 25 pmol analyte on target) at 26 mm/s stage movement speed for singly charged bradykinin using DHB as matrix. (c) Mass spectrum obtained under the above high-throughput screening conditions from all (3) scans of one liquid AP-MALDI sample. (d) Mass spectrum obtained under the above high-throughput screening conditions from all (3) scans of one solid AP-MALDI sample prepared with DHB. (e) Mass spectrum obtained from one solid AP-MALDI sample prepared with CHCA but manually acquired over 100 scans (>100 laser shots). For solid AP-MALDI samples prepared with CHCA, bradykinin was not detected under the above automated high-throughput screening conditions using similar laser energies needed for DHB to produce bradykinin ion signals.

samples with the penicillinase-incubated ampicillin (Figure 2d). These ion signals can be assigned to the sodium adduct ions of the decarboxylated hydrolyzed ampicillin, a typical product of lactamase treatment. As seen in Figure 2, unambiguous identification of treated and untreated ampicillin samples can be made. Virtually no carryover between the samples was observed.

Importantly, the analytical speed demonstrated by the analysis of these assay samples is >5.5 samples per second, which is twice as fast as the latest published data for HTS analysis of large sample sets by mass spectrometry.[9,18] However, the current maximum laser pulse repetition rate and the instrument's scan and interscan delay times arguably result in some limitations with respect to the ion signal intensity and stability, explaining some of the ion signal fluctuations in Figure 2. At a laser pulse repetition rate of 30 Hz and a stage speed of 26 mm/s each sample will be irradiated by only three laser shots, since the sample diameter is ~2.5 mm. Thus, as indicated earlier some samples will be irradiated with two laser shots hitting the laser beam-facing side of the dome-shaped sample droplet and one laser shot hitting the shadow side of the droplet while others will have the opposite irradiation pattern as there is no synchronization between laser pulse repetition rate and sample presentation rate. Thus, higher laser pulse repetition rates (1 kHz or more)

and a reduction of the instrument's scan and interscan delay times should allow for analytical speeds well beyond 10 samples per second with much-improved ion signal abundance and stability.

With the above-mentioned restrictions of the faster stage and speed, 88 samples of bradykinin were also analyzed using this new stage. For further comparison, both liquid and solid AP-MALDI MS data were acquired. As expected, the liquid AP-MALDI MS data of this experiment (see Figure 3a) show a similar ion signal stability compared to the penicillinase assay data but a slightly worse ion signal stability compared to the earlier bradykinin data due to the lower number of laser shots (≤3 vs approximately 15) and scans per sample and their associated limitations on ion signal stability as discussed above. However, the comparison to the solid AP-MALDI MS data (see Figure 3) clearly shows that the predominant analyte ion signal in solid AP-MALDI MS is the singly, not doubly, charged protonated bradykinin ion (see Figure 3c−e), and more importantly, that the ion signal intensity and stability is significantly worse with many samples (scans), showing only poor or no analyte ion signal (see Figure 3b).

Finally, this method was applied to the analysis of heterogeneous biofluid. Bovine milk was collected at the University of Reading's research farm at CEDAR, and after a short, one-pot sample preparation, samples were spotted as

described before. To achieve a good signal-to-noise ratio for analyte detection, somewhat longer acquisition times, that is, approximately 1 s per sample, were chosen with the stage moving fast from sample to sample while spending more time on each sample.

For all sample spots, mass spectra with good signal-to-noise ratios were obtained (see Figure 4), highlighting the suitability
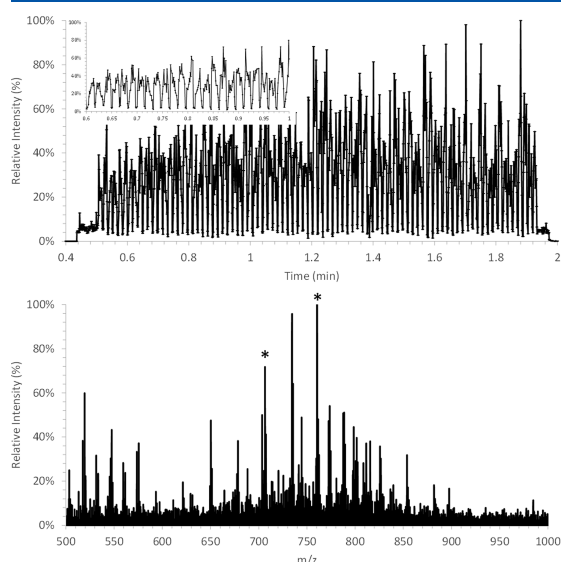

Figure 4. Liquid AP-MALDI MS analysis of 88 sample wells of bovine milk at 1.0 s/sample. Top panel: TIC with an enlargement of a part of the TIC as inset. Bottom panel: a representative mass spectrum for one sample (13 scans). Labeled peaks can be assigned to glycerophospholipids.

of liquid AP-MALDI for the fast analysis of complex biological samples. As the stage resides longer on each sample and more importantly on a specific similar spot on each sample, the ion signal for each spot becomes more rectangularly shaped, again indicating that similarly well-defined ion signals should be obtained with higher laser pulse repetition rates at faster stage movement (and faster scan times and less interscan delay). For selected peaks MS/MS data were acquired and characteristic fragment peaks at m/z 184.07 were found, indicating the loss of the headgroup of glycerophospholipids. Similar peaks for bovine milk were reported earlier.[28]

CONCLUSION

The data presented demonstrate that liquid AP-MALDI is suitable for high-throughput sample screening with a speed of greater than 5 samples per second for the analysis of peptides, lipids, and antibiotics. A simple biochemical assay was conducted and a clear distinction between converted and nonconverted substrate for each sample was achieved. The technique was successfully applied to complex raw milk extracts, although a somewhat lower analysis speed was chosen to obtain quality spectra with a multitude of lipid species. The sample throughput obtained with liquid AP-MALDI is higher compared to those recently reported for the RapifleX and RapidFire techniques. For the more complex milk samples,

currently lower speeds are applied, which are still highly competitive with ESI-based systems.

Further advancement toward higher throughput can be achieved using MALDI sample plate formats with smaller volumes and sample spacing. Preliminary experiments with 384-well plates using 0.4 μL sample volume have shown the importance of spotting reproducibility and the use of higher laser pulse repetition rates. For the 96-well plate (2.5 mm sample diameter) in this study, up to three laser pulses are used for one sample at 30 Hz laser pulse repetition rate and 26 mm/s sample movement speed. Thus, TIC variations may be due to only two laser shots hitting the sample and different laser fluences caused by the angle of the sample droplet. For lower volume plates, these effects will become even more pronounced. Hence, higher laser pulse repetition rates combined with less interscan delay and faster scan times should further enhance performance of the technique, especially regarding reproducibility.

AUTHOR INFORMATION

Corresponding Author

Rainer Cramer − *Department of Chemistry, University of Reading, Reading RG6 6AD, United Kingdom;* orcid.org/0000-0002-8037-2511; Email: r.k.cramer@reading.ac.uk

Authors

Henriette Krenkel − *Department of Chemistry, University of Reading, Reading RG6 6AD, United Kingdom*

Evita Hartmane − *Department of Chemistry, University of Reading, Reading RG6 6AD, United Kingdom*

Cristian Piras − *Department of Chemistry, University of Reading, Reading RG6 6AD, United Kingdom*

Jeffery Brown − *Department of Chemistry, University of Reading, Reading RG6 6AD, United Kingdom; Waters Corporation, , Wilmslow SK9 4AX, United Kingdom;* orcid.org/0000-0001-8569-7174

Michael Morris − *Waters Corporation, , Wilmslow SK9 4AX, United Kingdom*

Complete contact information is available at:
https://pubs.acs.org/10.1021/acs.analchem.9b05202

Author Contributions

The manuscript was written through contributions of all authors. All authors have given approval to the final version of the manuscript.

Notes

The authors declare no competing financial interest.

REFERENCES

(1) Haslam, C.; Hellicar, J.; Dunn, A.; Fuetterer, A.; Hardy, N.; Marshall, P.; Paape, R.; Pemberton, M.; Resemannand, A.; Leveridge, M. *J. Biomol. Screening* **2016**, *21* (2), 176−186.

(2) Beeman, K.; Baumgärtner, J.; Laubenheimer, M.; Hergesell, K.; Hoffmann, M.; Pehl, U.; Fischer, F.; Pieck, J.-C. *SLAS Discovery* **2017**, *22* (10), 1203−1210.

(3) Sun, S.; Kennedy, R. T. *Anal. Chem.* **2014**, *86* (18), 9309−9314.

(4) Roddy, T. P.; Horvath, C. R.; Stout, S. J.; Kenney, K. L.; Ho, P.-I.; Zhang, J.-H.; Vickers, C.; Kaushik, V.; Hubbard, B.; Wang, Y. K. *Anal. Chem.* **2007**, *79* (21), 8207−8213.

(5) Haarhoff, Z.; Wagner, A.; Picard, P.; Drexler, D. M.; Zvyaga, T.; Shou, W. *J. Biomol. Screening* **2016**, *21* (2), 165−175.

(6) Fang, X.; Zheng, Y.; Duan, Y.; Liu, Y.; Zhong, W. *Anal. Chem.* **2019**, *91* (1), 482−504.

(7) Inglese, J.; Johnson, R. L.; Simeonov, A.; Xia, M.; Zheng, W.; Austin, C. P.; Auld, D. S. *Nat. Chem. Biol.* **2007**, *3* (8), 466−79.

(8) Covey, T.; Kovarik, P.; Liu, C. High Speed System for Analysis of Biological Samples that Corrects for ESI Ionization Suppression in Real Time. In *Poster at 67th ASMS Conference*; ASMS, 2019.

(9) Winter, M.; Ries, R.; Kleiner, C.; Bischoff, D.; Luippold, A. H.; Bretschneider, T.; Büttner, F. H. *SLAS Technol.* **2019**, *24* (2), 209−221.

(10) Kempa, E. E.; Hollywood, K. A.; Smith, C. A.; Barran, P. E. *Analyst* **2019**, *144* (3), 872−891.

(11) Wang, C.; Wang, M.; Han, X. *Mol. BioSyst.* **2015**, *11* (3), 698−713.

(12) Smyth, W. F.; McClean, S.; Massaro, C. F.; Smyth, T. J.; Brooks, P.; Robledo, V. R. *Anal. Lett.* **2015**, *48* (17), 2661−2675.

(13) Hilton, G. R.; Benesch, J. L. P. *J. R. Soc., Interface* **2012**, *9* (70), 801−816.

(14) Kaltashov, I. A.; Bobst, C. E.; Abzalimov, R. R.; Wang, G.; Baykal, B.; Wang, S. *Biotechnol. Adv.* **2012**, *30* (1), 210−222.

(15) Ladwig, P. M.; Barnidge, D. R.; Willrich, M. A. V. *Clin. Vaccine Immunol.* **2017**, *24* (5), e00545−16.

(16) Zehender, H.; Mayr, L. M. *Curr. Opin. Chem. Biol.* **2007**, *11* (5), 511−517.

(17) Bretschneider, T.; Ozbal, C.; Holstein, M.; Winter, M.; Buettner, F. H.; Thamm, S.; Bischoff, D.; Luippold, A. H. *SLAS Technol.* **2019**, *24* (4), 386−393.

(18) Sinclair, I.; Bachman, M.; Addison, D.; Rohman, M.; Murray, D. C.; Davies, G.; Mouchet, E.; Tonge, M. E.; Stearns, R. G.; Ghislain, L.; Datwani, S. S.; Majlof, L.; Hall, E.; Jones, G. R.; Hoyes, E.; Olechno, J.; Ellson, R. N.; Barran, P. E.; Pringle, S. D.; Morris, M. R.; Wingfield, J. *Anal. Chem.* **2019**, *91* (6), 3790−3794.

(19) Wleklinski, M.; Loren, B. P.; Ferreira, C. R.; Jaman, Z.; Avramova, L.; Sobreira, T. J. P.; Thompson, D. H.; Cooks, R. G. *Chem. Sci.* **2018**, *9* (6), 1647−1653.

(20) Chandler, J.; Haslam, C.; Hardy, N.; Leveridge, M.; Marshall, P. *SLAS Discovery* **2017**, *22* (10), 1262−1269.

(21) Hale, O. J.; Cramer, R. *Anal. Bioanal. Chem.* **2018**, *410* (5), 1435−1444.

(22) Ryumin, P.; Brown, J.; Morris, M.; Cramer, R. *Int. J. Mass Spectrom.* **2017**, *416*, 20−28.

(23) Ryumin, P.; Cramer, R. *Anal. Chim. Acta* **2018**, *1013*, 43−53.

(24) Towers, M.; Cramer, R. *Spectroscopy* **2007**, *22* (11), 29−32.

(25) Hale, O. J.; Morris, M.; Jones, B.; Reynolds, C. K.; Cramer, R. *ACS Omega* **2019**, *4* (7), 12759−12765.

(26) Cramer, R.; Pirkl, A.; Hillenkamp, F.; Dreisewerd, K. *Angew. Chem., Int. Ed.* **2013**, *52* (8), 2364−2367.

(27) Ryumin, P.; Brown, J.; Morris, M.; Cramer, R. *Methods* **2016**, *104*, 11−20.

(28) Calvano, C. D.; De Ceglie, C.; Aresta, A.; Facchini, L. A.; Zambonin, C. G. *Anal. Bioanal. Chem.* **2013**, *405* (5), 1641−1649.

2.3. Ultra-high-speed sample analysis using modified SONAR (Article 2)

Foremost, sample analysis speed depends on the creation of enough ions from a sample to obtain a signal-to-noise ratio that will allow reproducible identification of the ion of interest. If the time required for the analysis of one sample is in this context satisfactory, additional challenges for fast analysis of subsequent samples arise. Those include the sample introduction (change between samples) and data acquisition, transfer and processing.

2.3.1. Laser pulse repetition rate

For the experiments described in article 2, higher laser pulse repetition frequencies (PRFs) were used compared to the setup used previously (see article 1). Using LAP-MALDI on a similar setup, an increase in analyte ion signal intensity was previously observed with increasing laser pulse repetition rates of up to $1\,000\,\text{Hz}$.[121] However, signal stability at higher pulse repetition rates was decreased and the samples did not last for long.[121] These results are consistent with data obtained during this work (see Figure 2.2). The influence of the laser pulse repetition rate for higher PRFs remains ambiguous. Between $1\,000\,\text{Hz}$ and $5\,000\,\text{Hz}$ the increase in signal intensity was less pronounced and especially between $2\,000\,\text{Hz}$ and $5\,000\,\text{Hz}$ nearly no increase was observed[121] on a similar setup whereas a nearly linear increase in signal intensity was observed until $5\,000\,\text{Hz}$ in this study. Two main experimental differences can contribute to this different behaviour. Firstly, samples in the previous study were irradiated for significantly longer (approximately $25\,\text{s}$ instead of $3\,\text{s}$ used here). The prolonged laser irradiation time might cause sample depletion effects which reduce the ion signal intensity. Although no ion signal reduction with time was observed, local effects might play a role.

Secondly, a different matrix was used (2,5-dihydroxybenzoic acid (2,5-DHB) instead of α-CHCA as used here). For conventional solid-state MALDI, pronounced differences between these two matrix compounds were noted for increased laser pulse repetition rates.[122] The influence of the laser pulse repetition rate on ion yields and ablation characteristics depend on the matrix, the laser beam profile, laser pulse energies as well as the raster speed.[122] It was argued that for typical thermal diffusivity values of the solid matrix, the energy of laser pulses is dissipated and heats the location where the next
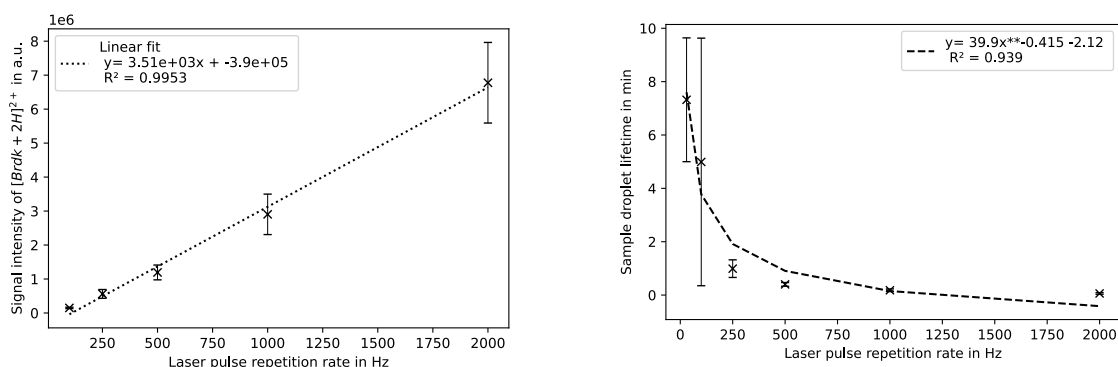
Figure 2.2.: Influence of laser pulse repetition frequency on a α-CHCA sample of bradykinin. (a) Influence of laser pulse repetition rate on ion signal intensity. (b) Influence of laser pulse repetition rate on sample droplet lifetime.

laser pulse hits the sample at elevated raster speeds.[122] For LAP-MALDI the situation is more complex as besides thermal conduction also convection contributes to heat dissipation. Coarse estimates can be carried out for a circular heat dissipation with radius r (and area A) using the thermal diffusivity α of ethylene glycol (see Appendix A.1) and the time between successive laser pulses t.

$$r = \sqrt{\frac{A}{\pi}} = \sqrt{\frac{\alpha t}{\pi}} = \sqrt{\frac{9.2 \cdot 10^{-8}\,\mathrm{m^2/s}\,1 \cdot 10^{-3}\,\mathrm{s}}{\pi}} = 5.4\,\mathrm{\mu m} \qquad (2.1)$$

Accordingly, at a laser pulse repetition rate of $1\,000\,\mathrm{Hz}$ the heat would have travelled approximately $5\,\mathrm{\mu m}$ during the time between laser pulses. This means that above a sample stage speed of $5\,\mathrm{mm/s}$ successive laser pulses will not contribute to the ablation induced by the previous laser pulse.

When using lasers with high PRF samples need to be moved faster to avoid sample depletion. For imaging experiments using solid-state MALDI the phenomenon of oversampling is discussed to yield low data quality.[123] Other studies do not report decreasing image quality with increasing speed.[124] PRF, laser pulse energy and sample movement speed are interrelated parameters and need to be optimised together to get maximum analyte signal intensity.[125] Higher PRF are beneficial at higher sample movement speeds.[125] At low pulse energies, the PRF does not impact analyte signal intensity significantly.[125] Different combinations of sample movement speed and PRF which yield the same number of laser pulses per sample were found to have an influence on the ratio of ions detected.[125] At slower speeds (and hence lower PRFs) more protonated and at higher speeds (and higher PRFs) more sodiated analyte was detected.[125] At higher laser energies, more sodi-

ated ions were observed.[125] The optimal PRF (highest analyte signal intensity) depends on the laser energy, the velocity of sample movement and the analyte.[125] In imaging experiments the total number of ions decreased by 30 % when the analysis speed increased by a factor of app. 5 (same number of laser pulses per area).[124] The relative ion intensities are not significantly affected by analysis speed (but the mass resolution on an orbitrap).[124]

The trend towards higher PRF laser is also evident in commercial instrumentation (see Bruker Rapidflex Tissuetyper 10 kHz, Shimadzu MALDI-7090 2 kHz, Waters MRT 2.5 kHz).

2.3.2. Number of emitted and detected ions

The ion transmission y_{tot} on the Synapt G2-Si can be estimated using the following equation:[122]

$$y_{tot} = y_{optics} * y_{duty\ cycle} * y_{ToF} \tag{2.2}$$

The transfer efficiency of the ion optics y_{optics} was estimated to be around 0.3.[122] It should be noted that this value was given for the in-built MALDI source. Hence, the first ion optics are different compared to the setup used in this work. Namely, a hexapole was used instead of the ion block mounted when using the modified ESI inlet. Ion transmission of atmospheric pressure sources is generally lower compared to vacuum or intermediate-vacuum sources. Hence, the transmission efficiency of transfer optics on the LAP-MALDI source is assumed to be below 0.3.

The duty cycle $y_{duty\ cycle}$ of the orthogonal ToF depends on the selected mass range and the mass of the analyte (see Equation 2.3[122]). For an m/z range up to 2000, the ion transfer efficiencies due to the duty cycle for N-Hippuryl-His-Leu, bradykinin and angiotensin I as used in section 2.3.5 are between 10 and 17 %. Taking into account the transmission efficiency of the ToF y_{ToF} in resolution mode of 43 %,[122] the overall transmission for the investigated analytes is around 1 %.

$$y_{duty\ cycle} = 0.225 * \sqrt{\frac{(\frac{m}{z})_i}{(\frac{m}{z})_{max}}} \tag{2.3}$$

The number of transmitted ions can be estimated from the ion intensity I, the ion transmission y and a conversion factor called single ion intensity SI (see Equation 2.4[122*]). The single ion intensities are determined in ESI experiments and are m/z dependent. As variations between analytes are negligible,[122] values from the regularly performed detector setup can be used which are stored in the meta data for each acquired data file.

$$
\begin{aligned}
n_i &= \frac{1}{y_i} * \frac{I_i}{SI_i} \\
n_i &= \frac{1}{0.01} * \frac{1.3e5}{36} \\
n_i &= 361100
\end{aligned}
\tag{2.4}
$$

Normally, most ToF instruments use an analog-to-digital converter (ADC) which samples the output from the detector at given time intervals and stores a digital signal depending on the original signal intensity.[126] Modern mass spectrometers use 10-bit-ADCs[127] to accurately represent the dynamic range of mass spectral peaks.

In contrast, when using a time-to-digital converter (TDC) the amplified detector signal is passed by a discriminator to evaluate whether the signal is above a set threshold. If so, the TDC registers the exact time difference between the signal arrival and the flight start time. The arrival time distributions per flight experiment (per pusher signal) are saved in memory and summed over the scan time.[126]

In section 2.3, Figure S6, a TDC was used for the analysis. The ion signal width for one sample of bradykinin was approximately 80 ms and around 1012 doubly-charged analyte ions were registered per sample (see table 2.1). A PRF of 2 000 Hz was used which means that one laser shot is emitted every 0.5 ms. So, within 80 ms approximately 160 laser shots were emitted. Taking into account an estimated ion transmission of 1 % (see equation 2.2), approximately 630 doubly-charged bradykinin ions enter the mass spectrometer per laser shot. Summing the signal obtained for the $[M+H]^+$, $[M+Na]^+$, $[M+2H]^{2+}$ and $[M+H+Na]^{2+}$, approximately 2400 ions are detected. Thus, around 1500 analyte-related ions enter the mass spectrometer per laser shot. For conventional solid MALDI using a home-built mass spectrometer, around 5000 peptide ions were reported to having been created per laser shot.[128] The different collection efficiencies of the generated plume in vacuum and atmospheric pressure probably play a mayor role

---

*the inverse of the transmission is used in contrast to the cited reference

in the observed discrepancies. Although no such efficiency is reported for LAP-MALDI, studies using ESI report transfer efficiencies of 2 to 18 %.[129]

Table 2.1.: Number of bradykinin ions per sample peak from section 2.3, supplementary figure 6. Peaks are automatically picked using MassLynx algorithm. The intensities for the first 3 isotopologues are summed.

	1	2	3	4	5	6	7	8	9	10
$[M+2H]^{2+}$	1020	1111	1015	1043	1005	1018	1018	1052	919	919
mean	1012	standard deviation	34							

A crucial aspect for determining the number of ions is to ensure the detector was not saturated. In the case of the TDC, only one ion is registered at a time and the following dead-time. One way to test for detector saturation is to check the isotopic distribution for distortions[130].[128]

For bradykinin, the theoretical distribution of isotopologues for the $[M+2H]^{2+}$ is 100% : 61% : 20% : 5% (see chemcalc.org). However, the apparent distributions from 10 example peaks deviate from the theoretical distribution (see table 2.2). It can be concluded that the detector was saturated as the main isotopologue appears underestimated. Hence, the overall ion count is expected to be higher than estimated above. Taking into account the underestimation of the number of ions due to the detector saturation and the uncertainty of ion transmission, the estimated value for LAP-MALDI might be of the same order of magnitude than for conventional solid-state MALDI. The apparent total ion count (TIC) in LAP-MALDI is several orders of magnitude lower than what is normally observed in ESI. However, due to the ultra-fast ion generation these numbers of ions might still be challenging for the detection system.

Table 2.2.: Isotopic distribution of doubly-protonated bradykinin for 10 samples from section 2.3, supplementary figure 6. Ratio of centred peak intensities are compared to the first isotopologue.

	theory	1	2	3	4	5	6	7	8	9	10
2nd	**61%**	79%	82%	85%	89%	87%	84%	86%	83%	88%	86%
3rd	**20%**	49%	51%	54%	51%	55%	51%	47%	47%	46%	48%
4th	**5%**	18%	21%	20%	21%	27%	18%	19%	19%	20%	19%

2.3.3. Sample introduction

The analysis of subsequent samples without manual intervention requires several steps. Firstly, samples need to be introduced. In MALDI, tens, hundreds or even thousands of samples are typically spotted onto one target plate and can easily be analysed by moving the target plate thanks to the contactless, laser-based desorption. The motorised, translational stages used in the setup, allow a software-controlled movement of the mounted target plate. The new generation of stages used for this experiment allow a faster movement with higher accelerations and faster communication compared to previously used ones. To control these, a script in python was written (see Appendix A.3) and different movement patterns were tested (see Figure 2.3).
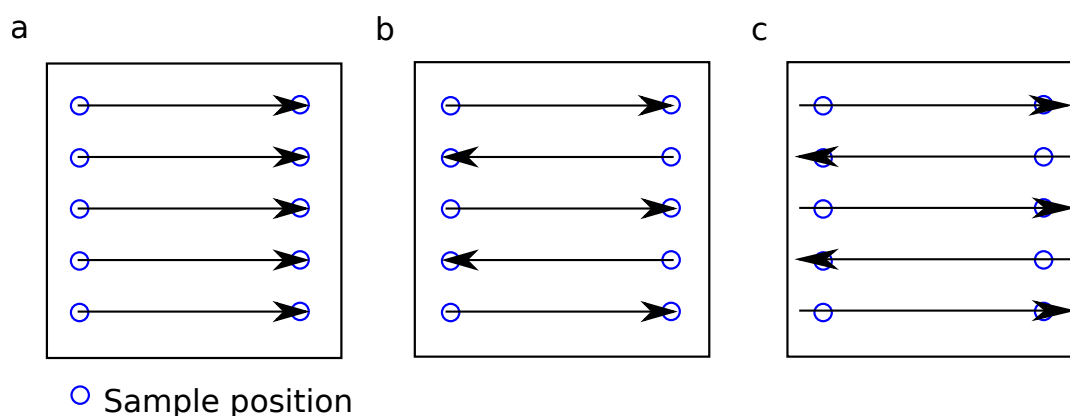
Figure 2.3.: Different stage movement patterns: a) All rows are analysed in the same direction, b) subsequent rows are measured in alternating direction, c) as b) but horizontal movement goes slightly further than the last sample.

A simple uni-directional pattern (a) is disadvantageous compared to one where back- and forward movement is used for sample analysis (b) due to prolonged sample analysis times caused by the time lost by moving to the start of the row. Although b) is the fastest pattern tested, it produced irregular ion signal shapes for some samples, as the last positions on each row have longer residency times due to the deceleration of the stage. To circumvent this behaviour, the horizontal movement was extended over the last sample position in each row (c), which resulted in slightly slower overall speeds (approximately -15%), but more homogeneous data. Hence, the last pattern was adopted for further analysis.

Interestingly, in previously published MALDI imaging experiments raster type a) was

found to yield higher quality data than type b) due to a difference in ion intensity as a function of the direction of movement.[123] It was hypothesised that this is caused by the deposition of ablated material from the preceding sample or a heterogeneity of the laser beam.[131] This was not observed for the LAP-MALDI analyses. Similar to imaging experiments, continuous movement of the sample (imaging terminology: continuous vs. spot mode[124]) is beneficial for analysis speed in LAP-MALDI as mechanical constrains due to the stage acceleration and deceleration are avoided.

In recent commercial MALDI instrumentation (e.g. Bruker Rapiflex Tissuetyper), a combination of sample and laser movement is used to efficiently direct the laser beam to different sample locations.[132] This approach enhances the analysis speed and causes less problems with translational sample movement.[131] This required advanced hardware modifications and is thought unnecessary for LAP-MALDI analysis due to the inherently more homogeneous samples.[38]

Besides the mode of movement, the stage acceleration and velocity were optimised. For the acceleration an upper limit of $4\,\mathrm{m/s}$ was defined above which the setup became mechanically instable. The velocity of the stage was adapted for each project according to the data quality obtained. The velocity of sample stage v_{stage} and the diameter of the sample d_{sample} determine the number of laser shots per sample (see Equation 2.5) for a given PRF.

$$n_{laser\ shots\ per\ sample} = \frac{PRF\ d_{sample}}{v_{stage}} \tag{2.5}$$

As a result, for slower sample movement, the PRF might need to be lowered to avoid sample depletion.

In a commercial instrument sample movement, laser movement and data acquisition are synchronised to allow fast analysis and automatic connection of mass spectrometry data with the sample location.[132] Here, two approaches were taken to connect the sample location with the mass spectrometry data. As described in 2.3, the start and end of each row were marked by a sample with known analyte and the sample positions in-between were calculated. In contrast, for 2.4, each mass spectral scan was labelled with the sample location as the data acquisition was coupled to the translational stage using a custom script developed in previous projects.

2.3.4. Scan rate considerations

The mass spectrometer's ability to produce and save spectral information at a very fast pace is crucial for high-speed analyses and also important for imaging experiments to reduce the acquisition time of high-resolution images.[123] In practice, the instrument control software allows to set the so-called scan time, the time for which ToF spectra are accumulated. After each scan the detector is reset and data are transferred. During this inter-scan delay (ISD) no mass spectral information is acquired. The ISD is 15 ms by default and can be set to 10 ms. The estimated width of analyte ions created by one laser shot is around 5 ms[133] and thus can be completely lost, if arriving at the detector during an ISD. The optimal scan time is a compromise between the temporal sampling resolution of samples, with a minimum around seven data points per sample, and the increased data loss due to an increased number of ISDs. Hence, scan times are adjusted for a given sample movement speed.

To alleviate the loss of sample information due to ISDs, the instrument manufacturer developed a modified acquisition software. Based on the data-independent acquisition (DIA)-mode SONAR,[134] the software was adapted for the Synapt G2-Si. An option to disable the quadrupole scanning was integrated and the instrument was used in ion mobility mode to enable the splitting of one scan in 200 bins (see Figure 2.4b) with disabled mobility separation. As a result, a fine temporal resolution of mass spectra was achieved while lowering the relative number of ISDs per data point compared to the normal scan mode.
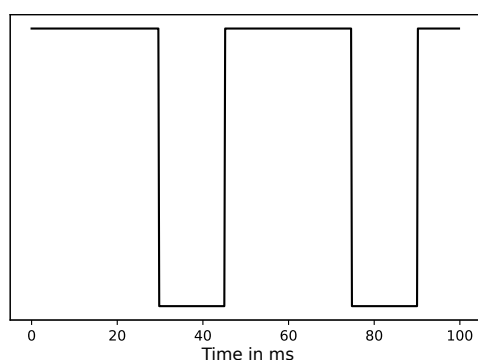
(a) Standard scan mode: 1 scan yields 1 mass spectrum
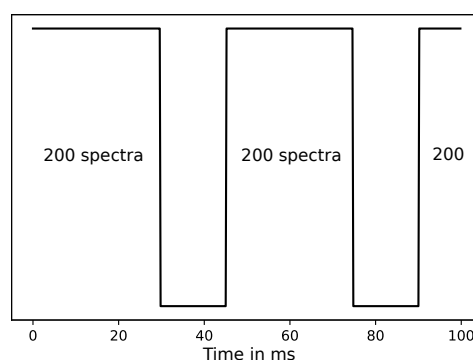
(b) SONAR scan mode: 1 scan yields 200 mass spectra

Figure 2.4.: Schematic representation of different MS scan modes for scan time = 30 ms, inter-scan delay = 15 ms.

At fast sample movement speeds, the times required for spectrum acquisition and data processing/storage become significant contributors to the overall analysis time.[131] Spectrum acquisition times largely depend on the type of mass spectrometer used. Instruments based on Fourier transformation, like Orbitrap instruments, require trapping times to record transients. In contrast, ToF instruments can almost continuously detect ions. In both cases, the analysis time depends on the desired mass resolution, as longer detection times in the trap give better resolution, and longer flight paths require longer intervals between ion injection. However, the time duration of mass analysis is generally much smaller on a ToF compared to trapping instruments. On trapping instruments, transients are typically around 500 ms. The ToF analysis time depend on the hardware setup (e.g. length of the flight path) and the m/z range. The flight time can be estimated by using Equation 1.6: for a flight path of 2 m, an ion of m/z 1000 and a potential difference of 10 000 V, the flight time is around 45 µs. For example, the pusher of the Synapt G2-Si deflects ions into the flight tube every 69 µs for an m/z range of 100 to 2000. A simple spectrum can this be acquired within less than 70 µs, although multiple spectra are summed over a set scan time.

At short scan times, the data transfer time also becomes an important factor to take into account. When moving from the data acquisition workflow used in section 2.2 to higher analysis speeds, issues of inconsistent scan times over analysis time were noted. With the help of the instrument manufacturer, it was noted that the ISD was automatically extended after an initial period. This was due to a slow data transfer rate between the mass spectrometer and the instrument control computer (pc). After eliminating the network switch between the instrument and the pc the issue occurred less frequently. Initially, the scan times and ISD were monitored using an oscilloscope on the scan-in-progress signal output at the rear of the instrument. Later, the network connection between the (internal) embedded computer of the instrument (epc) and the pc was used via a software solution to query the epc for the scan time and ISD. ISDs were extended when using sensitivity mode but not when using resolution mode. The difference between the two modes is an additional radial clipping of the ion beam before entering the ToF. As a result, less ions with a narrower spatial distribution enter the flight tube and reach the detector which results in a lower sensitivity but higher resolution. As a precaution, ISDs were monitored and logged for each experiment but no extension was apparent when using resolution mode. A similar effect was obtained when using the DRE-lens to deflect part of the ion beam. These observations are in good agreement with the signs of detector saturation when operating in TDC mode (see section 2.3.2).

2.3.5. Article

analytical chemistry

Ultrahigh-Throughput Sample Analysis Using Liquid Atmospheric Pressure Matrix-Assisted Laser Desorption/Ionization Mass Spectrometry

Henriette Krenkel, Jeffery Brown, Keith Richardson, Emmy Hoyes, Michael Morris, and Rainer Cramer*

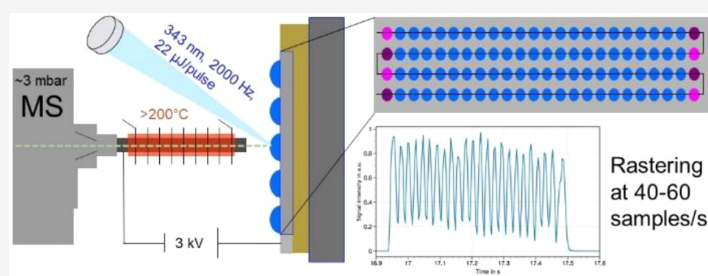Cite This: *Anal. Chem.* 2022, 94, 4141−4145

Read Online

ACCESS | Metrics & More | Article Recommendations | Supporting Information

Rastering at 40-60 samples/s

ABSTRACT: Mass spectrometry (MS) allows for automated analysis of complex samples at high resolution without the need for labeling/derivatization. Liquid atmospheric pressure matrix-assisted laser desorption/ionization (LAP-MALDI) enables rapid sample preparation and MS analysis using microtiter-plate formats and high-performing mass spectrometers. We present a step change in high-speed, large-scale MS sample analysis of peptides at 20 samples/s and an enzymatic assay at 40 samples/s, i.e., an order of magnitude faster than current MS platforms. LAP-MALDI requires only low amounts of sample volume (<2 μL), of which only a fraction (<1%) is typically consumed, and allows for multiplexing and high-speed MS/MS analysis, demonstrated at ∼10 samples/s. Its high ion signal stability and similarity to electrospray ionization enables CVs below 10% and the analysis of multiply charged peptide ions at these extreme speeds. LAP-MALDI MS fulfills the speed requirements for large-scale population diagnostics and compound screening with the potential of analyzing >1 million samples per day.

Label-free, high-throughput MS analysis has recently pushed the limits of sample throughput for compound library screening and inhibitor studies. Especially ambient ionization techniques such as AMI (Acoustic Mist Ionization)[1] (2−3 samples/s), MAI (Matrix-Assisted Ionization)[2] (1 sample/s), DESI (Desorption ElectroSpray Ionization)[3] (2.7 samples/s), ESI (ElectroSpray Ionization)[4] (0.4 samples/s), and ADE (Acoustic Droplet Ejection)[5] (0.45 samples/s), as well as conventional MALDI (Matrix-Assisted Laser Desorption/Ionization)[6] (2.5 samples/s) or hybrid techniques[7] (0.5− 1.3 samples/s for IR-MALDESI (Infrared Matrix-Assisted Laser Desorption Electrospray Ionization)) have produced encouraging results with respect to analytical speed. Although having clear advantages over the routinely used label-based photometric readouts, MS-based fast analysis applications are still not widely employed.

However, ADE,[8] as well as LAP-MALDI MS,[9] recently demonstrated new speeds of up to 6 samples/s, reliably producing stable ion signals that are well-separated from each other. The latter of these two approaches is a new addition to the high-speed MS analysis tools with the inherent speed advantage of laser-based techniques. Additional advantages of LAP-MALDI are high ion signal stability,[10,11] which is crucial for fast sample scanning, and the production of multiply charged analyte ions,[12] thus allowing the employment of high-performing mass analyzers such as orbitraps and modern Q-TOF instruments. In combination with its low matrix background, LAP-MALDI facilitates the simultaneous detection of low-molecular weight (metabolites, lipids) and high-molecular weight (peptides, proteins) analytes,[13] outperforming conventional solid MALDI on axial TOF instruments. LAP-MALDI MS and its associated (offline) upfront sample preparation support large-scale analyses, by using microtiter-plate format and multiple robotic preparation platforms to feed one LAP-MALDI mass spectrometer.

Importantly, LAP-MALDI is inherently fast. On a commercial Q-TOF instrument, recorded ion packets from
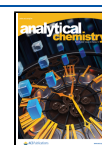
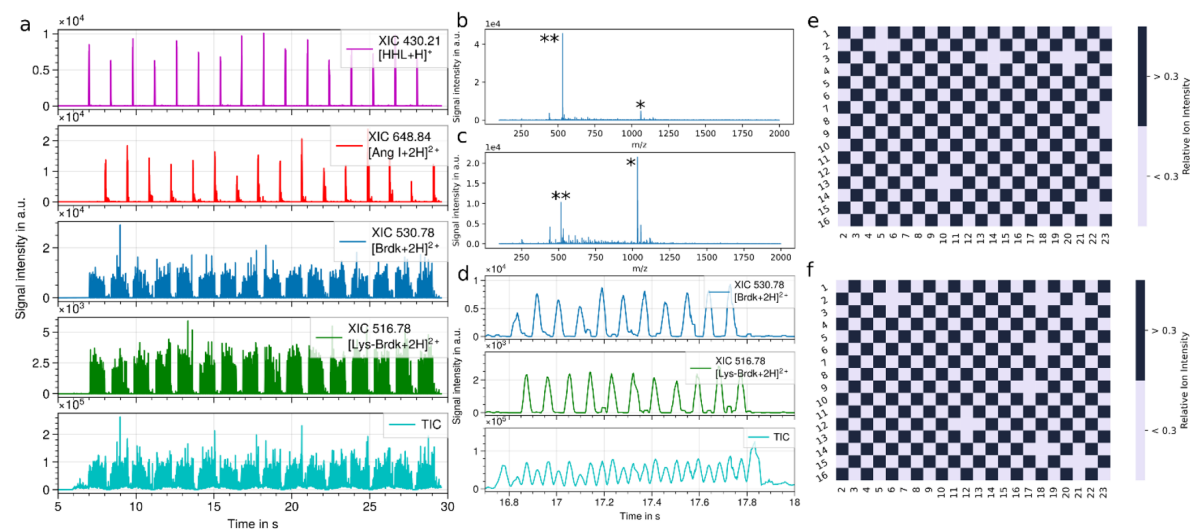**Figure 1.** LAP-MALDI MS analysis of a 384-well plate with alternating Brdk and Lys-Brdk samples and different standards at the start and end of each sample row at 20 samples/s for each row (average of 17 samples/s for the entire plate). a) From top to bottom: extracted ion chromatogram (XIC) of $[HHL+H]^+$ (m/z 430.21, start marker), $[Ang+2H]^{2+}$ (m/z 648.84, end marker), $[Brdk+2H]^{2+}$ (m/z 530.78), $[Lys-Brdk+2H]^{2+}$ (m/z 516.78), and total ion chromatogram (TIC). Mass spectra of first (b) (Brdk) and last (c) (Lys-Brdk) peptide sample of the plate. Singly (*) and doubly (**) charged analyte ions are labeled. d) Enlargement of one row of analyte ion signals. From top to bottom: XIC of $[Brdk+2H]^{2+}$ (m/z 530.78), $[Lys-Brdk+2H]^{2+}$ (m/z 516.78), and total ion chromatogram (TIC). Analyte ion signal intensities for Brdk (e) and Lys-Brdk (f) using a 30% threshold.

individual desorption events are <5 ms wide,[14] allowing an acquisition rate of up to 200 desorption events per second. Thus, we further developed LAP-MALDI with Q-TOF instrumentation by optimizing instrumental bottlenecks such as spectral scan rates, laser repetition rate, sample plate movement, and sample number per plate (see additional experimental details in the Supporting Information), in order to push the speed limits toward tens and ultimately hundreds of samples per second.

■ EXPERIMENTAL SECTION

LAP-MALDI and MS Setup. The general LAP-MALDI setup can be found elsewhere.[9] For this work, a diode-pumped solid-state (DPSS) laser was used with a wavelength of 343 nm and a pulse repetition rate of 2000 Hz (Flare NX 343-0.2-2, Coherent, Santa Clara, USA). MALDI sample plates were rastered as described in the Supporting Information. The acquisition mode SONAR[15] (Waters) was used with the quadrupole scanning being disabled and in RF-only mode. Ion mobility gases were turned off. Each of the SONAR TOF 'scans' were stored in 200 consecutive spectra or 'bins', allowing the acquisition and storage of up to 1000 spectra/s, while the temporal resolution increased up to 0.93 ms per spectrum/bin.

Matrix Preparation and Sample Spotting. CHCA was dissolved in acetonitrile and water (1:1; v/v) to a concentration of 5 mg/mL. After short sonication, propylene glycol (PG) was added at 60% by volume. The matrix was mixed with a sample at a ratio of 1:1 (v/v), and 1 or 0.3 μL of the mixture was spotted onto the stainless-steel sample plate using a 384- or 1536-well format, respectively.

Peptide Analysis. A total of 10 pmol of peptide was used for each LAP-MALDI sample. The MALDI samples were analyzed in each row by moving the sample plate at a constant

speed of 50−200 mm/s. To ease postacquisition data processing, the start and end of each sample row was marked with a sample using the analyte standard Angiotensin I (Ang I) (40 pmol) and N-Hippuryl-His-Leu hydrate (HHL) (10 pmol), respectively.

Enzyme Assay. Angiotensin-converting enzyme (ACE) was dissolved in 50 mM Tris buffer at pH 8.5 to yield 0.1 U/mL and mixed with the substrate 1:1 (v/v, 320 pmol/μL Ang I or 100 pmol/μL HHL). The mixture was incubated at 37.5 °C for several hours.

Additional experimental details can be found in the Supporting Information.

■ RESULTS AND DISCUSSION

For initial testing, a 384-well microtiter-format sample plate was prepared by alternatingly spotting two peptides: bradykinin (Brdk) and [Lys-des-Arg^9]-bradykinin (Lys-Brdk). The sample plate was automatically rastered with an analysis speed of >20 samples/s per row. The overall speed for the sample plate was slightly reduced to 17 samples/s, as additional time was needed to move from the last sample in each row to the first sample in the next row due to restrictions in the sample stage movement and data processing software (see additional experimental details in Supporting Information). The total data acquisition time for an entire sample plate based on the microtiter-plate format was less than 23 s. Figure S1 shows a diagrammatic scheme of the LAP-MALDI source as used in this study.

The data obtained from this initial analysis clearly show well-separated ion signals for all samples without any analyte carryover (see Figure 1a−d). As previously reported, predominantly doubly charged peptide ions are observed.[12] Mass spectrometer scan rates were adjusted to yield at least 10 data acquisitions across each sample, keeping the detection

deadtime (interscan delays; ISDs) to a minimum. This is important as data acquisition gaps caused by ISDs lead to the loss of some or all ion signals from a sample.

Heatmaps for both peptides using simple ion signal intensity thresholds (see Figure 1e,f) reveal a detection (classification) accuracy of >95% over multiple analyses (n = 3, see Figure S2). Greater accuracy is achieved at slightly lower throughput (~99% at 10 samples/s, n = 3, see Figure S3). Sample position effects, e.g., edge effects, are not evident (see Figure S4). The few failures in the correct sample assignment are currently mostly due to sample spotting, which is envisaged to be improved by adequate robotic liquid handlers capable of handling small volumes of liquid (<1 μL) for MALDI sample preparation. To further automate the entire workflow, plate-changing robotics can be used, which can achieve sample plate-swapping in around 5 s.[16] Overall high-throughput analysis time could therefore be around 30 s per plate, allowing 120 plates to be analyzed per hour with an adequate multistage robotic feeding system. In 24 h, more than a million samples could be screened, in principle.

This level of sample throughput is desirable for compound and assay screening in pharmaceutics. Consequently, the platform's applicability to enzyme assays was also tested by monitoring the conversion of an enzyme substrate and its product's appearance simultaneously (see Figure 2). ACE showed full transformation of its natural substrate Ang I and HHL, commonly used in fluorescence experiments. The substrate ion signal intensity substantially decreased after enzyme treatment, and new ion signals at m/z 269.1589 and m/z 1046.5422 appeared, which can be attributed to cleaved protonated His-Leu and converted Angiotensin II (Ang II) with a mass measurement accuracy of 7 and 4 ppm, respectively. Although some ion suppression due to the buffer can be observed (data not shown), reproducible and visibly time-resolved peaks were observed at the same acquisition speed as used for the peptide standards (see Figure 2). With increasing mass (mainly above 1000 Da), we observe the appearance of additional (temporally delayed) low-intensity analyte ion peaks at these high-speed acquisitions. These are most likely due to the complex ion path within the employed Q-TOF/ion mobility instrument and are currently under investigation.

To further increase sample throughput, two other bottlenecks were addressed. First, the speed of the translational stage for sample plate movement was increased by a factor of up to 4 (from 50 to 200 mm/s). Second, the sample plate layout was changed to the 1536-well format. Samples were spotted closer to each other and made smaller as actual sample consumption per desorption event is minimal (less than 1‰[12]).

Tighter sample spotting and a stage speed of 200 mm/s were first tested with the ACE assay (see Figure 3). These changes led to well-resolved peaks at >40 samples/s. With faster sample movement (≥200 mm/s), acceleration and deceleration of the translational stage clearly show a broadening effect for the first and last samples in each row. In addition, the above-mentioned double-peaking for higher masses and the reduced number of sampling points per sample currently limit the maximum analysis speed to 40 samples/s for analytes with a mass >1000 Da. Interestingly, the analysis of the lower-mass substrates (m/z 430.21) and products (m/z 269.15) clearly shows baseline-resolved analyte ion signals between the alternating samples at a speed of 40 samples/s (Figure 3a).
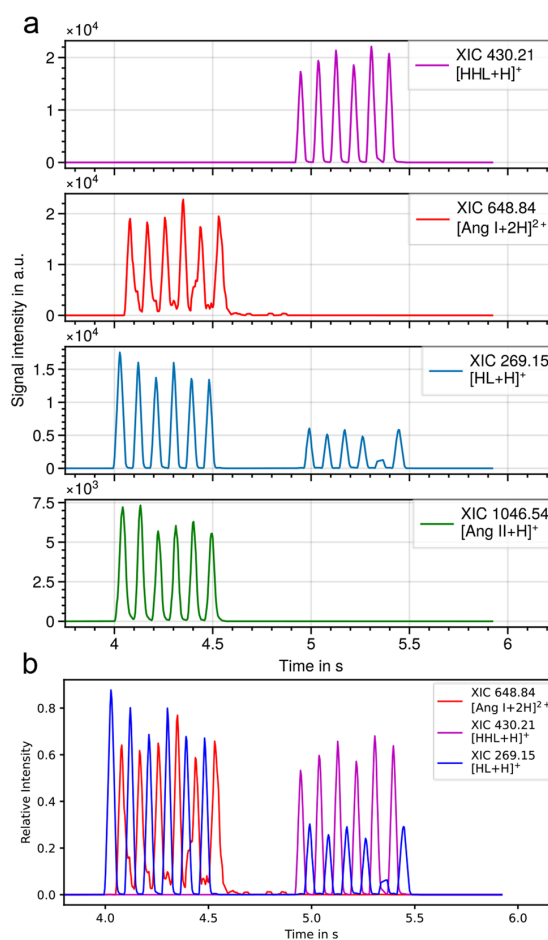

Figure 2. LAP-MALDI MS analysis of an angiotensin-converting enzyme assay with alternating enzyme-treated and untreated samples for Angiotensin I (Ang I, first row) and *N*-Hippuryl-His-Leu hydrate (HHL, second row). a) From top to bottom: XIC of [HHL+H]$^+$ (m/z 430.21, substrate), [Ang I + 2H]$^{2+}$ (m/z 648.84, substrate), His-Leu (m/z 269.15, product), and Angiotensin II [Ang II + H]$^+$ (m/z 1046.54, product). b) Overlay of chromatograms shown in a. Average data acquisition speed was 16 samples/s using a stage speed of 100 mm/s.

Next, extreme sample throughput levels were tested by analyzing HHL (see Figure 4). While the first and last samples in each row are only slightly broadened due to stage acceleration/deceleration at a speed around 40 samples/s, peak broadening worsens and expands to other samples at even higher speeds. Nonetheless, samples can still be separated in their TICs (total ion chromatograms) and XICs (extracted ion chromatograms) at 60 samples/s (see Figure S5a,b). By analyzing several samples of Brdk multiple times, coefficients of variation (CVs) below 10% (<5% for [HHL+H]$^+$) were achieved at conditions corresponding to a speed of 9 samples/s (see Figure S6). Other MS-based techniques result in similar variability but at significantly lower sample throughput.[17,18] Currently, higher speeds result in higher CVs, e.g., 15% at 20 samples/s.

Finally, ultrahigh-throughput LAP-MALDI tandem mass spectrometry (MS/MS) was demonstrated by analyzing Brdk
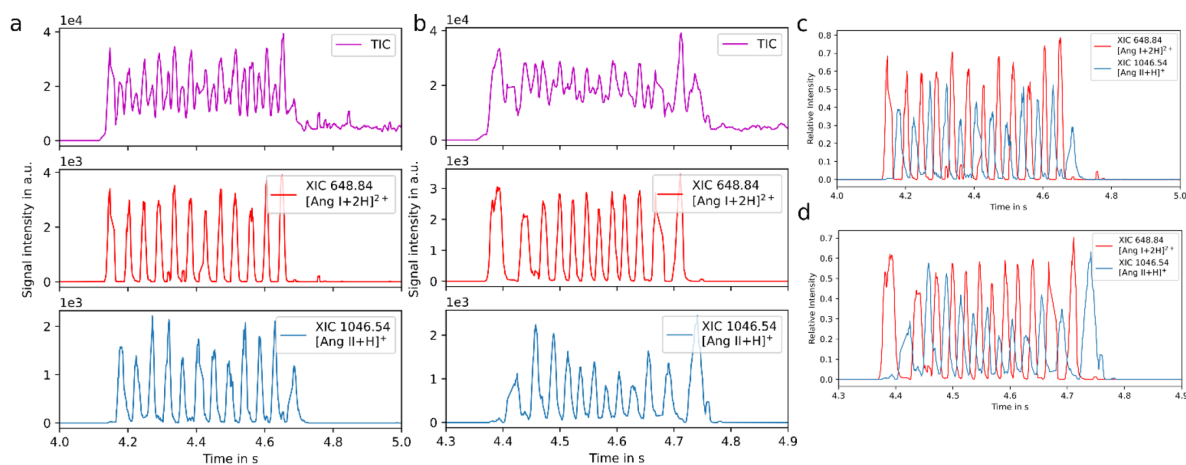
Figure 3. LAP-MALDI MS analysis of an angiotensin-converting enzyme assay alternating enzyme-treated and untreated samples for Angiotensin I using a 1536-well plate layout. a) 40 samples/s (stage movement speed of 100 mm/s); b) 60 samples/s (stage movement speed of 200 mm/s); c) overlay of XICs shown in a; d) overlay of XICs shown in b. TIC: total ion chromatogram; XIC: extracted ion chromatogram.
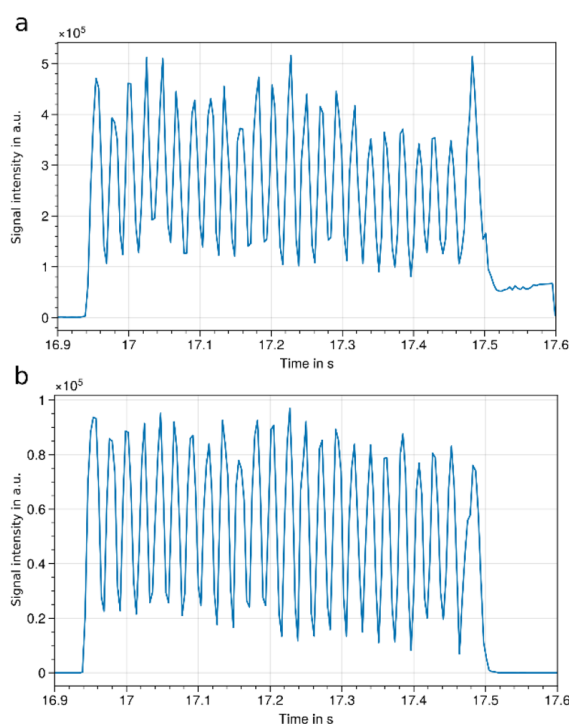

Figure 4. LAP-MALDI MS analysis of HHL using a 1536-well plate layout. a) TIC and b) XIC of $[HHL+H]^+$ at 41 samples/s. TIC: total ion chromatogram; XIC: extracted ion chromatogram.

and its collision-induced dissociation (CID) fragment ions using a fixed window quadrupole. Typical CID peptide fragment ions such as y- and b-type ions were detected at a speed of 12 samples/s per row (see Figure S7). This initial data shows the potential of LAP-MALDI for high-speed SRM/MRM applications.

■ CONCLUSION

In summary, we have shown a step change in the speed for analyzing individual samples by mass spectrometry. So far, up to 60 samples per second can be well separated at the fwhm level by their analyte ion signal. These significant speed increases by an order of magnitude or more compared to previously published reports were achieved by overcoming several bottlenecks such as data acquisition speed (adjusted for ISD deadtimes), laser pulse repetition rate (increased to 2,000 Hz), and sample plate stage speed (increased to 200 mm/s) as well as tighter sample spotting and the use of liquid matrices with their high MALDI ion signal stability. Without the latter, the practical analysis speed would be severely compromised due to the fluctuating ion signal, typically observed with MALDI, thus impeding automated data processing. As used in LAP-MALDI MS, liquid matrices also allow for the generation of multiply charged ions, and together with an atmospheric ion source, high-performing mass spectrometers and superior MS/MS analyses can be employed; in addition, sample plates can be exchanged significantly more quickly in AP-MALDI than in vacuum MALDI sources. MS/MS analysis at these extreme speeds will take screening of large sample sets to an even higher level, in particular with respect to specificity and multiplexing using SRM/MRM approaches.

The method described here can be applied to a vast set of analytes, and the demonstrated analysis speed is even greater than the speed reported for MALDI imaging on commercial instrumentation,[19] which currently achieves around 20 pixels/s (without gaps between samples). Future modifications of the mass spectrometry acquisition software should allow data acquisition without data loss between scans (due to ISD). Lower scan times and thus higher temporal resolution will provide an additional boost to speed. In general, the theoretical speed limit of the method is determined by the temporal width of the ion plume formed during desorption. Further advancements can be made by using adequate robotics for tighter sample positioning (e.g., 6144-well microtiter-plate format) and employing sample stages with even higher speed as well as acceleration/deceleration. In contrast to other techniques like ADE,[18] sample volumes can be <1 μL, and tighter sample

layouts do not result in increased analysis times but lead to a significant throughput improvement.

Potential application areas for LAP-MALDI MS are in large-scale (multiplex) population diagnostics and in screening of compound libraries within the pharmaceutical industry, where a throughput of 1 million samples per day or more is highly desirable.

ASSOCIATED CONTENT

Ⓢ Supporting Information

The Supporting Information is available free of charge at https://pubs.acs.org/doi/10.1021/acs.analchem.1c05614.

Additional experimental details, triplicate measurements of 384-well plates at 2 analysis speeds, and data on variability including edge effects (PDF)

AUTHOR INFORMATION

Corresponding Author

Rainer Cramer − *Department of Chemistry, University of Reading, Reading RG6 6DX, U.K.;* ⓘ orcid.org/0000-0002-8037-2511; Phone: 0118 378 4550; Email: r.k.cramer@reading.ac.uk

Authors

Henriette Krenkel − *Department of Chemistry, University of Reading, Reading RG6 6DX, U.K.*

Jeffery Brown − *Waters Corporation, Wilmslow SK9 4AX, U.K.;* ⓘ orcid.org/0000-0001-8569-7174

Keith Richardson − *Waters Corporation, Wilmslow SK9 4AX, U.K.;* ⓘ orcid.org/0000-0001-5224-0688

Emmy Hoyes − *Waters Corporation, Wilmslow SK9 4AX, U.K.*

Michael Morris − *Waters Corporation, Wilmslow SK9 4AX, U.K.*

Complete contact information is available at:
https://pubs.acs.org/10.1021/acs.analchem.1c05614

Author Contributions

R.C. and H.K. designed and interpreted experiments and wrote the manuscript. H.K. conducted experiments and data analysis. K.R., E.H., and J.B. developed the custom MS software for fast data acquisition. R.C. conceived and supervised the study. R.C. and M.M. acquired the funding. All authors read and edited the manuscript.

Notes

The authors declare no competing financial interest.
Data supporting the results reported in this paper are openly available from the University of Reading Research Data Archive at 10.17864/1947.000338.

REFERENCES

(1) Sinclair, I.; Bachman, M.; Addison, D.; Rohman, M.; Murray, D. C.; Davies, G.; Mouchet, E.; Tonge, M. E.; Stearns, R. G.; Ghislain, L.; Datwani, S. S.; Majlof, L.; Hall, E.; Jones, G. R.; Hoyes, E.; Olechno, J.; Ellson, R. N.; Barran, P. E.; Pringle, S. D.; Morris, M. R.; Wingfield, J. *Anal. Chem.* **2019**, *91* (6), 3790−3794.

(2) Hoang, K.; Trimpin, S.; McEwen, C. N.; Pophristic, M. *J. Am. Soc. Mass. Spectrom* **2021**, *32* (1), 124−132.

(3) Wleklinski, M.; Loren, B. P.; Ferreira, C. R.; Jaman, Z.; Avramova, L.; Sobreira, T. J. P.; Thompson, D. H.; Cooks, R. G. *Chem. Sci.* **2018**, *9* (6), 1647−1653.

(4) Bretschneider, T.; Ozbal, C.; Holstein, M.; Winter, M.; Buettner, F. H.; Thamm, S.; Bischoff, D.; Luippold, A. H. *SLAS Technol.* **2019**, *24* (4), 386−393.

(5) Wagner, A.; Zhang, J.; Liu, C.; Covey, T. R.; Olah, T. V.; Weller, H. N.; Shou, W. Z. *Anal. Chem.* **2020**, *92* (19), 13525−13531.

(6) Winter, M.; Ries, R.; Kleiner, C.; Bischoff, D.; Luippold, A. H.; Bretschneider, T.; Büttner, F. H. *SLAS Technol.* **2019**, *24* (2), 209−221.

(7) Pu, F.; Radosevich, A. J.; Sawicki, J. W.; Chang-Yen, D.; Talaty, N. N.; Gopalakrishnan, S. M.; Williams, J. D.; Elsen, N. L. *Anal. Chem.* **2021**, *93* (17), 6792−6800.

(8) Zhang, H.; Liu, C.; Hua, W.; Ghislain, L. P.; Liu, J.; Aschenbrenner, L.; Noell, S.; Dirico, K. J.; Lanyon, L. F.; Steppan, C. M.; West, M.; Arnold, D. W.; Covey, T. R.; Datwani, S. S.; Troutman, M. D. *Anal. Chem.* **2021**, *93* (31), 10850−10861.

(9) Krenkel, H.; Hartmane, E.; Piras, C.; Brown, J.; Morris, M.; Cramer, R. *Anal. Chem.* **2020**, *92* (4), 2931−2936.

(10) Towers, M. W.; McKendrick, J. E.; Cramer, R. *J. Proteome Res.* **2010**, *9* (4), 1931−1940.

(11) Palmblad, M.; Cramer, R. *J. Am. Soc. Mass. Spectrom* **2007**, *18* (4), 693−697.

(12) Cramer, R.; Pirkl, A.; Hillenkamp, F.; Dreisewerd, K. *Angew. Chem. Int. Ed* **2013**, *52*, 2364−2367.

(13) Piras, C.; Hale, O. J.; Reynolds, C. K.; Jones, A. K.; Taylor, N.; Morris, M.; Cramer, R. *Sci. Rep* **2021**, *11* (1), 3305.

(14) Brown, J. *Instrumental Development of an Atmospheric Pressure Liquid UV-MALDI Mass Spectrometer Source and Interface for the Analysis of Multiply Protonated Peptide Ions*; University of Reading: 2020.

(15) Gethings, L. A.; Richardson, K.; Wildgoose, J.; Lennon, S.; Jarvis, S.; Bevan, C. L.; Vissers, J. P. C.; Langridge, J. I. *Rapid Commun. Mass Spectrom.* **2017**, *31* (19), 1599−1606.

(16) Cramer, R. *Mol. Cell Proteomics* **2020**, *19* (11), 1760−1766.

(17) Wen, X.; Liu, C.; Ghislain, L.; Tovar, K.; Shah, V.; Stout, S. J.; Cifelli, S.; Satapati, S.; O'Donnell, G.; Sheth, P. R.; Wildey, M. J.; Datwani, S. S.; Covey, T. R.; Bateman, K. P.; McLaren, D. G. *Anal. Chem.* **2021**, *93* (15), 6071−6079.

(18) Simon, R. P.; Häbe, T. T.; Ries, R.; Winter, M.; Wang, Y.; Fernández-Montalván, A.; Bischoff, D.; Runge, F.; Reindl, W.; Luippold, A. H.; Büttner, F. H. *SLAS Discov* **2021**, *26* (8), 961−973.

(19) Müller, M. A.; Kompauer, M.; Strupat, K.; Heiles, S.; Spengler, B. *J. Am. Soc. Mass. Spectrom* **2021**, *32* (2), 465−472.

Supporting Information

Ultrahigh-throughput sample analysis using liquid atmospheric pressure (LAP) matrix-assisted laser desorption/ionisation (MALDI) mass spectrometry

Henriette Krenkel,[1] Jeffery Brown[2], Keith Richardson[2], Emmy Hoyes[2], Michael Morris[2], Rainer Cramer[1]*

[1] Department of Chemistry, University of Reading, Whiteknights, Reading RG6 6DX, UK

[2] Waters Corporation, Stamford Avenue, Wilmslow SK9 4AX, UK

* R. Cramer
Department of Chemistry
University of Reading
Whiteknights, Reading RG6 6DX, United Kingdom
E-mail: r.k.cramer@reading.ac.uk
Homepage: www.reading.ac.uk/chemistry/about/staff/r-k-cramer.aspx

Table of Content

Additional Experimental details

Materials. Angiotensin I (Ang I) was bought from Enzo Life Sciences (Farmingdale, USA). α-Cyano-4-hydroxycinnamic acid (CHCA), propylene glycol (PG), Angiotensin Converting Enzyme from rabbit lung (ACE), N-Hippuryl-His-Leu hydrate (HHL), Bradykinin (Brdk) and [Lys-des-Arg[9]]-Bradykinin (Lys-Brdk) were bought from Merck (Darmstadt, Germany). Tris Plus One was purchased from Amersham Biosciences. HPLC-grade water was purchased from Fisher Scientific (Loughborough, UK). Acetonitrile (Chromasolve, HPLC grade) was bought from Honeywell Riedel-de-Haën (Charlotte, USA).

LAP-MALDI and MS setup. The general LAP-MALDI setup can be found elsewhere[1]. Briefly, a Synapt G2-Si (Waters, Wilmslow, UK) was modified with a home-built LAP-MALDI ion source using a heated ion transfer tube. The control and acquisition software used was MassLynx 4.2 (Waters).

Two hardware improvements were necessary to allow higher sample throughput. Firstly, instead of a 30-Hz nitrogen laser, a diode-pumped solid-state (DPSS) laser at 343 nm with a pulse repetition rate of 2000 Hz (Flare NX 343-0.2-2, Coherent, Santa Clara, USA) was used to increase the number of laser shots per sample while decreasing the residence time on each sample spot. Secondly, the target plate speed was increased by using a faster linear actuator (X-LSQ, Zaber, Vancouver, Canada), featuring an encoder for precise position readback.

In general, MALDI sample plates were continuously rastered row-wise by starting the next row with the sample closest to the sample analysed last in the previous row. To achieve the same data acquisition time for each sample, and thus facilitating post-acquisition data processing, the sample raster was adapted to move slightly beyond the end of each row before moving to the next, thus avoiding prolonged residence time on the last sample due to the deceleration needed for turning to the next row. As additional time was therefore needed to move from the last sample in each row to the first sample in the next row, there was a slightly reduced overall speed for the analysis of an entire plate.

A 384-well MALDI target plate in the microtiter plate-format was used to allow easy interfacing with standard robotics and sample preparation. Therefore, a 3d-printed holder was designed to allow the use of standard and non-standard target plates.

Due to data acquisition rate limitations, the commercial instrument software does not provide a readout for every single ToF spectrum (as the oaTOF is pushing ion packets at tens of kHz). Instead, an appropriate accumulation of ToF spectra is obtained for each spectral "scan". For the Synapt, the MassLynx 4.2 ToF spectral accumulation time has a minimum setting of 16 ms per scan and an InterScan Delay (ISD) of at least 10 ms between every scan. This does not allow sufficient temporal resolution for ultrafast throughput analysis. Hence, the recently developed acquisition mode SONAR[2] (Waters) was used in an adapted way. The quadrupole scanning was disabled and used in RF-only mode and ion mobility gases were turned off, while TRAP TWAVES were optimised to guide ion packages through at maximum speed. Each of the SONAR ToF "scans" were stored in 200 consecutive spectra or "bins". Thus, ISDs occur after each scan but not after each spectrum/bin. As a consequence, if the scan time was set at 0.2 seconds (for example), individual consecutive spectra could be acquired and stored at approximately 1000 spectra/s and the temporal resolution increased to 0.93 ms per spectrum/bin.

Data processing. Raw files recorded in the adapted SONAR format were converted to MassLynx-readable files using a custom-made software (for software access contact K.R.). Ion signals for each sample were automatically detected and spatially labelled by custom-made data processing software (for software access contact E.H.) by detecting marker ion signals at the start and end samples for each row and evenly distributing the number of scans between into the specified number of samples with the help of MassLynx SDK. Separate files were created for each sample's ion signals, allowing further standard data post-processing. Data were smoothed using Savitzky-Golay algorithm. Ion intensities for heatmaps were extracted using specproc (https://sourceforge.net/projects/specproc/).

Matrix preparation and sample spotting. CHCA was dissolved in acetonitrile and water (1:1; v/v) to a concentration of 5 mg/mL. After short sonication, 60 % PG was added by volume. The matrix was mixed with sample at a ratio of 1:1 (v/v), and 1 µL or 0.3 µL of the mixture was spotted onto the stainless-steel target plate using a 384- or 1536-well format, respectively.

Peptide analysis. A total of 10 pmol of peptide was used for each LAP-MALDI sample. The MALDI samples were analysed in each row by moving the sample plate at a constant speed of 50-200 mm/s. To ease post-acquisition data processing, the start and end of each sample row was marked with a sample using the analyte standard Ang I (40 pmol) and HHL (10 pmol), respectively.

Enzyme assay. ACE was dissolved in 50-mM tris buffer at pH 8.5 to yield 0.1 U/mL and mixed with substrate 1:1 (v/v, 320 pmol/µL Ang I or 100 pmol/µL HHL). The mixture was incubated at 37.5°C for several hours.

Coefficient of Variation (CV) measurements. Four samples of Brdk were spotted on the target plate in rows of two. HHL and Ang I were used for marking each row as described above. The translational stage was set to cycle trough the samples to measure Brdk 96 times. The detector mode was set to time-to-digital-converter (TDC). Peak detection was performed in MassLynx (Savitzky-Golay smooth, peak separation 30 %, peak threshold 10 % relative height).

Tandem mass spectrometry. Twelve samples of Brdk (20 pmol each on target) were analysed with a fixed quadrupole window around m/z 530.78. A collisional voltage in the trap cell of 25 V was applied.

References

1.   Krenkel, H.; Hartmane, E.; Piras, C.; Brown, J.; Morris, M.; Cramer, R., Advancing Liquid Atmospheric Pressure Matrix-Assisted Laser Desorption/Ionization Mass Spectrometry Toward Ultrahigh-Throughput Analysis. *Analytical Chemistry* **2020,** *92* (4), 2931-2936.
2.   Gethings, L. A.; Richardson, K.; Wildgoose, J.; Lennon, S.; Jarvis, S.; Bevan, C. L.; Vissers, J. P. C.; Langridge, J. I., Lipid profiling of complex biological mixtures by liquid chromatography/mass spectrometry using a novel scanning quadrupole data-independent acquisition strategy. *Rapid Communications in Mass Spectrometry* **2017,** *31* (19), 1599-1606.

Figures
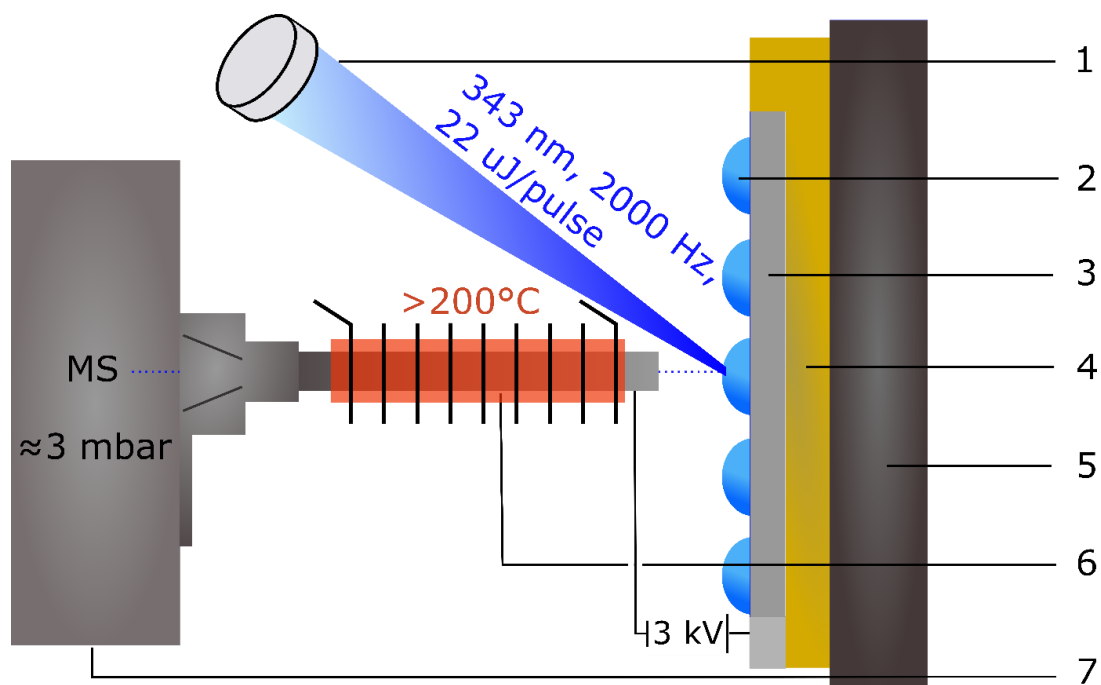
Figure S1: General LAP-MALDI setup: 1) UV laser, 2) liquid sample at atmospheric pressure, 3) sample plate, 4) sample plate holder, 5) 2-dimensional translational stage, 6) inlet tube heated by resistance wire and 7) Q-TOF mass spectrometer
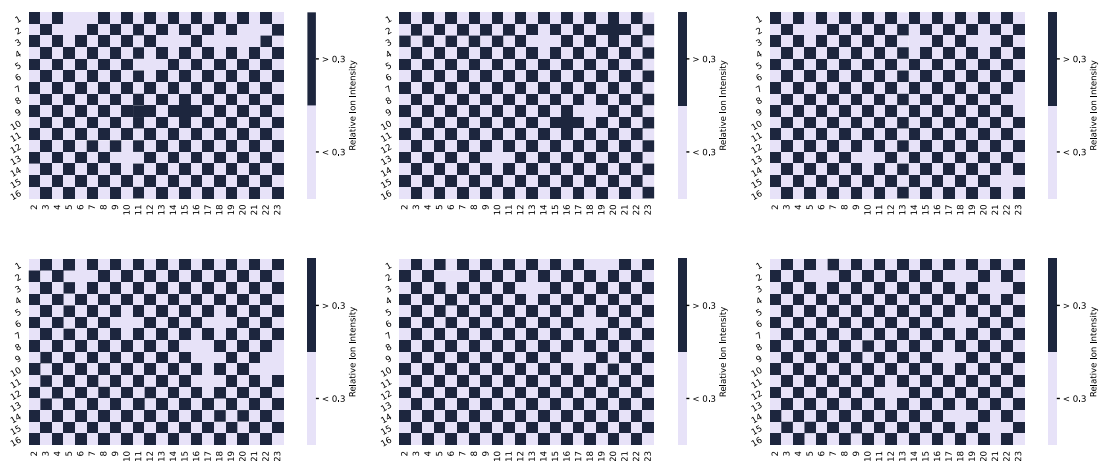
Figure S2: LAP-MALDI MS analysis of a 384-well plate with alternating Brdk and Lys-Brdk samples and different standards at the start and end of each sample row at 20 samples/s for each row (average of 17 sample/s for the entire plate). Analyte ion signal intensities for Brdk (top) and Lys-Brdk (bottom) for three runs using a 30 % threshold.
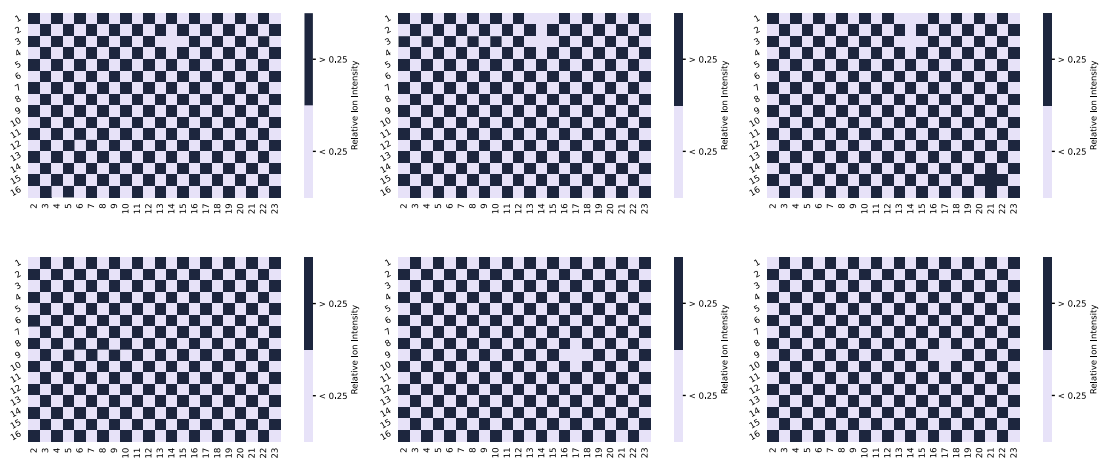
Figure S3: LAP-MALDI MS analysis of a 384-well plate with alternating Brdk and Lys-Brdk samples and different standards at the start and end of each sample row at 10 samples/s for each row (average of 9 sample/s for the entire plate). Analyte ion signal intensities for Brdk (top) and Lys-Brdk (bottom) for three runs using a 25 % threshold.
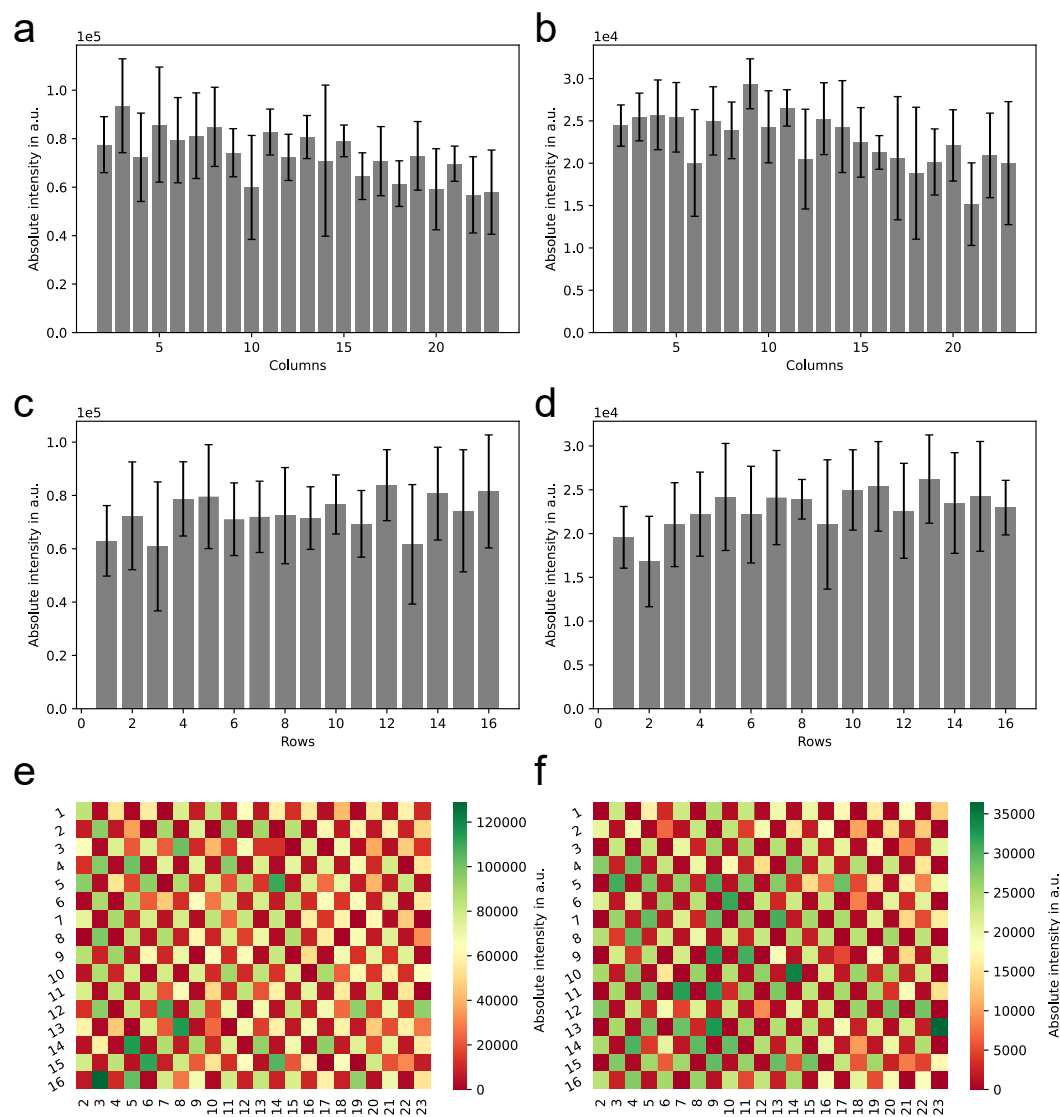
Figure S4: Graphical analysis of analytical performance and variability. LAP-MALDI MS analysis of a 384-well plate with alternating Brdk and Lys-Brdk samples and different standards at the start and end of each sample row at 20 samples/s for each row (average of 17 sample/s for the entire plate). Mean and standard deviation over each column (a,b) and each row (c,d) for Brdk and Lys-Brdk. Heatmaps for absolute ion intensity for Brdk (e) and Lys-Brdk (f).
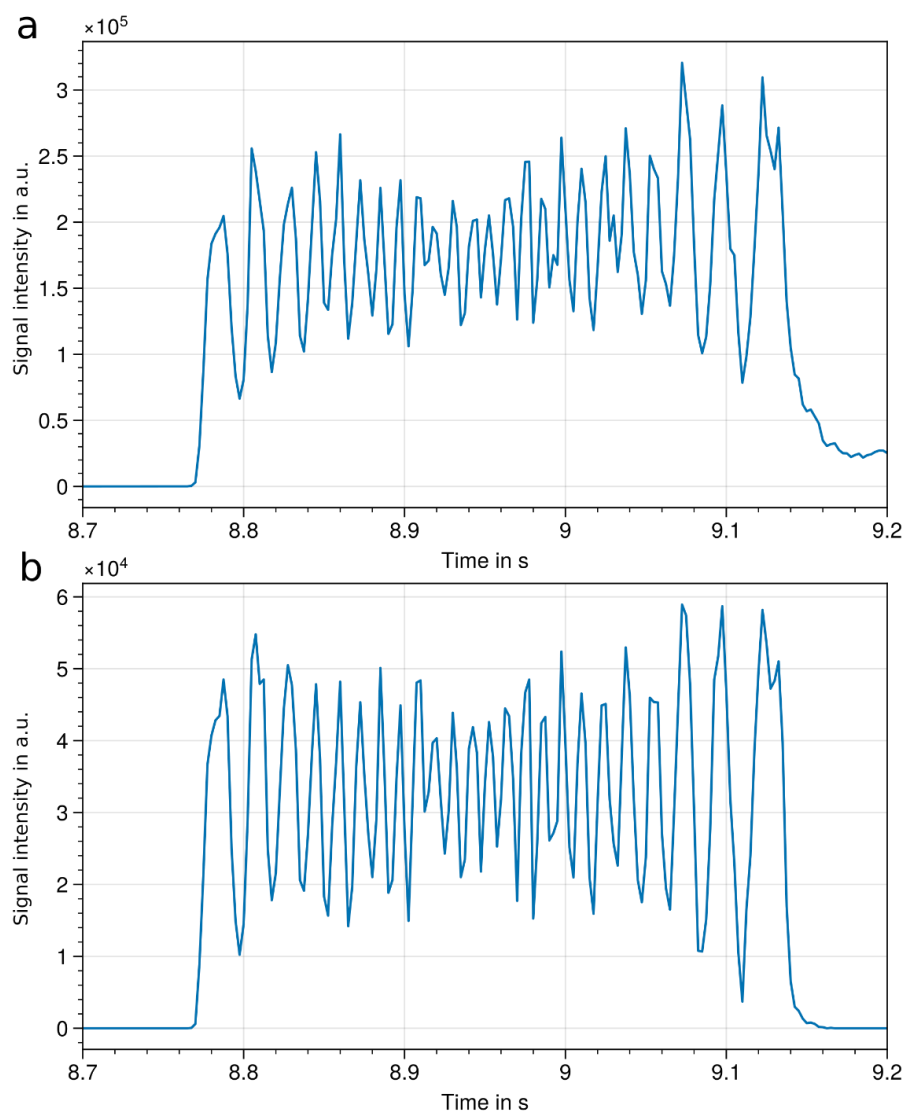
Figure S5: LAP-MALDI MS analysis of HHL using a 1536-well plate layout. a) total ion chromatogram, and b) extracted ion chromatogram at 60 samples/s.
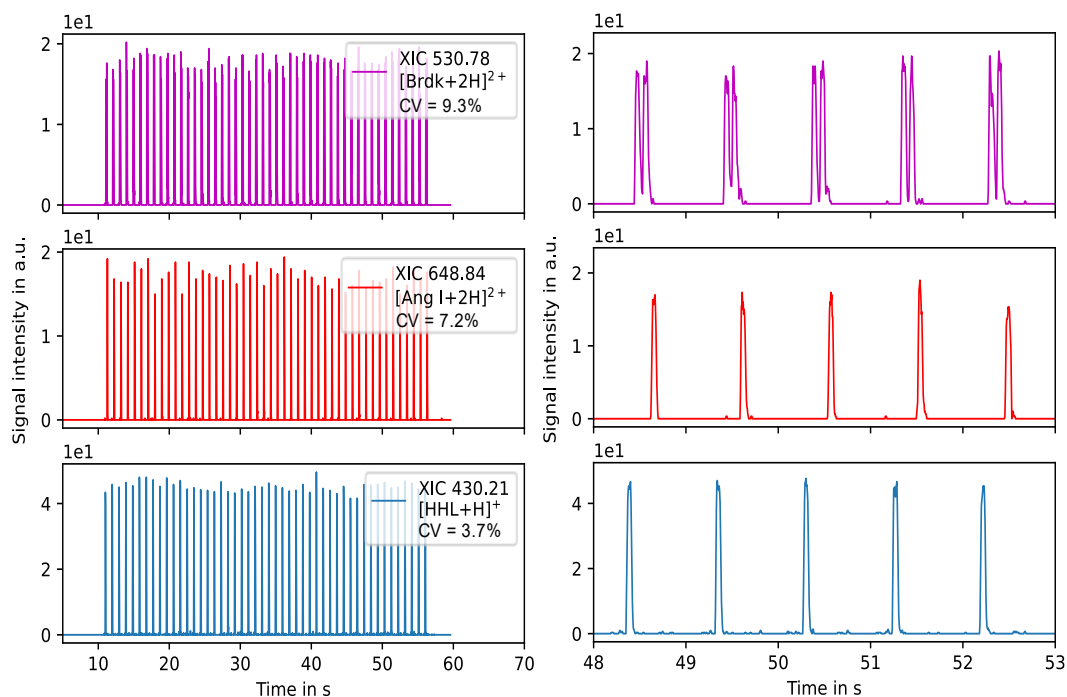
Figure S6: Variability of peptide analysis in TDC mode. 48 consecutive LAP-MALDI analyses of 2x2 sample spots of Brdk and different standards at start and end at 50 mm/s stage speed. Enlargement on right side.
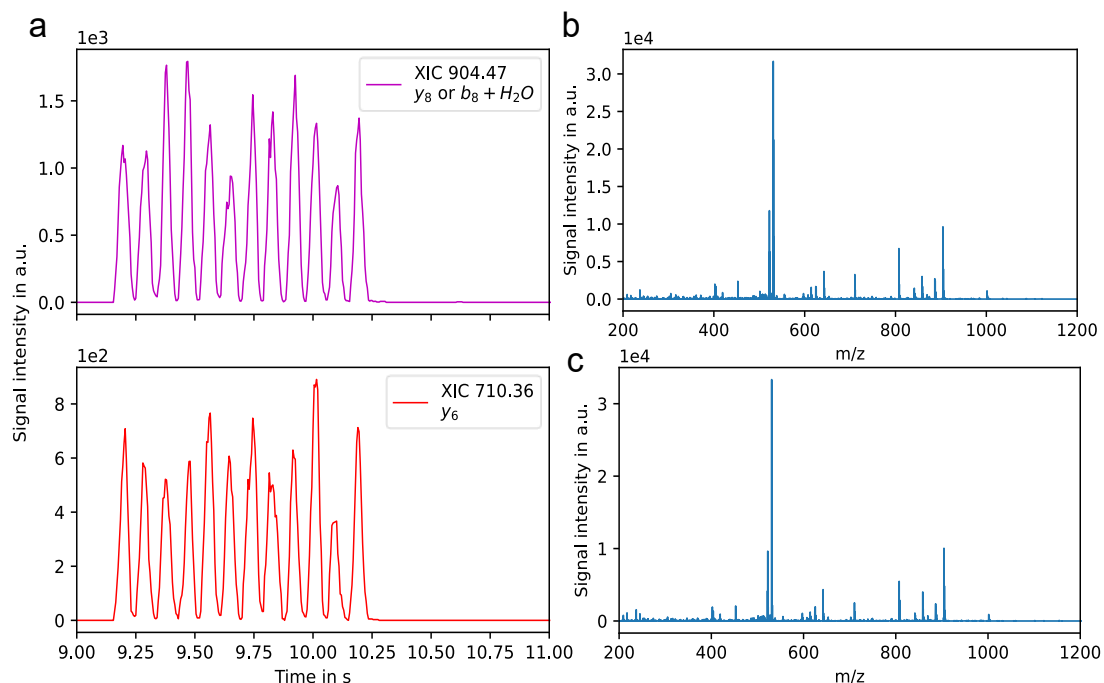
Figure S7: Tandem mass spectrometry at 50 mm/s. 12 samples of Brdk with quadrupole filtering around m/z 530.78 and trap collisional voltage at 25 V. a) Extracted ion chromatogram of two fragment ions; b) Mass spectrum of first sample; c) Mass spectrum of last sample.

2.4. LAP-MALDI MS tolerance against additives (Article 3)

LAP-MALDI has been shown to be suitable for HTS. During the analysis of the enzymatic assay used in section 2.3, significant ion suppression due to the addition of tris buffer was observed. The promotion or suppression of ionisation as well as the formation of different types of ions is of importance when establishing new assays or transferring existing assays to LAP-MALDI. To facilitate this development, a systematic study of the influence of compounds commonly used in biochemical assays on ion signal intensity and adduct formation was carried out.
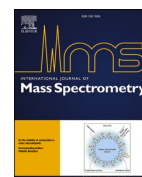
The use of salts, buffers and surfactants in LAP-MALDI MS

Henriette Krenkel [a], Jeffery Brown [b], Michael Morris [b], Rainer Cramer [a],[*]

[a] *Department of Chemistry, University of Reading, Whiteknights, Reading, RG6 6DX, UK*
[b] *Waters Corporation, Stamford Avenue, Wilmslow, SK9 4AX, UK*

A B S T R A C T

Biological samples such as tissue extracts and enzymatic assays typically have a complex composition, which can interfere with analyte ionisation and detection in mass spectrometry (MS). Ionisation techniques such as electrospray ionisation (ESI) are often coupled online to an upfront chromatographic separation, whereas sample preparations for techniques such as conventional matrix-assisted laser desorption/ionisation (MALDI) are performed offline and, in the case of MALDI, rely on sample clean-up owing to different crystallisation behaviour. Liquid atmospheric pressure matrix-assisted laser desorption/ionisation (LAP-MALDI) MS is a hybrid ionisation technique that has been previously used to analyse a wide range of biological samples at fast acquisition rates. Here we report data from a systematic investigation of the influence of various buffer compounds, salts, surfactants, and other compounds necessary for biological sample preparation reflected in the signal intensity of a standard peptide mixture. Tricine showed the least signal reduction from the buffer compounds tested as did octyl-β-D-glucopyranoside for the surfactants. It can be concluded that LAP-MALDI MS can be used to analyse biological samples directly without major sample clean-up if their content of additives is not too high.

1. Introduction

Many compounds that are naturally present in biological samples or are often added to such samples to provide favourable conditions for biological processes can have a significant impact on analyte detection in mass spectrometric analyses [1]. For example, salts are ubiquitous in biological matrices and can be essential for protein folding [2], enzyme activity [3,4] and cell viability [5–7]. However, their adverse effects on mass spectrometric analysis are well known [8]. Non-volatile salts typically contaminate the mass spectrometer's inlet, and hence can cause significant down-time in larger studies. They also provide different ionisation pathways in addition to protonation, reducing the analyte signal-to-noise ratio [1]. Beyond salts, substantial loss in analyte ion signal due to the presence of other compounds can be the result of a competition for charge either in the post-desorption gas phase or, for ionisation techniques like electrospray ionisation (ESI), already in the pre-desorption liquid phase. This competition for charge can lead to analyte suppression and is influenced by the compounds' spatial distribution in the pre-desorption solid or liquid phase of the sample [8] as well as the setup-specific desorption/ablation characteristics [1], and adds to the intrinsic differences in ionisation efficiency between analytes.

Sample clean-up prior to analysis is therefore often needed but, due to time and cost implications, its avoidance and mitigation strategies involving instrumental and chemical modifications are preferred. In ESI,

substances are commonly added to the spraying solution [9] or in the gas phase [10,11], and spraying configurations are modified to yield smaller initial droplets [12]. Matrix-assisted laser desorption/ionisation (MALDI) also frequently employs additives [13–17], specially tailored matrix compounds [18,19] and specific sample preparation techniques [20,21] to minimise ion suppression and adduct formation.

Liquid atmospheric pressure matrix-assisted laser desorption/ionisation (LAP-MALDI) mass spectrometry (MS) is suitable for a variety of analytes [22–24] and complex biological matrices [25,26] even at high analysis speeds [27]. For conventional solid-state MALDI the suitability of screening assay buffers was investigated [28]. However, a systematic study of the suitability of different compounds typically encountered in biological mass spectrometry for LAP-MALDI MS is missing to date. In this work, we show the influence of different additives on the signal intensity of a peptide mixture which can act as a guideline for future studies and experimental design.

2. Materials and methods

2.1. Materials

α-Cyano-4-hydroxycinnamic acid (CHCA), propylene glycol (PG), bradykinin acetate salt (Brdk), angiotensin I human acetate salt hydrate (Ang), leucine enkephalin acetate salt hydrate (LeuEnk), melittin from honey bee venom and synthetic melittin (Mel), substance P acetate salt

---

hydrate (SubP), bovine serum albumin (BSA), 3-((3-cholamidopropyl) dimethylammonio)-1-propanesulfonate (CHAPS), triton™ X-100, triton X-114, tween® 20, tris(hydroxymethyl)aminomethane (tris), amidosulfobetaine-14 (ASB-14), sodium deoxycholate (SDC), octyl-β-D-glucopyranoside (OGP), sodium dodecyl sulphate (SDS), sodium chloride, potassium chloride, ammonium chloride, magnesium chloride hexahydrate, magnesium acetate, 3-(N-morpholino)propanesulfonic acid (MOPS), 2-(N-morpholino)ethanesulfonic acid (MES), 4-(2-hydroxyethyl)-1-piperazineethanesulfonic acid (HEPES), L-serine, ammonium tartrate dibasic, ammonium hydroxide solution, ethylenediaminetetraacetic acid (EDTA), urea, and LC-MS-grade formic acid (FA) were purchased from Sigma-Aldrich (Gillingham, UK). HPLC-grade water, calcium chloride and phosphate buffered saline (PBS) 10X, ammonium sulphate, LC-MS-grade trifluoroacetic acid (TFA), HPLC-grade acetonitrile (Chromasolv™; Honeywell Riedel-de-Haën™) and dimethyl sulfoxide (DMSO) were purchased from Fisher Scientific (Loughborough, UK). NP-40 alternative was obtained from Calbio-Chem® (Nottingham, UK) and ammonium acetate was bought from BDH (Poole, UK). Sodium acetate, ammonium dihydrogenphosphate, ammonium oxalate monohydrate and ammonium citrate dibasic were purchased from Fluka (Dorset, UK). Tricine was bought from Acros Organics (Geel, Belgium).

2.2. Methods

2.2.1. Sample preparation

The MALDI matrix was prepared by dissolving CHCA in acetonitrile and water (1:1; v/v) to a concentration of 5 mg/mL. After sonication, 60% PG (v/v) was added. The analyte mixture was prepared by mixing aqueous peptide stock solutions to give concentrations of 16 pmol/μL for Ang, 10 pmol/μL for Brdk, 20 pmol/μL for LeuEnk, 20 pmol/μL for SubP and 12.5 pmol/μL for Mel (see SI Table 1 for further information). The MALDI matrix and analyte mixture were mixed in a ratio of 3:1 (v/v). The additives (or water) were added to this matrix/analyte solution in a ratio of 1:1 (v/v) and thoroughly mixed. Samples were prepared in replicates and from each replicate one LAP-MALDI sample with a volume of 0.3 μL was spotted on a Waters™ 384-well MALDI sample plate unless otherwise stated. Surfactant-containing samples were mixed and spotted using reverse pipetting to limit foaming.

EDTA was prepared using ammonium hydroxide solution for dissolution. For evaluating the capability of certain compounds to reduce salt adduct formation, additives were mixed with water or aqueous 10 mM NaCl solutions before being mixed with the matrix/analyte solution.

2.2.2. LAP-MALDI MS

LAP-MALDI MS analysis was performed on a modified SYNAPT™ G2-Si (Waters Corp., Wilmslow, UK) Q-ToF instrument as described before [29] using a 343-nm diode-pumped solid-state Yb:YAG laser. For automated sample acquisition, custom WREnS (Waters Research Enabled Software) scripts controlled the sample plate movement and labelled mass spectral scans with the sample position for post-processing using a modified MassLynx™ (Waters) version. Each LAP-MALDI sample was irradiated by the laser with a pulse repetition rate of 500 Hz for 5 s with acquisition scan times of 0.25 s and interscan delays of 10 ms.

2.2.3. Data processing

Separate data files were created for each sample's ion signal according to the labelled sample position on the sample plate using a custom slicing script, similar to previously reported scripts [30]. Batch processing of these files, including the summation of scans, smoothing, and extracting signal intensities, was performed with specproc (https://sourceforge.net/projects/specproc/). For analyte ion intensity values, peaks were selected using an m/z tolerance window of $\pm$ 25 ppm and the requirement to be present in at least 2 out of 3 replicates using a Python script. Peaks were assigned according to their m/z value. Please note that for substance P non-oxidised potassiated and oxidised sodiated ion

species might in some cases be undistinguishable as their mass difference is approximately 0.021 Da. Similarly, for ion signals with imperfect peak shape, e.g. due to low signal-to-noise, the m/z assignment might in some cases fall outside the Python script's m/z tolerance window of $\pm$ 25 ppm. On the other hand, background noise might contribute to the ion signal if it falls within the above window.

Chemical structures were drawn with ChemDraw® 17.1 (Perkin Elmer, Waltham, US).

3. Results and discussion

3.1. Buffers

Buffers are widely used in sample preparations for biological samples [31] to mimic physiological conditions and allow enzyme activity. A list of useful buffer compounds was compiled by Good et al. [32] and was amended over time [33,34]. Here, buffers with a morpholinic ring (MES, MOPS), piperazinic ring (HEPES) and tris-derived buffers (tris, tricine) were tested against a still widely used phosphate-based buffer (PBS). Structures and pK_a values can be found in SI Table 2.

When mixing 100 mM tris with the matrix/analyte mixture, a colour change from clear to bright yellow was observed, which is an indicator of a chemical reaction occurring. The same colour change can be observed when only the matrix is mixed with tris (see SI Fig. 1). Accounts for the reactivity of the tris amine can be found in the literature [31,35,36] and present a strong argument against the use of tris as a buffer.

For HEPES, MES and MOPS, clusters of $[nM+H]^+$ (where M is the buffer compound) are observed in the LAP-MALDI mass spectra. Furthermore, MES yields similar clusters by sodiation $[nM+Na]^+$. In contrast, tris and tricine only show intense protonated monomer molecules $[M+H]^+$. Some buffer compound adducts were observed with peptides. Singly charged SubP showed adducts with CHCA, MES, MOPS, HEPES and tris (as well as CHCA-tris, see SI Fig. 2). Doubly protonated Brdk was detected with HEPES as an adduct.

General trends for the influence of the buffers on peptide ion signal intensity were similar for all peptides analysed (see Fig. 1). Although structurally similar, tris and tricine performed differently, especially at higher concentrations. At ≥ 5 mM, tris severely suppressed analyte ion signal, whereas tricine led to increased protonated and overall signal intensities at 5 mM for most of the peptides compared to all other solutions at 5 mM as well as the water control. PBS showed substantial ion suppression for concentrations of $\geq 5\%$, for LeuEnk even at 0.5%. MES, MOPS and HEPES generally reduced the peptides' ion signals at 5 mM or more although the degree of suppression varied between analytes. Compared to water (with the caveat of a few larger error bars for some ion signals), all peptides showed overall higher ion signal intensities at 0.05 mM HEPES, and at 0.005 mM, 0.05 mM, and 0.5 mM concentrations for MES and MOPS, apart from 0.5 mM MOPS for SubP and Mel.

For proteins, spectral degradation above 50 mM tris or 20 mM phosphate buffer was reported for solid MALDI MS in an earlier study [37]. In general, phosphate buffers are not recommended for solid MALDI MS analysis owing to interfering background signals [38] and impeded crystallisation for many MALDI matrices [39]. PBS severely suppressed the ion signal intensity of small molecules using the ESI-based ECHO® MS system despite large dilutions [40]. As phosphate is not considered inert in biological systems, its use as a buffer is inherently limited. However, as the data for LAP-MALDI MS shows, the use of PBS of up to 0.5% or higher results in no significant analyte ion signal loss and therefore presents a comparative advantage to solid MALDI and ESI MS.

Another study analysing proteins with solid MALDI found that up to 50 mM tris had no impact on signal intensity but yielded broader peaks due to a less homogeneous crystallisation [39] whereas HEPES and MOPS gave greater signal intensities than in pure water [39]. These detrimental effects on resolution are not expected on a Q-ToF instrument

H. Krenkel et al.

Fig. 1. Influence of buffer compounds on peptide ion signal for a) leucine enkephalin, b) bradykinin, c) angiotensin I, d) substance P and e) melittin. The error bars denote the standard deviation between replicates (n=3 for additives, n=15 for water) or the data point range for n=2 where the signal is below the signal-to-noise threshold of 3 (see SI Table 3). Ion signals with minor contributions to the total ion signal (<5% of total ion signal in all samples), e.g. from rare adduct ion formation, were omitted for clarity.

compared to an axial-ToF instrument that was used for the above study. For peptide analysis, 100 mM tris was successfully used in solid MALDI MS analysis in combination with various detergents [41]. This potentially higher resilience of solid MALDI against buffer compounds compared to LAP-MALDI can be partly attributed to the crystallisation process which can purify the sample. In contrast, the presence of buffers can potentially impede crystallisation, which also depends on the matrix employed [39].

ESI and nanoESI have been reported to yield protein spectra with acceptable signal-to-noise in 100 mM tris buffer [42], although with a signal loss of more than an order of magnitude. For the acoustic droplet ejection (ADE) [43] as implemented on the ECHO® MS system, a residual concentration of 10 μM tris was acceptable [44].

Apart from suppressing analyte ion signal intensity, buffers can also have an impact on operational conditions, particularly in high-throughput screening (HTS) workflows. For example, the ECHO® MS system requires adjustment of the ADE conditions depending on the buffer composition [44]. The data presented here for LAP-MALDI MS, which has been previously shown to be capable to acquire data at a speed of up to 50–60 samples per second [29], were acquired using the same conditions for all additives and no adjustments were required.

3.2. Metal salts

The presence of various salts in biological matrices was mimicked by adding several concentrations of sodium, potassium, magnesium and calcium salts to study the effect on signal intensity. As expected, the mode of ionisation shifted from mainly protonated molecules for low salt concentrations to sodiated and potassiated molecules for higher sodium/potassium salt concentrations (see Fig. 2). This shift resulted in lower signal intensity for the protonated species, and at higher salt concentrations even the sum over all observed analyte ions is significantly decreased. It should be noted that the presence of potassium appears to be more detrimental than the presence of sodium. In contrast, magnesium chloride and calcium chloride did suppress overall analyte ion signal intensity (above a concentration of 0.05–0.5 mM) without forming magnesium or calcium adducts. Ammonium chloride gave the best results of all salts analysed independent of the type of peptide. Here, it should be noted that 0.5 and 0.05 mM ammonium chloride generally provided higher protonated and overall analyte signals than the water control. Apart from these, some other lower (<5 mM) salt concentrations showed slightly higher overall peptide ion signal intensities than the water control.

To exclude an effect of the chloride anion, acetate salts of sodium, magnesium and ammonium were analysed. For salts containing the same cation, e.g. acetate and chloride salts of magnesium, the same trend was observed. Thus, the influence of the anion on analyte signal intensity was minor compared to the influence of the cation. For analyses in negative ion mode this might be different. However, magnesium acetate always gave slightly more intense overall peptide ion signal intensities compared to the chloride whereas ammonium chloride gave higher intensities compared to the acetate. It is recommended not to use sodium acetate with solid-state MALDI as its hygroscopic nature results in wet sample surfaces [38], which is naturally not an issue for LAP-MALDI.

The recorded analyte ion signal intensities did not vary linearly with the salt concentration in all cases. For instance, the ion signal intensity of leucine enkephalin decreases with increasing ammonium chloride concentration (lowest at 50 mM) while the highest overall ion signal of angiotensin I for this chloride was obtained at a concentration of 50 mM.

In LAP-MALDI MS mostly multiply charged peptide ions are observed, which were reported to form less adducts than singly protonated molecules [24]. This behaviour was also reported for nESI where slightly less sodium adduction was observed for higher charge states [9]. For the peptide mixture used in this study (see SI Fig. 3), the protonated-to-sodiated molecular signal ratio was greater for higher

charge states of angiotensin I and bradykinin than for their singly charged ion species while this effect is absent for large parts of the data for SubP.

Typical salt concentrations in biological samples are summarised in SI Table 5. In biofluids, sodium is typically present in concentrations around 5–150 mM. Potassium is present between 5 and 50 mM while magnesium and calcium are less abundant with calcium below 5 mM and magnesium below 1 mM. For the MS analysis of biological samples by LAP-MALDI (as well as by other ionisation techniques), the natural occurrence of sodium can therefore be a limiting factor for mass spectral quality compared with the other salts investigated. Hence, strategies to reduce the sodium concentration of biological samples are recommended for LAP-MALDI MS analysis.

3.3. Salt remediation

Additives are often used in MALDI and ESI to alleviate the effects of salts without resorting to extensive sample clean-up. The addition of ammonium salts can decrease metal cation adducts for peptide analysis in conventional MALDI MS [45] and liquid MALDI MS [46], and ammonium acetate is commonly used in ESI [47–49]. The previously used peptide mixture was mixed with a 10-mM NaCl solution, and various ammonium salt and L-serine solutions were added to study the effect on the protonated, sodiated and overall peptide signal intensity (see SI Fig. 5). For some additives, like ammonium acetate (see Fig. 3), the same trend was observed for all peptides. In contrast, for ammonium tartrate, Ang and Brdk display a similar pattern while the other three analytes follow a different trend. Neither analyte basicity nor molecular size seem to be a predictor for these patterns.

Even for aqueous peptide mixture solutions without any NaCl, several additives enhanced the protonated molecule signal intensities (see Fig. 4). L-serine significantly increased the protonated and total ion signal intensity for Ang and Brdk when used at high concentrations. Most ammonium salts worked best at low concentrations but suppressed ion signals at higher concentrations.

The use of the 10-mM NaCl solution clearly suppressed not only protonated but also overall ion signal intensity for all analytes (see Fig. 4 and SI Fig. 5). For LeuEnk, SubP and Mel none of the additives were able to restore the ion signal to levels obtained in pure water. For Brdk and Ang, the peptide ion signal intensity recovered upon the addition of some additives and even exceeded the pure-water intensities at some additive concentrations.

Ammonium dihydrogen phosphate added to pure aqueous solutions reduced peptide ion signals with increasing concentrations but provided for most additive concentrations an increased Brdk and Ang ion signal intensity compared to pure water solutions. Added to the NaCl solution, the Brdk and Ang ion signals increased with the additive concentration and were greater than in pure water at the three higher concentrations. For conventional solid MALDI MS analysis of tryptic digests, the addition of around 10 mM ammonium dihydrogen phosphate increased peptide ion signals and reduced matrix clusters [15]. Higher and lower concentrations were found to be less effective [15]. Other studies reported increased peptide signals between 5 and 20 mM [50] and 0.5 and 50 mM [16]. Similar effects were observed for tryptic digest analysis by liquid vacuum MALDI, using concentrations between 10 and 100 mM [46]. Thus, LAP-MALDI MS data presented here follow a similar trend of signal enhancement. Although phosphate is not compatible with liquid chromatography [51], it can be a valuable additive for MALDI MS analysis.

There were no substantial ion signal-enhancing effects for ammonium acetate, which was even detrimental at higher concentrations. In nanoESI under native conditions, 7 M ammonium acetate was required to obtain a visible reduction of sodium adducts in protein analysis and no effect was typically obtained at 100 mM [9]. The NaCl concentration investigated here might have been not high enough to observe a similar effect. However, in standard-flow ESI a reduction in protein ion signal is
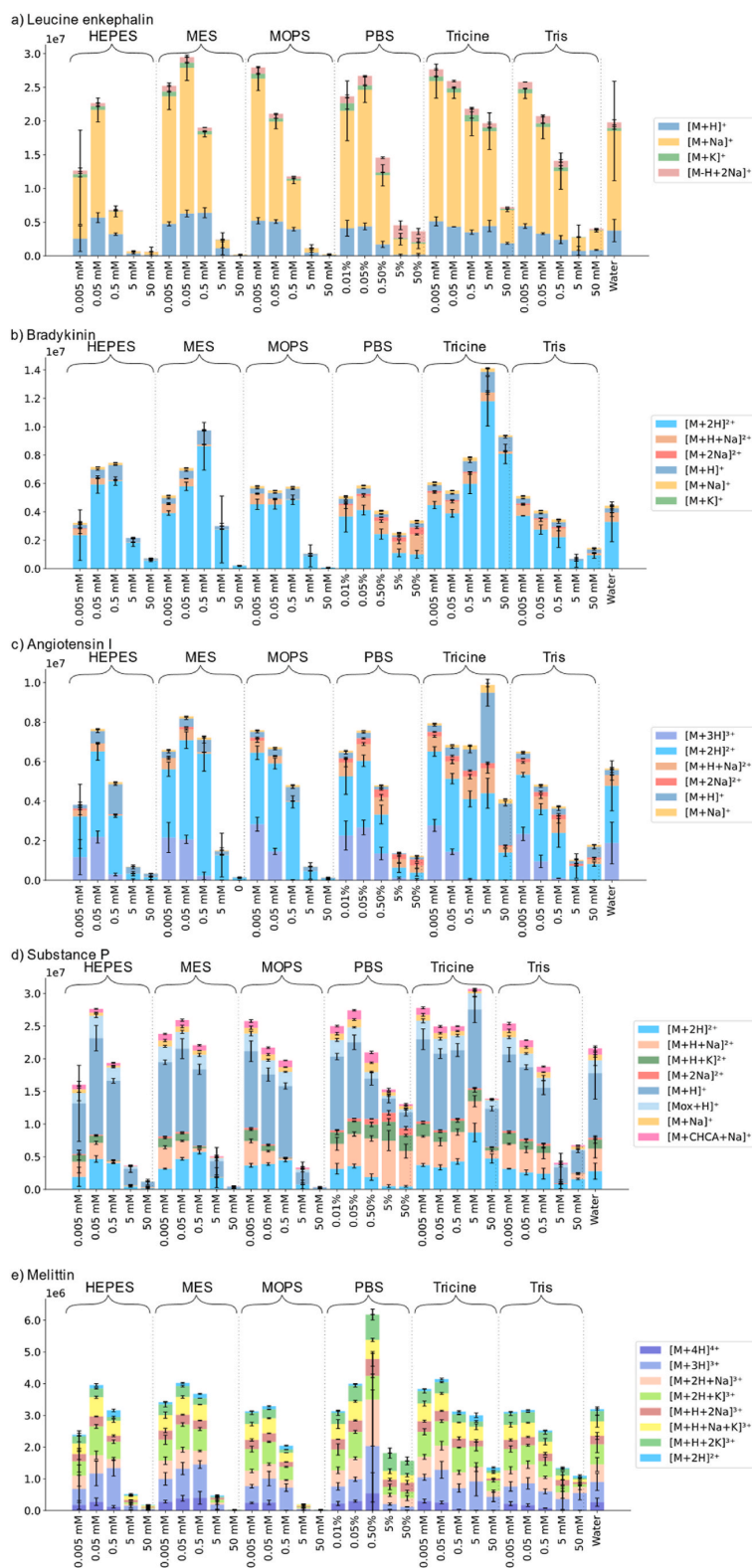
H. Krenkel et al.

Fig. 2. Influence of salts on peptide ion signal for a) leucine enkephalin, b) bradykinin, c) angiotensin I, d) substance P and e) melittin. The error bars denote the standard deviation between replicates (n=3 for additives, n=15 for water) or the data point range for n=2 where the signal is below the signal-to-noise threshold of 3 (see SI Table 4). Ion signals with minor contributions to the total ion signal (<5% of total ion signal in all samples), e.g. from rare adduct ion formation, were omitted for clarity.
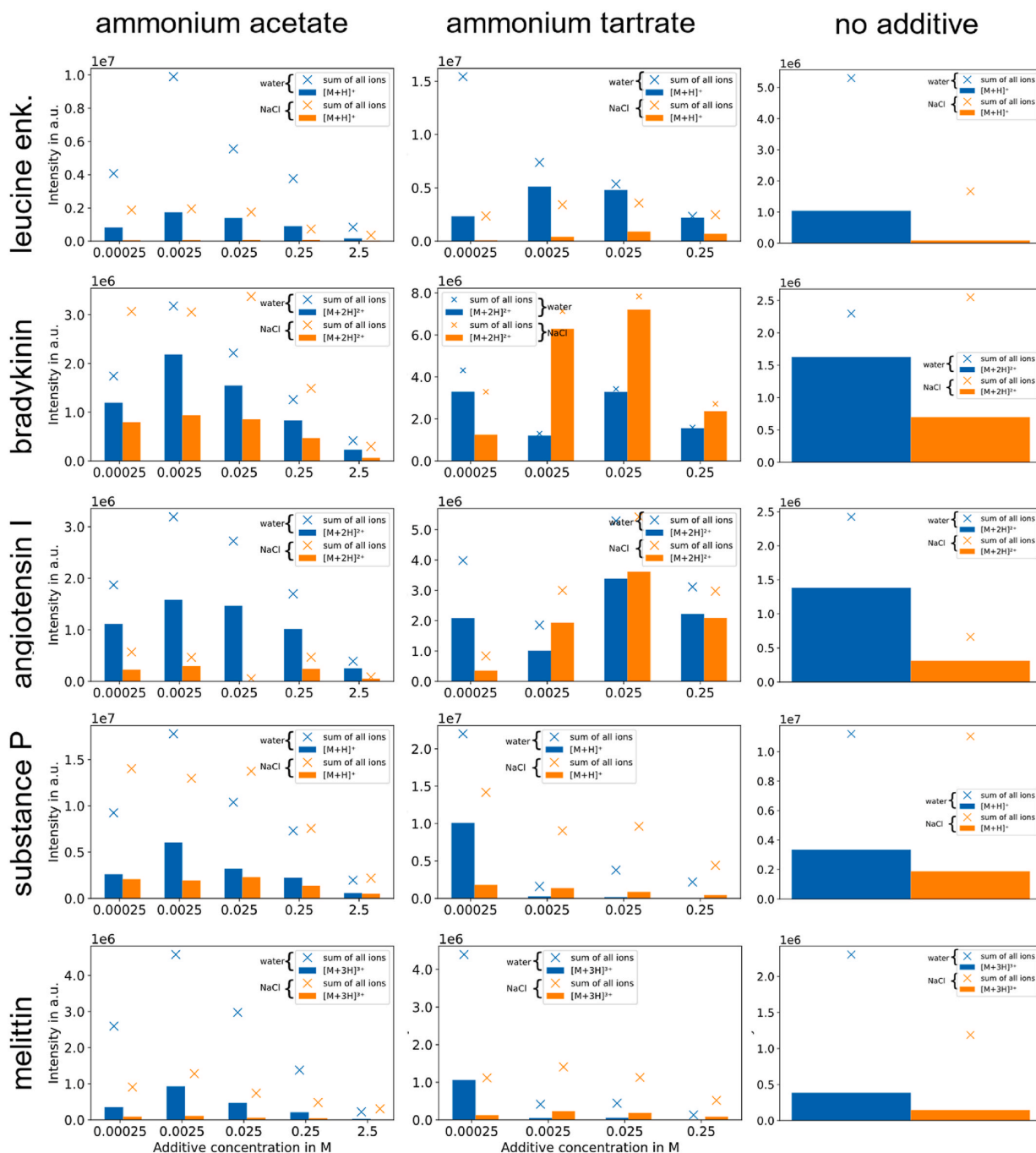
Fig. 3. Influence of ammonium acetate and ammonium tartrate on ion signal intensity in pure water and a 10-mM NaCl solution.

observed with increasing ammonium acetate concentration [52] which is in line with the data presented here. Hence, an influence of the initial droplet size created during the ablation might play a role in adduct formation. In solid MALDI, up to 10 mM did not have significant effects on the analyte ion signal in the analysis of small molecules [28].

The addition of ammonium citrate significantly increased protonated signal intensity for Ang and Brdk in the presence of NaCl. Ammonium citrate is known to reduce sodium adducts [53] and enhance signal intensity [51] in solid MALDI MS analysis. Citrate was found to be more

effective than other ammonium salts [45] although a reduction in signal was reported above 5 mM [16].

Similar to citrate, oxalate and tartrate salts were investigated as sterically hindered ions are thought to result in less adducts than smaller ammonium salts [17] and provide several ammonium ions per molecule (see SI Fig. 4). Ammonium tartrate follows similar trends as citrate whereas oxalate is slightly inferior with regard to analyte ion signal intensities.

Finally, the addition of L-serine was analysed and a significant

H. Krenkel et al.
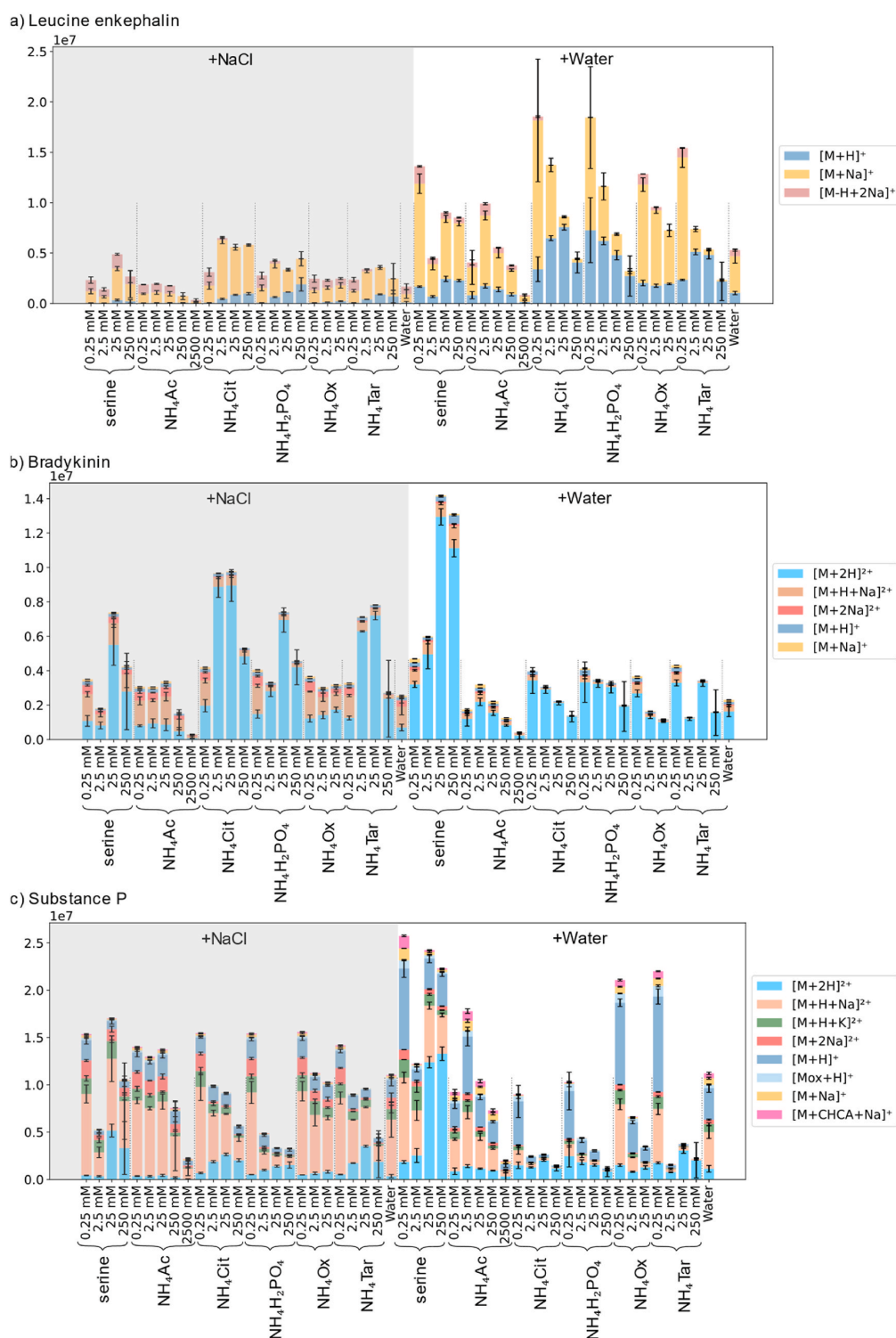
Fig. 4. Influence of the addition of ammonium salts and L-serine on ion signal intensity of peptides in a 10-mM NaCl solution and pure water, respectively, for a) leucine enkephalin, b) bradykinin and c) substance P. The error bars denote the standard deviation between replicates (n=3 for additives, n=15 for water with NaCl, n=9 for water) or the data point range for n=2 where the signal is below the signal-to-noise threshold of 3 (see SI Table 6). Ion signals with minor contributions to the total ion signal (<5% of total ion signal in all samples), e.g. from rare adduct ion formation, were omitted for clarity.

increase in protonated Brdk and Ang signals was observed at around 100 mM. This is consistent with conventional solid MALDI, for which the addition of serine improved the signal-to-noise ratio for protonated Ang species by a factor of 4 [14]. A similar effect was reported for DESI MS with L-serine-enhanced protein signal [54] and reduced sodium adducts even if used at less than stoichiometric amounts [55]. However, at higher concentrations (mM) a decrease in signal was observed [55], which is not in agreement with the data presented here. In ESI MS, the addition of ten times more serine than NaCl led to a reduction of Na adducts and an improvement in the signal-to-noise ratio for native proteins [56]. As no effect was observed above 2 mM sodium, it was hypothesised that the direct binding of Na to the amino acid prevents remediation by serine [56]. In the LAP-MALDI MS data presented here, an increase in peptide ion signal was observed for Brdk and Ang when serine was added in excess compared to sodium. No clear effect was visible for the other peptides analysed.

3.4. Surfactants

Surfactants are amphiphilic substances often used in biological sample preparations to help protein solubilisation, prevent adsorption [38] and aggregation [57] and generally assist with the analysis of hydrophobic peptides [58] and proteins [59]. Surfactants have a wide range of properties [60], e.g. being denaturing or not, and hence, need to be tailored to a specific application. Different types can be distinguished according to their molecular structure: anionic, cationic, zwitterionic or non-ionic. For this study, non-ionic (OGP), zwitterionic (CHAPS) and anionic (SDC) surfactants were analysed (see SI Table 7). Commonly used polymeric surfactants, e.g. Tween-20, triton (X-100 and 114) and NP40 alternative, were not further investigated as they caused a wide polymeric distribution over a large range of the mass spectrum which interfered with analyte detection.

With increasing surfactant concentration, the surface tension of the sample decreases and the droplet becomes unstable (see SI Fig. 6). Samples can spread out (and completely wet the sample plate surface), and the resulting film does not yield any analyte signal. With lower surfactant concentrations stable droplets can be obtained. The surface tensions for the investigated surfactants are summarised in SI Table 7. At the critical micelle concentration, these surface tensions are similar, although it must be noted that surface tension also depends on various other parameters such as electrolyte concentration [61], which can affect droplet stability in 'real-life' samples. Although droplet stability is somewhat correlated with surface tension and therefore inversely with surfactant concentration (see SI Table 8), SDS yields stable droplets even at the highest concentration investigated. Hence, other factors might play a role such as the affinity of the surfactant molecules to the stainless-steel sample plate. To circumvent unstable droplets, other sample plate surfaces were investigated, and a Bruker AnchorChip™ plate was used for analysis. Its hydrophobic surface area, surrounding the small hydrophilic sample spot areas, effectively prevented sample spreading and all samples (up to 10% w/v) yielded stable liquid MALDI sample droplets (see SI Fig. 6). Results obtained from stable samples on both plates are in good agreement apart from SDC, for which a discrepancy was observed at 0.1% (see Fig. 5 and SI Fig. 7).

For the surfactants, the variability between replicates was higher than for other experiments (see Fig. 5) as surfactant samples are more difficult to handle and the plate holder was not optimised for accommodating large plates with a microtiter plate format. In general, the lowest surfactant concentrations gave similar results to the water control. Samples containing 5% SDS solidified upon laser radiation, probably caused by solvent evaporation leading to a concentration of SDS beyond its solubility. For all surfactants, intense additional peaks (see SI Fig. 8) were observed which are not present in the water control and are dependent on the surfactant concentration. Putative assignments of surfactant clusters (mainly $[n \cdot M + H]^+$ and $[n \cdot M + Na]^+$, where M is the surfactant molecule) can be found in SI Table 9. For SDS, similar peaks

have been reported for ESI, although at higher SDS concentrations [62, 63].

Regarding analyte ion signal intensities, the same trend can be observed for all analytes for the addition of ASB, CHAPS and SDS. In most cases, ion suppression was observed around the 0.01% level (see Fig. 5). At this and higher concentrations ASB gave the worst results of all surfactants investigated while CHAPS led to slightly more intense analyte ion peaks compared to SDS. For the other surfactants, more diverse results were obtained. With increasing SDC concentration the signal intensity for LeuEnk, Ang and Mel decreased. For SubP, the opposite was observed apart from the highest concentration, at which no analyte ion signal could be obtained. As the peptides were analysed together as a mixture, no variation in sample preparation or analysis can account for these differences. The nature of the analytes and their relative differences in the ionisation process are the most probable origins of this behaviour. Comparing the isoelectric points (see SI Table 1), Brdk, SubP and Mel are significantly more basic than Ang and LeuEnk. However, this difference was not reflected in the SDC data. OGP was the only surfactant that provided analyte ion signals at 5%. Ang, Brdk and LeuEnk showed the strongest ion signal at 0.01% OGP; for Melittin 1% OGP was best.

Although detergents are widely used for biological sample preparations, most MS ionisation techniques require careful detergent removal. In ESI MS, surface-active compounds are generally detected at higher ion signal intensities due to their location at the droplet surface during droplet fission [64], which can suppress non-surface-active analytes. In conventional MALDI, the addition of surfactants can impede crystallisation [65].

For solid MALDI MS, contradictory results for the influence of surfactants on analyte signal are reported in the literature. In one study, no peptide or protein ion signals were obtained at 0.1% SDS or CHAPS but at 1% SDS or CHAPS protein ion signal was detected [66]. In other studies it was found that SDS concentrations of up to 0.1% [67] or 0.6% [42] were tolerable but interferences were seen at 1% [67]. CHAPS was found to be incompatible with solid MALDI MS analysis [67,68]. For solid MALDI MS analysis of acetylcholine, up to 0.6% CHAPS showed no significant effect on ion signal intensity [28]. Data obtained by LAP-MALDI MS show peptide ion signals at 0.1% SDS or CHAPS, but no signals at 1% of either for any of the peptides analysed. In an early study using solid MALDI, it was hypothesised that at low surfactant concentrations protein ion pairs were formed with the surfactant while at surfactant concentrations above the critical micelle concentration, the protein studied was well solubilised in micelles [66]. It was also suggested that higher surfactant concentrations lead to crystallisation of the surfactant around the matrix and therefore decrease the energy transfer to the sample [66]. In LAP-MALDI, crystallisation does not occur but increased surfactant concentrations can still change laser absorption due to a lower surface concentration of matrix molecules. For solid MALDI MS analysis of OGP-containing samples, it was reported that 0.1 and 1% OGP concentrations were suitable for peptide analysis [67] while the use of up to 5% OGP was reported for other studies [68]. This is in good agreement with the data reported here. Additionally, peak broadening and a mass shift were observed for some proteins when using OGP in solid MALDI MS [59]. This might indicate the formation of adducts. However, for LAP-MALDI MS analysis no OGP adducts were observed.

In a comparative MS study, ESI was found to be one order of magnitude less tolerant against surfactants than solid MALDI [68] with the exception of CHAPS, which ESI tolerated up to 1% [68]. Other studies showed that no protein ion signal was observed at 1% CHAPS [63] or only weak signal at 0.6% CHAPS [42]. In another study using proteins, SDS gave only 10% analyte ion signal compared to the water control at a concentration of 0.01% [63] but in a different study weak analyte ion signals were observed at 1.4% and good signal was obtained at 0.3% [42]. LAP-MALDI MS data presented here show comparatively good peptide ion signals at 0.001% SDS but weaker signals at 0.01–0.1% and therefore are in the same range as the literature values for ESI.
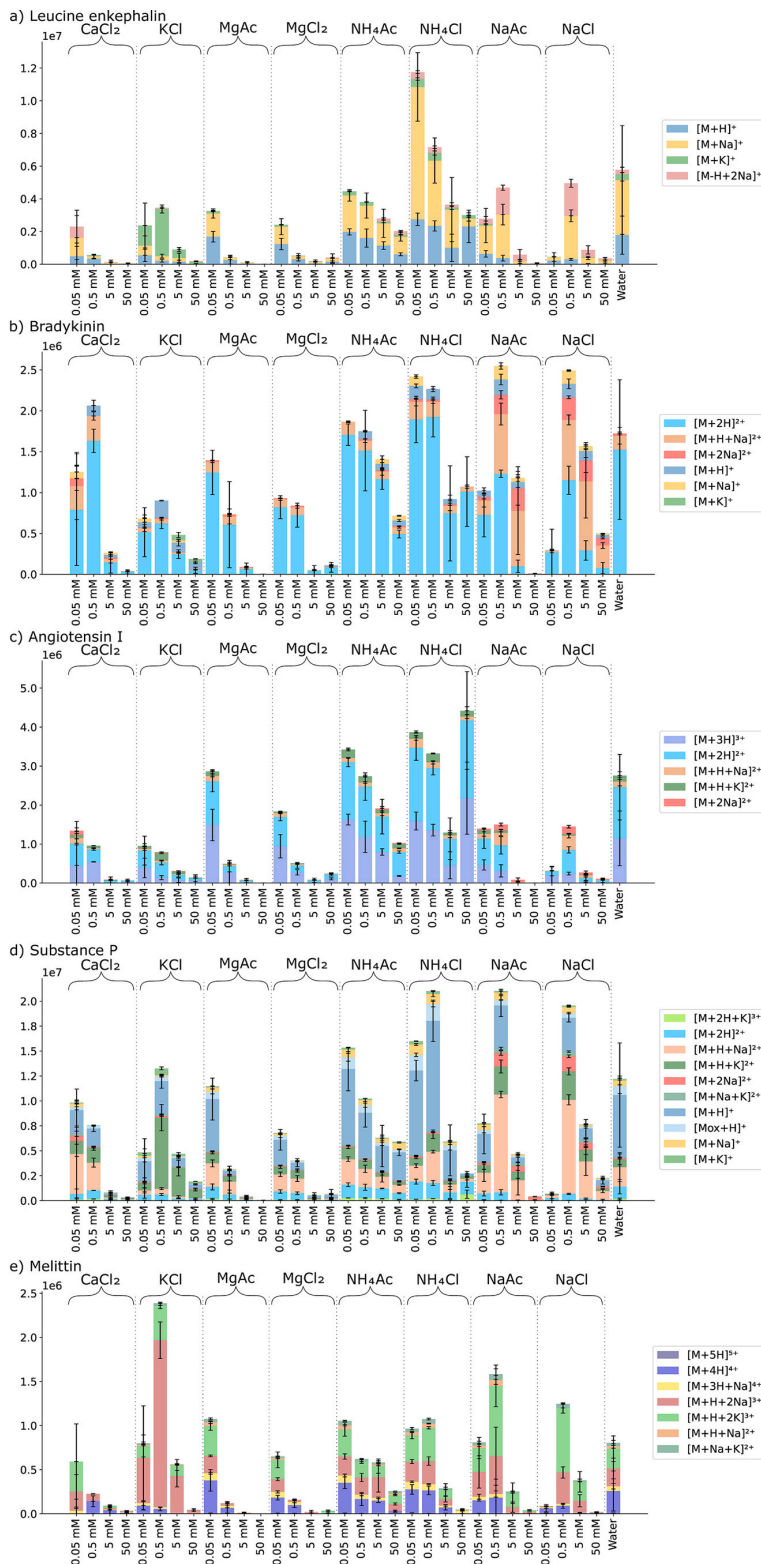
H. Krenkel et al.

Fig. 5. Influence of surfactants on peptide ion signal for a) leucine enkephalin, b) bradykinin, c) angiotensin I, d) substance P and e) melittin. The error bars denote the standard deviation between replicates (n=3 for additives, n=9 for water) or the data point range for n=2 where the signal is below the signal-to-noise threshold of 3 (see SI Table 10). Ion signals with minor contributions to the total ion signal (<5% of total ion signal in all samples), e.g. from rare adduct ion formation, were omitted for clarity.

Non-ionic saccharides gave best analyte ion signal in ESI compared with other surfactants as less background ions were generated, less Na adducts were observed and analyte ion signal suffered less suppression [63]. This is in very good agreement with the data presented here. In ESI, OGP still yielded analyte ion signal at 1% surfactant [63] while for LAP-MALDI MS peptide ion signal could still be observed at 5% OGP.

In HTS assays non-ionic surfactants are generally used at 0.01–0.1% to prevent aggregation [57]. As shown for OGP, LAP-MALDI MS does not suffer from severe ion suppression at these concentrations and it is assumed that this is also true for small molecules often used as screening targets. However, a shift from traditional assay detergents like triton and tween to surfactants more compatible with mass spectrometry is necessary.

3.5. Other compounds

BSA is used in cell-based assays to reduce nonspecific binding but is not advised for biochemical screens as it binds many compounds that are viable drug leads [69]. In small concentrations (2.5 pmol/μL, app. 0.02%) only a minor suppression of analyte ion signal is observed (see Fig. 6). This is comparable to other ionisation techniques like MALDI [28] and IR-MALDESI [70] for which no significant impact up to 0.01% was noticed. At higher concentrations, unresolved protein peaks dominate the mass spectra. However, resolved peaks can be probably obtained using different instrument settings [23].

DMSO is often used to store compound libraries, so HTS assays contain small amounts. At 1% DMSO, no ion signal suppression is observed for any analyte and for 5% only minor effects are noticeable. After dilution of the target compounds in assay buffer, no adverse effects on LAP-MALDI MS analysis are expected. In solid MALDI, DMSO is known to help with crystallisation [71,72], although heterogeneous crystallisation is observed at higher concentrations [73], and up to 1% is used to enhance tissue images of drugs [74].

The addition of 0.1 mM EDTA did not adversely affect LAP-MALDI MS analysis. At 1 mM suppression of analyte ion signal is observed, although the extent of signal reduction depends on the analyte and at 10 mM signal can still be obtained. Solid MALDI MS analyses suggest a reduction of analyte signal by approximately 50% at 50 mM [28], so is more tolerant against this additive. However, a small molecule was used as a test compound compared to peptides used in this study. In ESI MS, the addition of EDTA led to a significant improvement of phosphopeptide detection but caused issues with chromatographic separation and spray stability due to precipitation [51].

The use of acids in positive ionisation mode is thought to have a positive impact on analyte detection owing to the increased abundance of protons for ionisation and is therefore routinely used as an additive in ESI [75,76]. However, in LAP-MALDI MS the signal intensity for all analysed peptides decreased at 1% formic acid compared to water albeit at different factors and a significant decrease for all analytes is observed at 10%. As standard MALDI MS workflows for identification of microorganism recommend 35% formic acid [77], LAP-MALDI appears more susceptible to formic acid than conventional MALDI. When using TFA, droplets were not as stable and resulted in spread samples which increased signal variability (see Fig. 6). Nevertheless, analyte ion signal could be obtained for all dilutions (0.1–10% TFA on target). TFA is widely used as a mobile phase additive in liquid chromatography of peptides and proteins but is known to suppress protein ion signals in ESI by forming ion pairs with basic analytes [78]. Reported suppression factors range from 10 [76] to 250 [78] and can only be partially mediated [78]. Hence, LAP-MALDI MS is less affected by TFA.

If 1 M urea is added to the sample, significant ion signal suppression is observed and nearly no signal can be detected at 4 M. In solid MALDI no protein signal can be obtained at 8 M urea [19] and for nanoESI 4 M urea clogged the emitter [79]. However, 0.5 M was found to be compatible with nanoESI MS analysis and severe suppression occurred at around 2 M [79]. If urea is used in the sample preparation, sufficient

dilution is necessary to allow LAP-MALDI MS analysis.

For ammonium sulphate, ion signal intensity was influenced differently for the different analytes. For Ang, no suppression was observed at 10 and 100 mM, whereas Brdk and LeuEnk showed reduced ion signals for sodiated peaks which resulted in an overall decreased ion signal (see Fig. 6). For SubP and Mel, severe ion signal suppression was observed even at 10 mM. The poor performance of the 1 M sample for all analytes was attributed to crystallisation. After the MS analysis, some samples were found to be solidified which is thought to be caused by solvent evaporation due to the laser irradiation and heating of the inlet tube which increased the additive concentration beyond solubility. Ammonium sulphate is commonly used for protein precipitation at concentrations between 800 and 3200 mM [80].

4. Conclusion

A variety of sample additive compounds were tested for compatibility with LAP-MALDI MS analysis. Although some differences between the analysed peptides were observed, general trends could be deduced.

Amongst the investigated buffer compounds tricine showed the best ion signal intensities for all analysed peptides over a concentration range from 0.005 to 5 mM on target. Owing to the dilution with the LAP-MALDI matrix, a higher initial concentration during sample preparation can be chosen.

In the presence of salts, the mode of ionisation is changing from mainly protonated analyte molecules to the formation of salt adducts. Depending on the analyte and the concentration of salts (generally <0.5 mM) the overall analyte ion signal intensity might be enhanced compared to the signal obtained in pure water. As naturally occurring concentrations of salts, especially NaCl, are comparably high, strategies for salt removal are necessary to avoid lower signal-to-noise levels in LAP-MALDI MS analysis.

One relatively inexpensive and fast method to reduce salt effects is the addition of salt sequestering agents to the sample. Ammonium salts and L-serine were added to the peptide mix in pure water and in 10 mM NaCl. Signal intensity in salt-containing samples could not be completely restored (to the level of pure water) but some improvement was visible for most peptides. Best ion signal recovery was obtained by ammonium citrate when used stoichiometrically or in 10-times excess of NaCl. Addition of 0.25 mM of various additives also led to improvements of ion signal intensities in general, i.e. even in the samples without added NaCl. This might be due to the presence of salts in the 'pure' samples. The use of higher concentrations led to a decrease in analyte ion signal intensity. Interestingly, the addition of serine at higher concentrations (25–250 mM) led to signal increases in both sample sets, with and without added NaCl, in particular for the multiply charged analyte ion species.

The direct analysis of samples containing polymeric surfactants is unsuitable for LAP-MALDI MS. Even other types of surfactants create a range of surfactant-related ions which might interfere with analyte detection. In general, concentrations greater than 0.01% suppressed analyte detection. An exception is OGP, which yielded analyte ion signals over a comparably wide concentration range and is therefore recommended for analysis by LAP-MALDI MS. For some peptides, 0.1% SDC also resulted in good analyte ion signal intensity, although the mode of ionisation changed from protonation to sodiation.

Last, several compounds often used in sample preparation were tested for their suitability with LAP-MALDI MS analysis. For acids, FA rather than TFA should be chosen as higher signal intensities were obtained with the former for all peptides. DMSO often used for compound storage is not impeding analysis at concentrations normally present after reconstitution (≤5%). BSA used as a model for protein addition lowers analyte signal intensity but again in most laboratories only small concentrations are expected. For the use of urea in the sample preparation, its concentration should be lowered before LAP-MALDI MS analysis as 1 M decreases analyte ion signal intensity by more than 50%.

H. Krenkel et al.

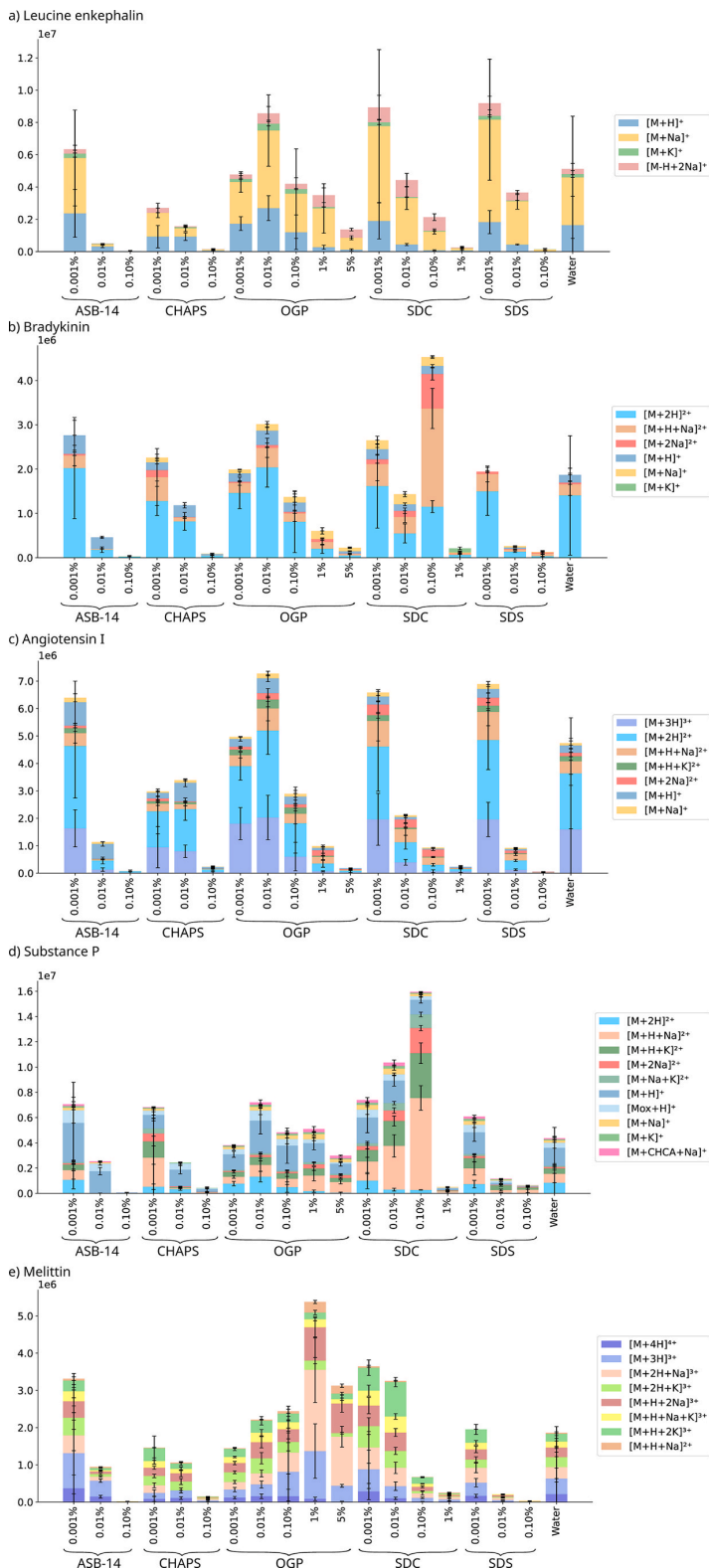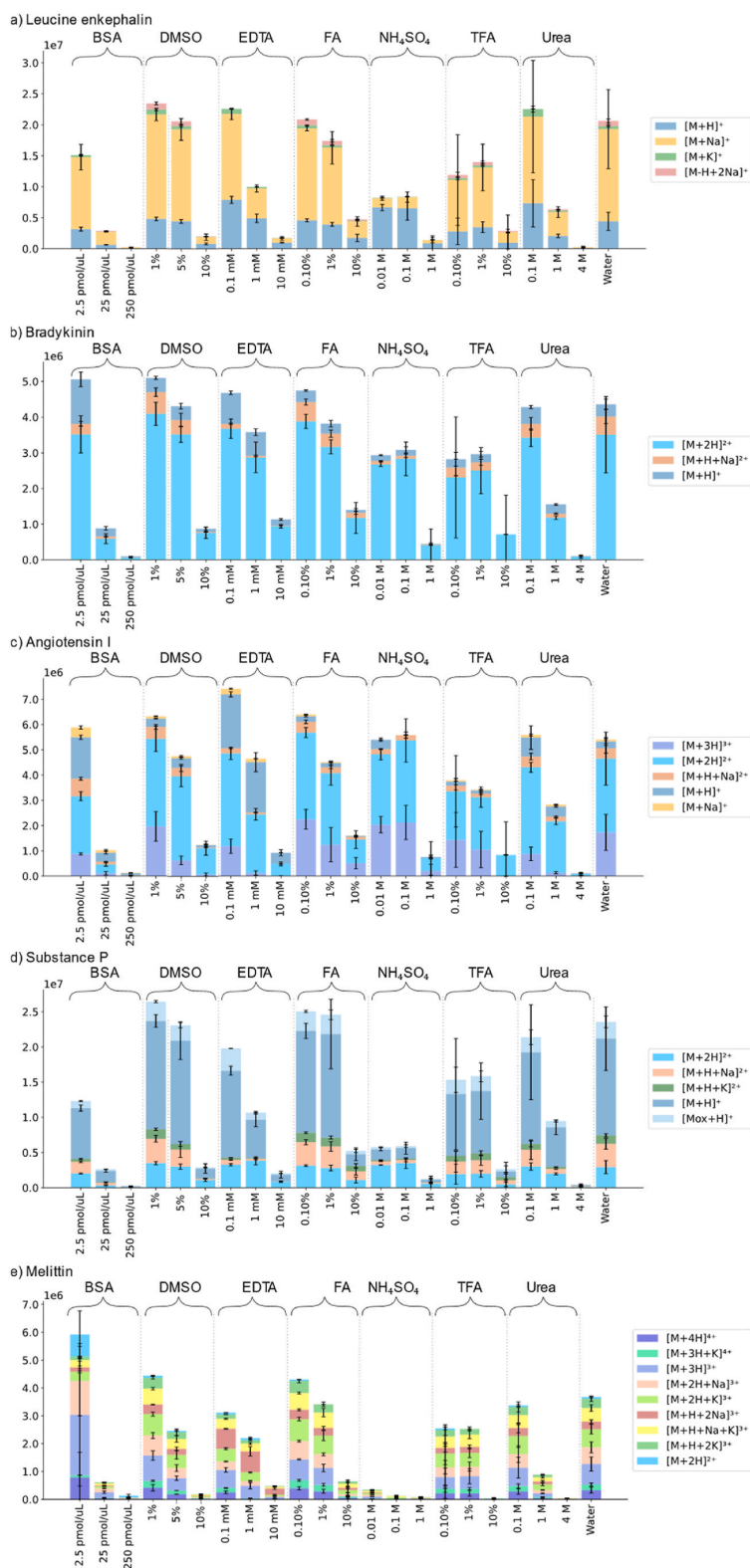**Fig. 6.** Influence of compounds often used in biological sample preparation on peptide ion signal for a) leucine enkephalin, b) bradykinin, c) angiotensin I, d) substance P and e) melittin. The error bars denote the standard deviation between replicates (n=3 for additives, n=9 for water) or the data point range for n=2 where the signal is below the signal-to-noise threshold of 3 (see SI Table 11). Ion signals with minor contributions to the total ion signal (<5% of total ion signal in all samples), e.g. from rare adduct ion formation, were omitted for clarity.

11

Author statement

Henriette Krenkel: methodology, software, formal analysis, investigation, writing, visualization.

Jeffery Brown: resources, writing – review & editing.

Michael Morris: resources, writing – review & editing, funding acquisition.

Rainer Cramer: conceptualization, methodology, resources, writing, visualization, supervision, funding acquisition.

Declaration of competing interest

The authors declare the following financial interests/personal relationships which may be considered as potential competing interests: Rainer Cramer reports financial support and equipment, drugs, or supplies were provided by Waters Corporation. Rainer Cramer reports a relationship with BSPR that includes: board membership.

Data availability

Data supporting the results reported in this paper are openly available from the University of Reading Research Data Archive at https://researchdata.reading.ac.uk/id/eprint/464.

Appendix A. Supplementary data

Supplementary data to this article can be found online at https://doi.org/10.1016/j.ijms.2023.117134.

References

[1] H. Metwally, R.G. McAllister, L. Konermann, Exploring the mechanism of salt-induced signal suppression in protein electrospray mass spectrometry using experiments and molecular dynamics simulations, Anal. Chem. 87 (2015) 2434–2442.

[2] H. Maity, A.N. Muttathukattil, G. Reddy, Salt effects on protein folding thermodynamics, J. Phys. Chem. Lett. 9 (2018) 5063–5070.

[3] C. Kütemeyer, M. Froeck, H.D. Werlein, B.M. Watkinson, The influence of salts and temperature on enzymatic activity of microbial transglutaminase, Food Control 16 (2005) 735–737.

[4] C. Park, R.T. Raines, Quantitative analysis of the effect of salt concentration on enzymatic catalysis, J. Am. Chem. Soc. 123 (2001) 11472–11479.

[5] M.J.V. Clausen, H. Poulsen, Sodium/potassium homeostasis in the cell, in: L. Banci (Ed.), Metallomics and the Cell, Springer Netherlands, Dordrecht, 2013, pp. 41–67.

[6] J.P. Morth, B.P. Pedersen, M.J. Buch-Pedersen, J.P. Andersen, B. Vilsen, M. G. Palmgren, P. Nissen, A structural overview of the plasma membrane Na+,K+-ATPase and H+-ATPase ion pumps, Nat. Rev. Mol. Cell Biol. 12 (2011) 60–70.

[7] L.M. Biga, S. Dawson, A. Harwell, R. Hopkins, J. Kaufmann, M. LeMaster, P. Matern, K. Morrison-Graham, D. Quick, J. Runyeon, 3.1 the cell membrane, in: Anatomy & Physiology, OpenStax/Oregon State University, 2019.

[8] F. Beaudry, P. Vachon, Electrospray ionization suppression, a physical or a chemical phenomenon? Biomed. Chromatogr. 20 (2006) 200–205.

[9] A.T. Iavarone, O.A. Udekwu, E.R. Williams, Buffer loading for countering metal salt-induced signal suppression in electrospray ionization, Anal. Chem. 76 (2004) 3944–3950.

[10] J.C. DeMuth, S.A. McLuckey, Electrospray droplet exposure to organic vapors: metal ion removal from proteins and protein complexes, Anal. Chem. 87 (2015) 1210–1218.

[11] J.T. Hopper, K. Sokratous, N.J. Oldham, Charge state and adduct reduction in electrospray ionization-mass spectrometry using solvent vapor exposure, Anal. Biochem. 421 (2012) 788–790.

[12] J. Hu, Q.Y. Guan, J. Wang, X.X. Jiang, Z.Q. Wu, X.H. Xia, J.J. Xu, H.Y. Chen, Effect of nanoemitters on suppressing the formation of metal adduct ions in electrospray ionization mass spectrometry, Anal. Chem. 89 (2017) 1838–1845.

[13] R.L. Griffiths, J. Bunch, A survey of useful salt additives in matrix-assisted laser desorption/ionization mass spectrometry and tandem mass spectrometry of lipids: introducing nitrates for improved analysis, Rapid Commun. Mass Spectrom. 26 (2012) 1557–1566.

[14] T. Nishikaze, M. Takayama, Disappearance of interfering alkali-metal adducted peaks from matrix-assisted laser desorption/ionization mass spectra of peptides with serine addition to alpha-cyano-4-hydroxycinnamic acid matrix, Rapid Commun. Mass Spectrom. 21 (2007) 3345–3351.

[15] Y. Ucal, A. Ozpinar, Improved spectra for MALDI MSI of peptides using ammonium phosphate monobasic in MALDI matrix, J. Mass Spectrom. 53 (2018) 635–648.

[16] X. Zhu, I.A. Papayannopoulos, Improvement in the detection of low concentration protein digests on a MALDI TOF/TOF workstation by reducing alpha-cyano-4-hydroxycinnamic acid adduct ions, J. Biomol. Tech. 14 (2003) 298–307.

[17] Y.F. Zhu, N.I. Taranenko, S.L. Allman, S.A. Martin, L. Haff, C.H. Chen, The effect of ammonium salt and matrix in the detection of DNA by matrix-assisted laser desorption/ionization time-of-flight mass spectrometry, Rapid Commun. Mass Spectrom. 10 (1996) 1591–1596.

[18] R. Chen, W. Xu, C. Xiong, X. Zhou, S. Xiong, Z. Nie, L. Mao, Y. Chen, H.C. Chang, High-salt-tolerance matrix for facile detection of glucose in rat brain microdialysates by MALDI mass spectrometry, Anal. Chem. 84 (2012) 465–469.

[19] S. Wang, Z. Xiao, C. Xiao, H. Wang, B. Wang, Y. Li, X. Chen, X. Guo, (E)-Propyl alpha-cyano-4-hydroxyl cinnamylate: a high sensitive and salt tolerant matrix for intact protein profiling by MALDI mass spectrometry, J. Am. Soc. Mass Spectrom. 27 (2016) 709–718.

[20] E.B. Monroe, B.A. Koszczuk, J.L. Losh, J.C. Jurchen, J.V. Sweedler, Measuring salty samples without adducts with MALDI MS, Int. J. Mass Spectrom. 260 (2007) 237–242.

[21] R.W. Garden, L.L. Moroz, T.P. Moroz, S.A. Shippy, J.V. Sweedler, Excess salt removal with matrix rinsing: direct peptide profiling of neurons from marine invertebrates using matrix-assisted laser desorption ionization time-of-flight mass spectrometry, J. Mass Spectrom. 31 (1996) 1126–1130.

[22] O.J. Hale, R. Cramer, Collision-induced dissociation of doubly-charged barium-cationized lipids generated from liquid samples by atmospheric pressure matrix-assisted laser desorption/ionization provides structurally diagnostic product ions, Anal. Bioanal. Chem. 410 (2018) 1435–1444.

[23] P. Ryumin, R. Cramer, The composition of liquid atmospheric pressure matrix-assisted laser desorption/ionization matrices and its effect on ionization in mass spectrometry, Anal. Chim. Acta 1013 (2018) 43–53.

[24] R. Cramer, A. Pirkl, F. Hillenkamp, K. Dreisewerd, Liquid AP-UV-MALDI enables stable ion yields of multiply charged peptide and protein ions for sensitive analysis by mass spectrometry, Angew Chem. Int. Ed. Engl. 52 (2013) 2364–2367.

[25] S.E. Lellman, R. Cramer, Bacterial identification by lipid profiling using liquid atmospheric pressure matrix-assisted laser desorption/ionization mass spectrometry, Clin. Chem. Lab. Med. 58 (2020) 930–938.

[26] O.J. Hale, M. Morris, B. Jones, C.K. Reynolds, R. Cramer, Liquid atmospheric pressure matrix-assisted laser desorption/ionization mass spectrometry adds enhanced functionalities to MALDI MS profiling for disease diagnostics, ACS Omega 4 (2019) 12759–12765.

[27] H. Krenkel, E. Hartmane, C. Piras, J. Brown, M. Morris, R. Cramer, Advancing liquid atmospheric pressure matrix-assisted laser desorption/ionization mass spectrometry toward ultrahigh-throughput analysis, Anal. Chem. 92 (2020) 2931–2936.

[28] J. Chandler, C. Haslam, N. Hardy, M. Leveridge, P. Marshall, A systematic investigation of the best buffers for use in screening by MALDI-mass spectrometry, SLAS Discov 22 (2017) 1262–1269.

[29] H. Krenkel, J. Brown, K. Richardson, E. Hoyes, M. Morris, R. Cramer, Ultrahigh-throughput sample analysis using liquid atmospheric pressure matrix-assisted laser desorption/ionization mass spectrometry, Anal. Chem. 94 (2022) 4141–4145.

[30] I. Sinclair, M. Bachman, D. Addison, M. Rohman, D.C. Murray, G. Davies, E. Mouchet, M.E. Tonge, R.G. Stearns, L. Ghislain, S.S. Datwani, L. Majlof, E. Hall, G.R. Jones, E. Hoyes, J. Olechno, R.N. Ellson, P.E. Barran, S.D. Pringle, M. R. Morris, J. Wingfield, Acoustic mist ionization platform for direct and contactless ultrahigh-throughput mass spectrometry analysis of liquid samples, Anal. Chem. 91 (2019) 3790–3794.

[31] C.M.H. Ferreira, I.S.S. Pinto, E.V. Soares, H.M.V.M. Soares, (Un)suitability of the use of pH buffers in biological, biochemical and environmental studies and their interaction with metal ions – a review, RSC Adv. 5 (2015) 30989–31003.

[32] N.E. Good, G.D. Winget, W. Winter, T.N. Connolly, S. Izawa, R.M.M. Singh, Hydrogen ion buffers for biological research, Biochemistry 5 (1966) 467–477.

[33] N.E. Good, S. Izawa, [3] Hydrogen ion buffers, in: Methods Enzymol., Academic Press, 1972, pp. 53–68.

[34] W.J. Ferguson, K.I. Braunschweiger, W.R. Braunschweiger, J.R. Smith, J. J. McCormick, C.C. Wasmann, N.P. Jarvis, D.H. Bell, N.E. Good, Hydrogen ion buffers for biological research, Anal. Biochem. 104 (1980) 300–310.

[35] E.A. Peroza, E. Freisinger, Tris is a non-innocent buffer during intein-mediated protein cleavage, Protein Expr. Purif. 57 (2008) 217–225.

[36] W.A. Bubb, H.A. Berthon, P.W. Kuchel, Tris buffer reactivity with low-molecular-weight aldehydes: NMR characterization of the reactions of glyceraldehyde-3-phosphate, Bioorg. Chem. 23 (1995) 119–130.

[37] K.K. Mock, C.W. Sutton, J.S. Cottrell, Sample immobilization protocols for matrix-asssisted laser-desorption mass spectrometry, Rapid Commun. Mass Spectrom. 6 (1992) 233–238.

[38] K.O. Börnsen, Influence of salts, buffers, detergents, solvents, and matrices on MALDI-MS protein analysis in complex mixtures, in: J.R. Chapman (Ed.), Mass Spectrometry of Proteins and Peptides: Mass Spectrometry of Proteins and Peptides, Humana Press, Totowa, NJ, 2000, pp. 387–404.

[39] U. Kallweit, K.O. Börnsen, G.M. Kresbach, H.M. Widmer, Matrix compatible buffers for analysis of proteins with matrix-assisted laser desorption/ionization mass spectrometry, Rapid Commun. Mass Spectrom. 10 (1996) 845–849.

[40] Y. Guo, M. Forbush, T.R. Covey, L. Ghislain, C. Liu, High-throughput analysis from complex matrices: acoustic ejection mass spectrometry from phase-separated fluid samples, Metabolites 11 (2021).

[41] F. Gharahdaghi, M. Kirchner, J. Fernandez, S.M. Mische, Peptide-mass profiles of polyvinylidene difluoride-bound proteins by matrix-assisted laser desorption/ionization time-of-flight mass spectrometry in the presence of nonionic detergents, Anal. Biochem. 233 (1996) 94–99.

[42] M.K. Mandal, L.C. Chen, Z. Yu, H. Nonami, R. Erra-Balsells, K. Hiraoka, Detection of protein from detergent solutions by probe electrospray ionization mass spectrometry (PESI-MS), J. Mass Spectrom. 46 (2011) 967–975.

[43] I. Sinclair, R. Stearns, S. Pringle, J. Wingfield, S. Datwani, E. Hall, L. Ghislain, L. Majlof, M. Bachman, Novel acoustic loading of a mass spectrometer: toward next-generation high-throughput MS screening, J. Lab. Autom. 21 (2016) 19–26.

[44] T. Hasegawa, R.M. Imamura, T. Suzuki, T. Hashiguchi, T. Nomura, S. Otsuguro, K. Maenaka, M. Sasaki, Y. Orba, H. Sawa, A. Sato, T. Okabe, T. Nagano, H. Kojima, Application of acoustic ejection MS system to high-throughput screening for SARS-CoV-2 3CL protease inhibitors, Chem. Pharm. Bull. (Tokyo) 70 (2022) 199–201.

[45] J.M. Asara, J. Allison, Enhanced detection of phosphopeptides in matrix-assisted laser desorption/ionization mass spectrometry using ammonium salts, J. Am. Soc. Mass Spectrom. 10 (1999) 35–44.

[46] R. Cramer, S. Corless, Liquid ultraviolet matrix-assisted laser desorption/ionization – mass spectrometry for automated proteomic analysis, Proteomics 5 (2005) 360–370.

[47] H. Hernandez, C.V. Robinson, Determining the stoichiometry and interactions of macromolecular assemblies from mass spectrometry, Nat. Protoc. 2 (2007) 715–726.

[48] U.H. Verkerk, P. Kebarle, Ion-Ion and ion-molecule reactions at the surface of proteins produced by nanospray. Information on the number of acidic residues and control of the number of ionized acidic and basic residues, J. Am. Soc. Mass Spectrom. 16 (2005) 1325–1341.

[49] L. Konermann, Addressing a common misconception: ammonium acetate as neutral pH "buffer" for native electrospray mass spectrometry, J. Am. Soc. Mass Spectrom. 28 (2017) 1827–1835.

[50] I.P. Smirnov, X. Zhu, T. Taylor, Y. Huang, P. Ross, I.A. Papayanopoulos, S. A. Martin, D.J. Pappin, Suppression of alpha-cyano-4-hydroxycinnamic acid matrix clusters and reduction of chemical noise in MALDI-TOF mass spectrometry, Anal. Chem. 76 (2004) 2958–2965.

[51] D. Winter, J. Seidler, Y. Ziv, Y. Shiloh, W.D. Lehmann, Citrate boosts the performance of phosphopeptide analysis by UPLC-ESI-MS/MS, J. Proteome Res. 8 (2009) 418–424.

[52] G. Wang, R.B. Cole, Effect of solution ionic strength on analyte charge state distributions in positive and negative ion electrospray mass spectrometry, Anal. Chem. 66 (1994) 3702–3708.

[53] U. Pieles, W. Zurcher, M. Schar, H.E. Moser, Matrix-assisted laser desorption ionization time-of-flight mass spectrometry: a powerful tool for the mass and sequence analysis of natural and modified oligonucleotides, Nucleic Acids Res. 21 (1993) 3191–3196.

[54] R. Javanshad, A.R. Venter, Effects of amino acid additives on protein solubility – insights from desorption and direct electrospray ionization mass spectrometry, Analyst 146 (2021) 6592–6604.

[55] R. Javanshad, E. Honarvar, A.R. Venter, Addition of serine enhances protein analysis by DESI-MS, J. Am. Soc. Mass Spectrom. 30 (2019) 694–703.

[56] D.J. Clarke, D.J. Campopiano, Desalting large protein complexes during native electrospray mass spectrometry by addition of amino acids to the working solution, Analyst 140 (2015) 2679–2686.

[57] N. Thorne, D.S. Auld, J. Inglese, Apparent activity in high-throughput screening: origins of compound-dependent assay interference, Curr. Opin. Chem. Biol. 14 (2010) 315–324.

[58] G.A. Breaux, K.B. Green-Church, A. France, P.A. Limbach, Surfactant-aided, matrix-assisted laser desorption/ionization mass spectrometry of hydrophobic and hydrophilic peptides, Anal. Chem. 72 (2000) 1169–1174.

[59] K.O. Börnsen, M.A. Gass, G.J. Bruin, J.H. von Adrichem, M.C. Biro, G.M. Kresbach, M. Ehrat, Influence of solvents and detergents on matrix-assisted laser desorption/ionization mass spectrometry measurements of proteins and oligonucleotides, Rapid Commun. Mass Spectrom. 11 (1997) 603–609.

[60] J.E. Coligan, Commonly used detergents, Curr Protoc Protein Sci, Appendix 1 (2001). Appendix 1B.

[61] E. Fuguet, C. Rafols, M. Roses, E. Bosch, Critical micelle concentration of surfactants in aqueous buffered and unbuffered systems, Anal. Chim. Acta 548 (2005) 95–100.

[62] I.F. Shieh, C.Y. Lee, J. Shiea, Eliminating the interferences from TRIS buffer and SDS in protein analysis by fused-droplet electrospray ionization mass spectrometry, J. Proteome Res. 4 (2005) 606–612.

[63] O.R.R. Loo, N. Dales, P.C. Andrews, The effect of detergents on proteins analyzed by electrospray ionization, in: J.R. Chapman (Ed.), Protein and Peptide Analysis by Mass Spectrometry, Humana Press, Totowa, NJ, 1996, pp. 141–160.

[64] N.B. Cech, C.G. Enke, Practical implications of some recent studies in electrospray ionization fundamentals, Mass Spectrom. Rev. 20 (2001) 362–387.

[65] R.R. Loo, J.A. Loo, Matrix-assisted laser desorption/ionization-mass spectrometry of hydrophobic proteins in mixtures using formic acid, perfluorooctanoic acid, and sorbitol, Anal. Chem. 79 (2007) 1115–1125.

[66] F.M.L. Amado, M.G. Santana-Marques, A.J. Ferrer-Correia, K.B. Tomer, Analysis of peptide and protein samples containing surfactants by MALDI-MS, Anal. Chem. 69 (1997) 1102–1106.

[67] N. Zhang, L. Li, Effects of common surfactants on protein digestion and matrix-assisted laser desorption/ionization mass spectrometric analysis of the digested peptides using two-layer sample preparation, Rapid Commun. Mass Spectrom. 18 (2004) 889–896.

[68] J. Funk, X. Li, T. Franz, Threshold values for detergents in protein and peptide samples for mass spectrometry, Rapid Commun. Mass Spectrom. 19 (2005) 2986–2988.

[69] M.R. Arkin, M.A. Glicksman, H. Fu, J.J. Havel, Y. Du, Inhibition of protein-protein interactions: non-cellular assay formats, in: S. Markossian, A. Grossman, K. Brimacombe, M. Arkin, D. Auld, C. Austin, J. Baell, T.D.Y. Chung, N.P. Coussens, J.L. Dahlin, V. Devanarayan, T.L. Foley, M. Glicksman, J.V. Haas, M.D. Hall, S. Hoare, J. Inglese, P.W. Iversen, S.C. Kales, M. Lal-Nag, Z. Li, J. McGee, O. McManus, T. Riss, P. Saradjian, G.S. Sittampalam, M. Tarselli, O.J. Trask Jr, Y. Wang, J.R. Weidner, M.J. Wildey, K. Wilson, M. Xia, X. Xu (Eds.), Assay Guidance Manual, Eli Lilly & Company and the National Center for Advancing Translational Sciences, 2004. Bethesda (MD).

[70] A.J. Radosevich, F. Pu, D. Chang-Yen, J.W. Sawicki, N.N. Talaty, N.L. Elsen, J. D. Williams, J.Y. Pan, Ultra-high-throughput ambient MS: direct analysis at 22 samples per second by infrared matrix-assisted laser desorption electrospray ionization mass spectrometry, Anal. Chem. 94 (2022) 4913–4918.

[71] J.J.A. van Kampen, P.C. Burgers, R. de Groot, A.D.M.E. Osterhaus, M.L. Reedijk, E. J. Verschuren, R.A. Gruters, T.M. Luider, Quantitative analysis of HIV-1 protease inhibitors in cell lysates using MALDI-FTICR mass spectrometry, Anal. Chem. 80 (2008) 3751–3756.

[72] J.H. Lee, H.S. Choi, K.A. Nasr, M. Ha, Y. Kim, J.V. Frangioni, High-throughput small molecule identification using MALDI-TOF and a nanolayered substrate, Anal. Chem. 83 (2011) 5283–5289.

[73] M.S. Unger, M. Blank, T. Enzlein, C. Hopf, Label-free cell assays to determine compound uptake or drug action using MALDI-TOF mass spectrometry, Nat. Protoc. 16 (2021) 5533–5558.

[74] S. Schulz, D. Gerhardt, B. Meyer, M. Seegel, B. Schubach, C. Hopf, K. Matheis, DMSO-enhanced MALDI MS imaging with normalization against a deuterated standard for relative quantification of dasatinib in serial mouse pharmacology studies, Anal. Bioanal. Chem. 405 (2013) 9467–9476.

[75] J.H. Eriksson, R. Mol, G.W. Somsen, W.L. Hinrichs, H.W. Frijlink, G.J. de Jong, Feasibility of nonvolatile buffers in capillary electrophoresis-electrospray ionization-mass spectrometry of proteins, Electrophoresis 25 (2004) 43–49.

[76] M.C. Garcıa, A.C. Hogenboom, H. Zappey, H. Irth, Effect of the mobile phase composition on the separation and detection of intact proteins by reversed-phase liquid chromatography–electrospray mass spectrometry, J. Chromatogr. A 957 (2002) 187–199.

[77] High-throughput identification of bacteria and yeast by matrix-assisted laser desorption ionization-time of flight mass spectrometry in conventional medical microbiology laboratories, in: S.Q. van Veen, E.C.J. Claas, J. Kuijper (Eds.), J. Clin. Microbiol. 48 (2010) 900–907.

[78] F.E. Kuhlmann, A. Apffel, S.M. Fischer, G. Goldberg, P.C. Goodley, Signal enhancement for gradient reverse-phase high-performance liquid chromatography-electrospray ionization mass spectrometry analysis with trifluoroacetic and other strong acid modifiers by postcolumn addition of propionic acid and isopropanol, J. Am. Soc. Mass Spectrom. 6 (1995) 1221–1225.

[79] M.K. Mandal, L.C. Chen, Y. Hashimoto, Z. Yu, K. Hiraoka, Detection of biomolecules from solutions with high concentration of salts using probe electrospray and nano-electrospray ionization, Anal. Methods 2 (2010) 1905–1912.

[80] P. Wingfield, Protein precipitation using ammonium sulfate, Curr Protoc Protein Sci, Appendix 3 (2001). Appendix 3F.

Supporting Information

The Use of Salts, Buffers and Surfactants in LAP-MALDI MS

Henriette Krenkel[1], Jeffery Brown[2], Michael Morris[2], Rainer Cramer[1]*

[1] Department of Chemistry, University of Reading, Whiteknights, Reading RG6 6DX, UK

[2] Waters Corporation, Stamford Avenue, Wilmslow SK9 4AX, UK

Corresponding author:

* R. Cramer
Department of Chemistry
University of Reading
Whiteknights, Reading RG6 6DX, United Kingdom
E-mail: r.k.cramer@reading.ac.uk
Homepage: www.reading.ac.uk/chemistry/about/staff/r-k-cramer.aspx

Table of Figures

Table of Tables

Table 1: Properties of analysed peptides

Peptide	Amino acid seq.	Empirical formula	Monoisotopic mass	pI[*]	Conc. of stock solution in pmol/ µL	Conc. on target in pmol/µL	Moles on target in mol
Leucine enkephaline	YGGFL	$C_{28}H_{37}N_5O_7$	555.2693	5.97	100	1.7	0.5
Bradykinin	RPPGFSPFR	$C_{50}H_{73}N_{15}O_{11}$	1059.5614	12.49	500	3.3	1
Angiotensin I	DRVYIHPFHL	$C_{62}H_{89}N_{17}O_{14}$	1295.6775	7.95	320	2.7	0.8
Substance P	RPKPQQFFGLM	$C_{63}H_{98}N_{18}O_{13}S$	1346.7282	11.56[^]	100	3.3	1
Melittin	GIGAVLKVLTTGLPALISWIKRKRQQ	$C_{131}H_{229}N_{39}O_{31}$	2844.7542	12.59[^]	500	2.1	0.625

[*]- calculated using https://www.bachem.com/knowledge-center/peptide-calculator/
[^]- calculated without terminal modification

Table 2: Structures of buffer compounds
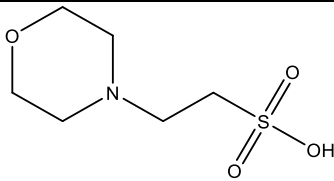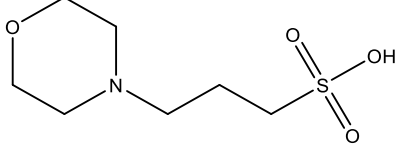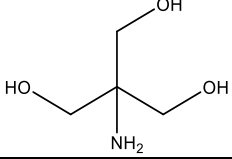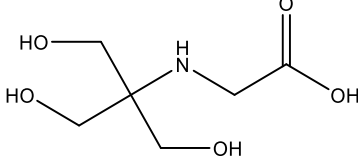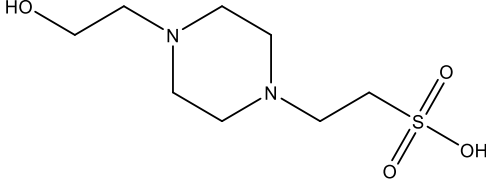
Buffer compound	Structure	pKa[1]
MES		6.270
MOPS		7.184
Tris		8.072
Tricine		8.135
HEPES		7.564

Table 3: Overview of detected ions with less replicates than n=3 for samples and n=15 for the water control for the buffer additives.

Analyte	m/z	Additive	Dilution	Number of replicates	Type of ion
Leucine enkephalin	556.277	MES	0.5 mM	2	[M+H]$^+$
	578.258	MES	0.5 mM	2	[M+Na]$^+$
	594.232	MES	0.5 mM	2	[M+K]$^+$
	600.24	MES	0.5 mM	2	[M-H+2Na]$^+$
Bradykinin	530.788	MES	0.5 mM	2	[M+2H]$^{2+}$
	541.779	MES	0.5 mM	2	[M+H+Na]$^{2+}$
	1060.569	MES	0.5 mM	2	[M+H]$^+$
	1060.569	MOPS	5 mM	2	[M+H]$^+$
Angiotensin I	432.9	MES	0.5 mM	2	[M+3H]$^{3+}$
	648.846	MES	0.5 mM	2	[M+2H]$^{2+}$
	659.837	MES	0.5 mM	2	[M+H+Na]$^{2+}$
	670.828	Tris	5 mM	2	[M+2Na]$^{2+}$
	1296.685	MES	0.5 mM	2	[M+H]$^+$
	1296.685	MOPS	5 mM	2	[M+H]$^+$
	1318.667	MES	0.5 mM	2	[M+Na]$^+$
	1318.667	MES	5 mM	2	[M+Na]$^+$
	1318.667	Tris	5 mM	2	[M+Na]$^+$
Substance P	674.371	MES	0.5 mM	2	[M+2H]$^{2+}$
	685.362	MES	0.5 mM	2	[M+H+Na]$^{2+}$
	693.349	MES	0.5 mM	2	[M+H+K]$^{2+}$
	696.353	MES	0.5 mM	2	[M+2Na]$^{2+}$
	1347.735	MES	0.5 mM	2	[M+H]$^+$
	1363.71	MES	0.5 mM	2	[Mox+H]$^+$
	1369.717	MES	0.5 mM	2	[M+Na]$^+$
	1558.76	MES	0.5 mM	2	[M+CHCA+Na]$^+$
Melittin	712.196	MES	0.5 mM	2	[M+4H]$^{4+}$
	949.259	MES	0.5 mM	2	[M+3H]$^{3+}$
	956.586	MES	0.5 mM	2	[M+2H+Na]$^{3+}$
	956.586	MOPS	5 mM	2	[M+2H+Na]$^{3+}$
	961.911	MES	0.5 mM	2	[M+2H+K]$^{3+}$
	963.913	MES	0.5 mM	2	[M+H+2Na]$^{3+}$
	969.238	MES	0.5 mM	2	[M+H+Na+K]$^{3+}$
	969.238	MOPS	5 mM	2	[M+H+Na+K]$^{3+}$
	974.563	MES	0.5 mM	2	[M+H+2K]$^{3+}$
	974.563	Tris	5 mM	2	[M+H+2K]$^{3+}$
	1423.384	MES	0.5 mM	2	[M+2H]$^{2+}$
	1423.384	MES	5 mM	2	[M+2H]$^{2+}$
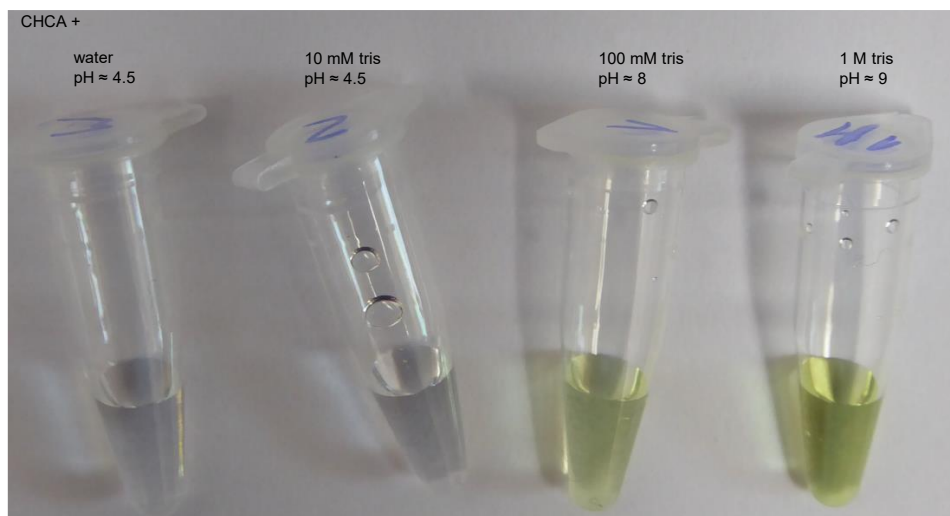
Figure 1: Colour change when mixing tris and the CHCA-based liquid support matrix.
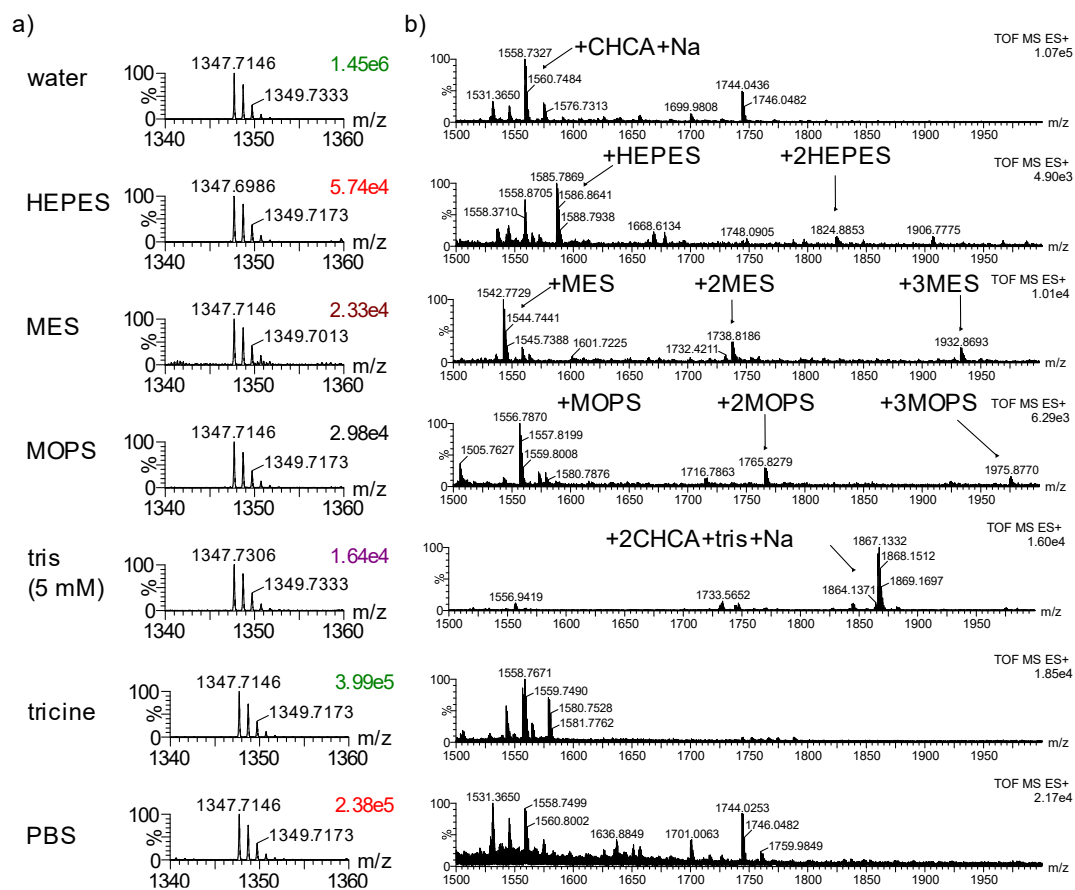
Figure 2: Adduct formation of singly charged substance P (a) with buffer compounds (b). All buffers are at a final concentration of 50 mM unless otherwise stated. Peak assignments are putative and based on monoisotopic m/z values.

5

Table 4: Overview of detected ions with less replicates than n=3 for samples and n=21 for the water control for the salts additives.

Analyte	m/z	Additive	Dilution	Number of replicates	Type of ion
Leucine enkephalin	578.258	MgCl2	5 mM	2	[M+Na]+
	600.24	MgCl2	5 mM	2	[M-H+2Na]+
	600.24	MgCl2	50 mM	2	[M-H+2Na]+
Bradykinin	552.77	MgAc	50 mM	2	[M+2Na]2+
	1060.569	CaCl2	5 mM	2	[M+H]+
	1060.569	CaCl2	50 mM	2	[M+H]+
	1082.551	CaCl2	5 mM	2	[M+Na]+
	1082.551	MgAc	0.5 mM	2	[M+Na]+
	1098.525	NaCl	50 mM	2	[M+K]+
Angiotensin I	667.824	CaCl2	5 mM	2	[M+H+K]2+
	667.824	MgAc	0.5 mM	2	[M+H+K]2+
	667.824	MgAc	5 mM	2	[M+H+K]2+
	670.828	CaCl2	0.05 mM	2	[M+2Na]2+
	670.828	CaCl2	5 mM	2	[M+2Na]2+
	670.828	MgAc	5 mM	2	[M+2Na]2+
Substance P	693.349	CaCl2	50 mM	2	[M+H+K]2+
	696.353	MgCl2	50 mM	2	[M+2Na]2+
	1363.71	MgCl2	50 mM	2	[Mox+H]+
	1385.691	MgCl2	0.5 mM	2	[M+K]+
	1385.691	MgCl2	5 mM	2	[M+K]+
Melittin	569.958	Water	-	19	[M+5H]5+
	712.196	CaCl2	5 mM	2	[M+4H]4+
	712.196	NaCl	0.05 mM	2	[M+4H]4+
	717.691	NH4Cl	50 mM	2	[M+3H+Na]4+
	717.691	NaAc	5 mM	2	[M+3H+Na]4+
	1434.375	KCl	5 mM	2	[M+H+Na]2+
	1434.375	MgAc	5 mM	2	[M+H+Na]2+
	1434.375	NH4Cl	50 mM	2	[M+H+Na]2+
	1453.353	CaCl2	50 mM	2	[M+Na+K]2+
	1453.353	KCl	50 mM	2	[M+Na+K]2+
	1453.353	MgCl2	50 mM	2	[M+Na+K]2+
	1453.353	NaAc	5 mM	2	[M+Na+K]2+
	1453.353	NaCl	0.05 mM	2	[M+Na+K]2+
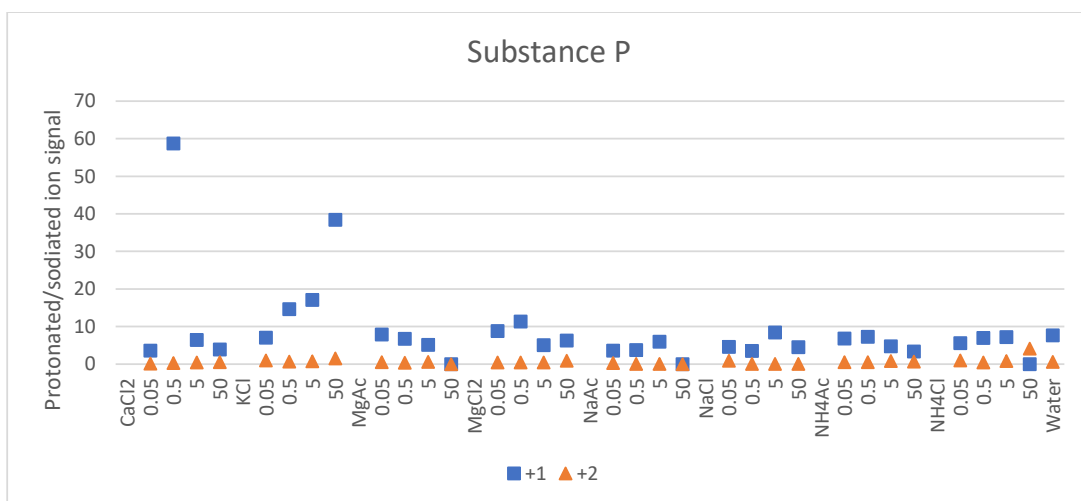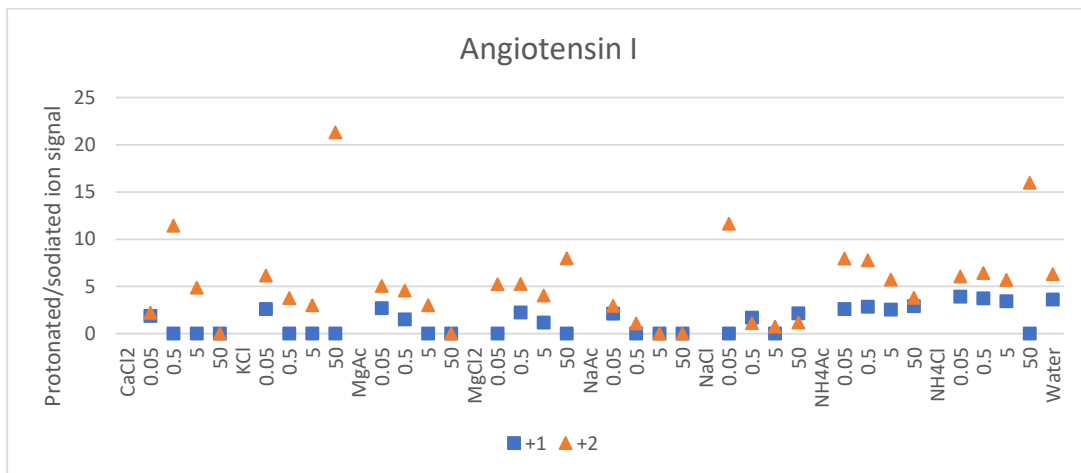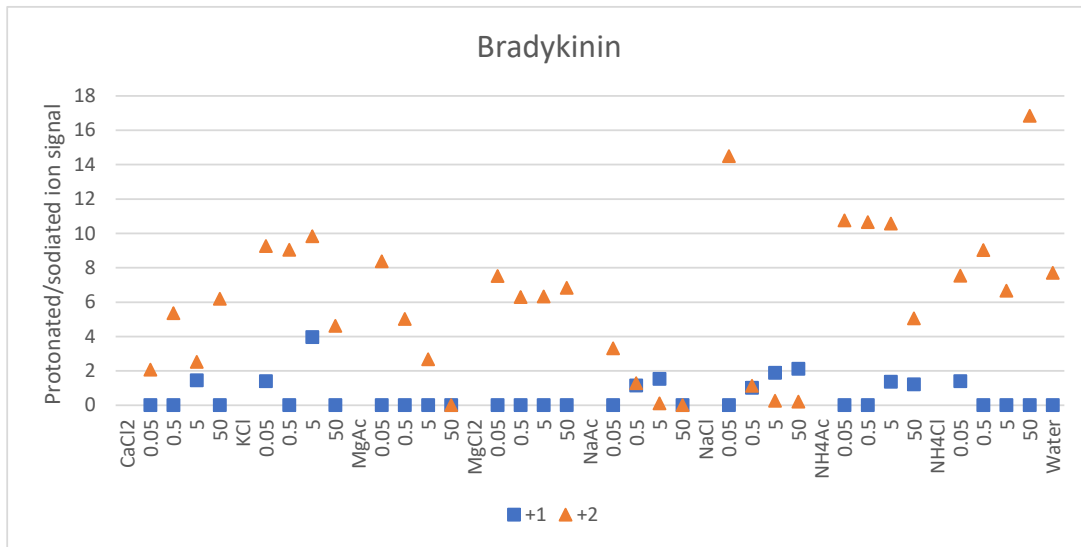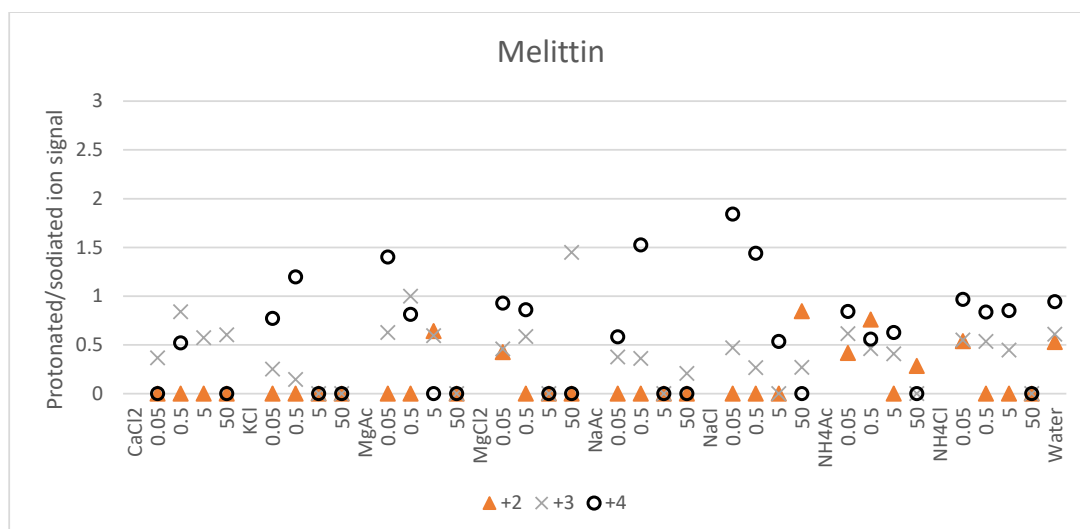
Figure 3: Comparison of adduct formation between charge states, displaying the ratio of protonated ion signal intensity to singly sodiated ion signal intensity per charge state. Blue rectangle: singly charged, orange triangle: doubly charged, grey cross: triply charged, black circle: quadruply charged.

Table 5: Salt concentrations in biological fluids in mM

	Na	K	Mg	Ca	Cl
Urine	41.8[2], 83[3]	25.6[2], 33[3]	0.06[2], 0.3501[4],2.6[3]	0.36[2], 0.6687[4], 4.4[3]	67.7[2], 77[3]
Saliva	7.87[5]	9.57[5]	0.2003[4]	1.17[5], 1.8987[4]	5-20[6]
Plasma	136-145[6]	3.4-4.5[6]	0.8556[4]	2.5150[4]	98-107[6]
Serum	142[7]	4.1[7]	0.66-1.04[6]	1.16-1.32[6]	98-107[6]
Cerebrospinal fluid	136-150[6]	2.5-3.2[6]	0.8885[4]	0.9606[4]	118-132[6]
Sweat	33[6]	4.4-15.6[6]	0.2698[4]	1.4122[4]	5-35[6]
Minimal essential medium	140.9[8]	5.4[8]	1[8]	1.8 or 0[8]	127[8]
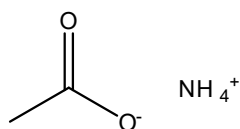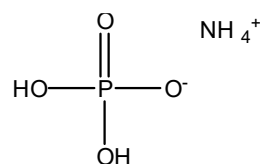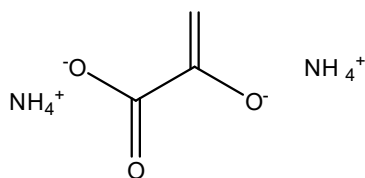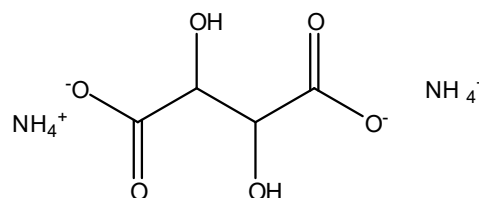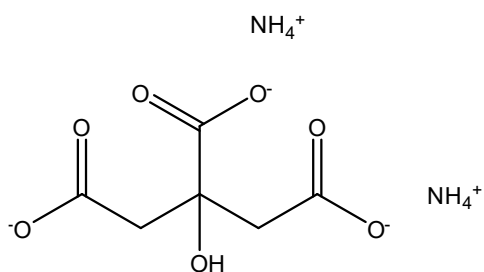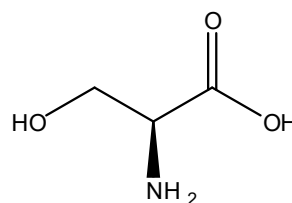
Figure 4: Structures of additives used as salt remediators.
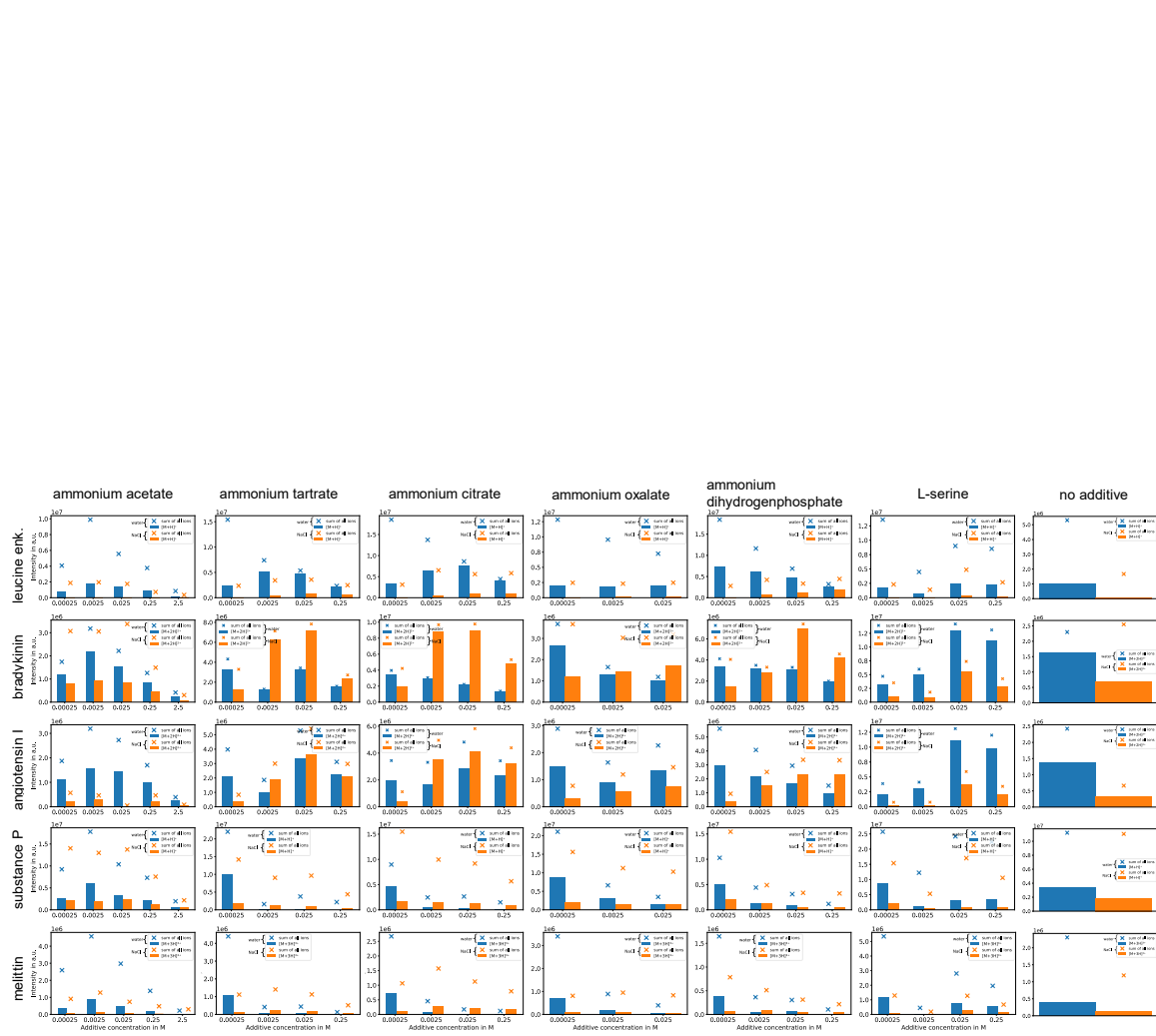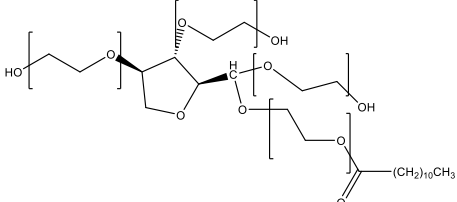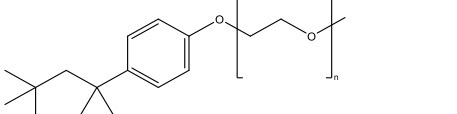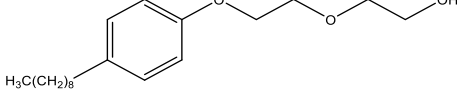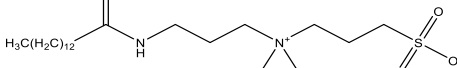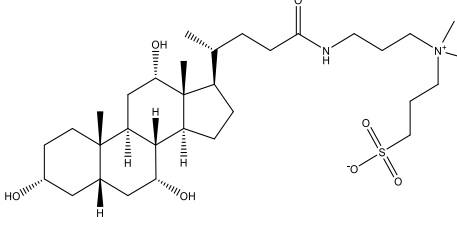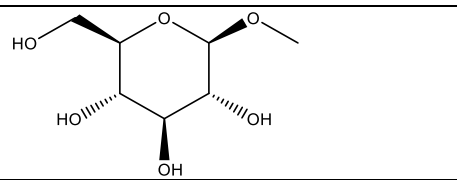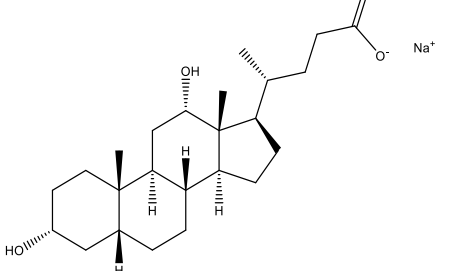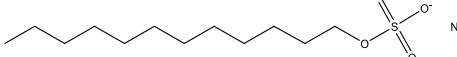
Figure 5: Influence of additives on ion signal intensities of peptides in pure water and a 10-mM NaCl solution.

Table 6: Overview of detected ions with less replicates than n=3 for samples, n=9 for water controls or n=15 for the water with NaCl control for 'salt remediation' additives.

Analyte	m/z	Additive	Dilution	Number of replicates	Type of ion
Bradykinin	1082.551	Water_NH$_4$Tar	250 mM	2	[M+Na]$^+$
Substance P	1369.717	Water_NH$_4$Cit	250 mM	2	[M+Na]$^+$
	1558.76	NaCl_NH$_4$Ac	250 mM	2	[M+CHCA+Na]$^+$
	1558.76	NaCl_NH4Cit	25 mM	2	[M+CHCA+Na]$^+$
	1558.76	Water_NH$_4$Tar	250 mM	2	[M+CHCA+Na]$^+$
Melittin	723.187	NaCl_L-serine	0.25 mM	2	[M+2H+2Na]$^{4+}$
	723.187	NaCl_NH$_4$Ox	0.25 mM	2	[M+2H+2Na]$^{4+}$
	961.911	Water_NH$_4$Cit	25 mM	2	[M+2H+K]$^{3+}$
	963.913	NaCl_NH$_4$H$_2$PO$_4$	250 mM	2	[M+H+2Na]$^{3+}$
	723.187	NaCl_Water	-	13	[M+2H+2Na]$^{4+}$

Table 7: Properties of surfactants

Surfactant	Structure	CAS number	Type*	Critical micelle concentration (CMC) in mM	Surface tension at CMC in mN/m
Tween-20		9005-64-5	NI	0.0169[9]	35[9]
Triton-X (n=9-10 X-100, n=7-8 X-114)		9036-19-5	NI	0.3[10]	28[11]
NP40-alternative		9016-45-9	NI	0.05-0.3[12]	
ASB-14		216667-08-2	ZW	0.119[13]	42[13]
CHAPS		75621-03-3	ZW	1.4[10]	45.2[14]
OGP		29836-26-8	NI	23[10]	41[15]
SDC		302-95-4	AI	5[10]	45[16]
SDS		151-21-3	AI	8[17]	38.5[14]

*ZW – zwitterionic, NI – non-ionic, AI – anionic

Table 8: Concentration of studied surfactant dilutions in mM. Values above the CMC in water are highlighted in orange.

On-target concentration in % (w/v)	ASB	CHAPS	OGP	SDS	SDC
10	23.01	16.26	34.20	NA	NA
5	11.50	8.13	17.10	17.34	NA
1	2.30	1.63	3.42	3.47	2.41
0.1	0.23	0.16	0.34	0.35	0.24
0.01	0.02	0.02	0.03	0.03	0.02
0.001	0.00	0.00	0.00	0.00	0.00

a)

b)

	1	2	3	4	5	6	7	8	9	10	11	12
A	W3	C3	S3	A3	O3	D3	W2	C2	S2	A2	O2	D2
B	W3	C3	S3	A3	O3	D3	W2	C2	S2	A2	O2	D2
C	W3	C3	S3	A3	O3	D3	W2	C2	S2	A2	O2	D2
D	C4	S4	A4	O4	C5	S5	W1	C1	S1	A1	O1	D1
E	C4	S4	A4	O4	C5	S5	W1	C1	S1	A1	O1	D1
F	C4	S4	A4	O4	C5	S5	W1	C1	S1	A1	O1	D1
G	A5	O5	A5	O5	A5	O5						

W: water, C: CHAPS, S: SDS, A: ASB, O: OGP, D: SDC
Conc. in % w/v: C/S/A/O/D: 1, 0.1, 0.01, 0.001, 0.0001

c)

d)

	1	2	3	4	5	6	7	8	9	10	11	12	13	14	15	16	17	18	19	20	21	22	23	24
B	W	A5	C5	O5	S5	D5	W	A4	C4	O4	S4	D4	W	A3	C3	O3	S3	D3	W	A2	C2	O2	S2	W
C	W	A5	C5	O5	S5	D5	W	A4	C4	O4	S4	D4	W	A3	C3	O3	S3	D3	W	A2	C2	O2	S2	W
D	W	A5	C5	O5	S5	D5	W	A4	C4	O4	S4	D4	W	A3	C3	O3	S3	D3	W	A2	C2	O2	S2	W
E												W	A1	C1	O1	W	A1	C1	O1	W	A1	C1	O1	W

W: water, C: CHAPS, S: SDS, A: ASB, O: OGP, D: SDC
Conc. in % w/v: C/A/O: 10, 5, 1, 0.1, 0.01 S: 5, 1, 0.1, 0.01 D: 1, 0.1, 0.01

Figure 6: Surfactant samples on Waters™ standard target plate (a, b), and AnchorChip™ target plate (c,d). Samples on the standard target plate were prepared once and spotted three times.
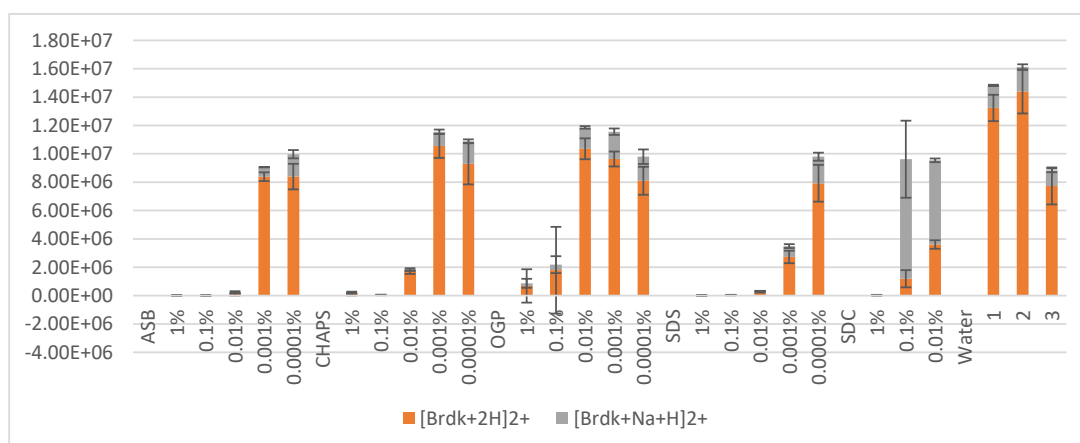
Figure 7: LAP-MALDI MS analysis of bradykinin with various surfactants at different concentrations using a Waters MALDI sample plate. All samples were prepared once and spotted 3 times. For higher concentrations, no signal could be generated due to droplet instability.
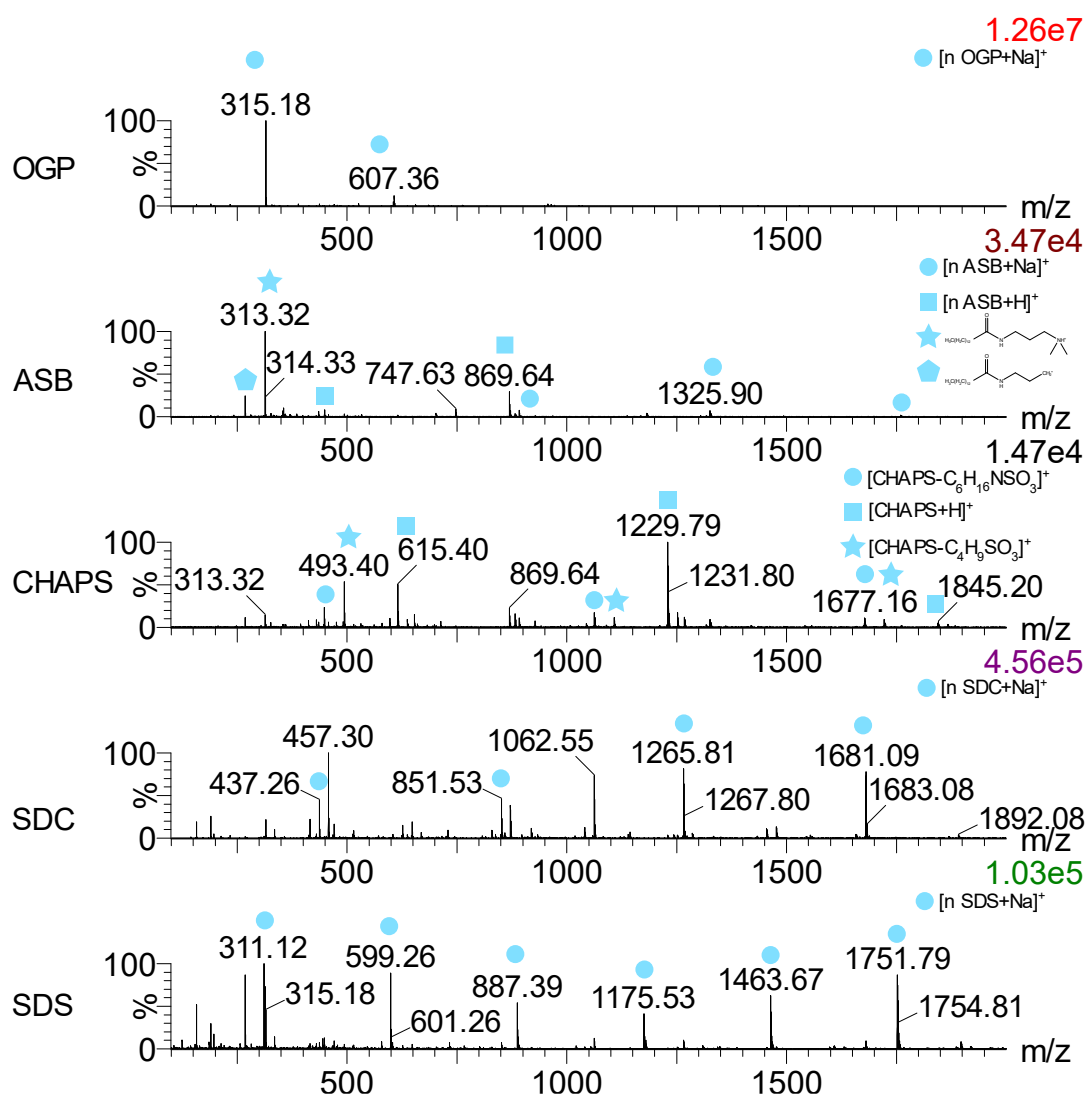
Figure 8: Mass spectra of peptide mix with surfactants and putatively identified signals originating from the surfactants. a) 34 mM OGP, b) 23 mM ASB, c) 16 mM CHAPS, d) 2.4 mM SDC, e) 3.5 mM SDS.

Table 9: Most abundant surfactant-related peaks observed in the mass spectra of the peptide mix. Theoretical values are calculated with chemcalc.org. Peaks denoted with * are also present in the control sample.

Surfactant	Type of ion	Theoretical m/z	Detected m/z	Mass error in ppm
ASB $C_{22}H_{46}N_2O_4S$	$[M+H]^+$	435.32511	435.3229*	5.08
	$[2M+H]^+$	869.64293	869.6343*	9.92
	$[3M+H]^+$	1303.96076	1303.9445	12.47
	$[M+Na]^+$	457.30705	457.3055*	3.39
	$[2M+Na]^+$	891.62488	891.6134*	12.88
	$[3M+Na]^+$	1325.94271	1325.9293*	10.11
	$[4M+Na]^+$	1760.26054	1760.2238	20.87
	$[M-(CH_2CH_2CH_2SO_3)+H]^+$	313.32134	313.3181*	10.34
	$[M-(NCH_3CH_3CH_2CH_2CH_2SO_3)]^+$	268.26349	268.2616*	7.05
CHAPS $C_{32}H_{58}N_2O_7S$	$[M+H]^+$	615.40375	615.4005	5.28
	$[2M+H]^+$	1229.80022	1229.7896	8.64
	$[3M+H]^+$	1844.19670	1844.1808	8.62
	$[M+Na]^+$	637.38569	637.3834	3.59
	$[2M+Na]^+$	1251.78217	1251.7723	7.88
	$[3M+Na]^+$	1866.17864	1866.1588	10.63
	$[M-(CH_2CH_2CH_2SO_3)+H]^+$	493.39998	493.3981*	3.81
	$[2M-(CH_2CH_2CH_2SO_3)+H]^+$	1107.79646	1107.7833	11.88
	$[3M-(CH_2CH_2CH_2SO_3)+H]^+$	1722.19293	1722.1769	9.31
	$[3M-(NCH_3CH_3CH_2CH_2CH_2SO_3)]^+$	1677.13508	1677.1226	7.44
	$[2M-(NCH_3CH_3CH_2CH_2CH_2SO_3)]^+$	1062.73861	1062.7328	5.47
	$[M-(NCH_3CH_3CH_2CH_2CH_2SO_3)]^+$	448.34214	448.3417*	0.98
OGP $C_{14}H_{28}O_6$	$[M+Na]^+$	315.17781	315.1767*	3.52
	$[2M+Na]^+$	607.36640	607.3624	6.59
SDS $CH_3(CH_2)_{11}OSO_3Na$	$[M+Na]^+$	311.12635	311.1244	6.27
	$[2M+Na]^+$	599.26347	599.2592	7.13
	$[3M+Na]^+$	887.40059	887.3923	9.34
	$[4M+Na]^+$	1175.53772	1175.5256	10.31
	$[5M+Na]^+$	1463.67484	1463.6611	9.39
	$[6M+Na]^+$	1751.81197	1751.7950	9.69
SDC $C_{24}H_{39}NaO_4$	$[M+Na]^+$	437.26382	437.2612	5.99
	$[2M+Na]^+$	851.53843	851.5314	8.26
	$[3M+Na]^+$	1265.81303	1265.8038	7.29
	$[4M+Na]^+$	1680.08764	1680.0741	8.06

Table 10: Overview of detected ions with less replicates than n=3 for samples and n=18 for the water control for 'surfactant' additives.

Analyte	m/z	Additive	Dilution	Number of replicates	Type of ion
Angiotensin I	1318.667	ASB-14	0.10%	2	$[M+Na]^+$
	1318.667	Water	-	17	$[M+Na]^+$
Substance P	685.362	CHAPS	0.10%	2	$[M+H+Na]^{2+}$
	1558.76	Water	-	16	$[M+CHCA+Na]^+$
Melittin	1434.375	CHAPS	0.10%	2	$[M+H+Na]^{2+}$
	1434.375	SDS	0.10%	2	$[M+H+Na]^{2+}$
	1434.375	Water	-	17	$[M+H+Na]^{2+}$

Table 11: Overview of detected ions with less replicates than n=3 for samples and n=9 for the water control for 'other' additives.

Analyte	m/z	Additive	Dilution	Number of replicates	Type of ion
Melittin	721.685	Urea	4 M	2	$[M+3H+K]^{4+}$

References

(1) Goldberg, R. N.; Kishore, N.; Lennen, R. M. Thermodynamic quantities for the ionization reactions of buffers. *Journal of Physical and Chemical Reference Data* **2002**, *31* (2), 231-370. DOI: 10.1063/1.1416902 (acccessed 2022/03/23).

(2) Kirchmann, H.; Pettersson, S. Human urine - Chemical composition and fertilizer use efficiency. *Fertilizer Research* **1995**, *40* (2), 149-154. DOI: 10.1007/bf00750100.

(3) Sviridov, D.; Hortin, G. L. Urine albumin measurement: effects of urine matrix constituents. *Clin. Chim. Acta* **2009**, *404* (2), 140-143. DOI: 10.1016/j.cca.2009.03.034 From NLM Medline.

(4) Aljerf, L.; Mashlah, A. Characterization and validation of candidate reference methods for the determination of calcium and magnesium in biological fluids. *Microchem. J.* **2017**, *132*, 411-421. DOI: 10.1016/j.microc.2017.03.001.

(5) Bel'skaya, L. V.; Kosenok, V. K.; Sarf, E. A. Chronophysiological features of the normal mineral composition of human saliva. *Arch Oral Biol* **2017**, *82*, 286-292. DOI: 10.1016/j.archoralbio.2017.06.024 From NLM Medline.

(6) Wu, A. H. B. *Tietz Clinical Guide to Laboratory Tests*; Saunders/Elsevier, 2006.

(7) Osanai, T.; Okuguchi, T.; Kamada, T.; Fujiwara, N.; Kosugi, T.; Saitoh, G.; Katoh, T.; Nakano, T.; Takahashi, K.; Guan, W.; et al. Salt-induced exacerbation of morning surge in blood pressure in patients with essential hypertension. *J. Hum. Hypertens.* **2000**, *14* (1), 57-64. DOI: 10.1038/sj.jhh.1000945 From NLM Medline.

(8) Eagle, H. Amino acid metabolism in mammalian cell cultures. *Science* **1959**, *130* (3373), 432-437. DOI: 10.1126/science.130.3373.432 (acccessed 2022/02/25). From NLM Medline.

(9) Niño, M. R. R.; Patino, J. M. R. Surface tension of bovine serum albumin and tween 20 at the air-aqueous interface. *Journal of the American Oil Chemists' Society* **1998**, *75* (10), 1241-1248. DOI: 10.1007/s11746-998-0169-6.

(10) Jones, O. T.; Earnest, J. P.; McNamee, M. G. Solubilization and reconstitution of membrane proteins. In *Biological membranes*, Findlay, J. B. C., Evans, W. H. Eds.; A Practical Approach, Oxford University Press, 1987.

(11) Nguyen, T. B.; Phan, C. M. Influence of Temperature on the Surface Tension of Triton Surfactant Solutions. *Journal of Surfactants and Detergents* **2019**, *22* (2), 229-235. DOI: https://doi.org/10.1002/jsde.12228.

(12) *NP-40 Alternative*. Merck KGaA, 2023. https://www.sigmaaldrich.com/GB/en/product/mm/492016 (accessed 2023 21/08/2023).

(13) D'Andrea, M. G.; Domingues, C. C.; Malheiros, S. V.; Neto, F. G.; Barbosa, L. R.; Itri, R.; Almeida, F. C.; de Paula, E.; Bianconi, M. L. Thermodynamic and structural characterization of zwitterionic micelles of the membrane protein solubilizing amidosulfobetaine surfactants ASB-14 and ASB-16. *Langmuir* **2011**, *27* (13), 8248-8256. DOI: 10.1021/la1037525 From NLM Medline.

(14) Razafindralambo, H.; Blecker, C.; Delhaye, S.; Paquot, M. Application of the Quasi-Static Mode of the Drop Volume Technique to the Determination of Fundamental Surfactant Properties. *J. Colloid Interface Sci.* **1995**, *174* (2), 373-377. DOI: 10.1006/jcis.1995.1404.

(15) Castro, G.; Amigo, A.; Brocos, P. Squeezing experimental measurements for a proper analysis of surfactant thermodynamics: Octyl-β-d-glucopyranoside as a case study. *Fluid Phase Equilibria* **2014**, *376*, 31-39. DOI: 10.1016/j.fluid.2014.05.035.

(16) Kumar, K.; Chauhan, S. Surface tension and UV-visible investigations of aggregation and adsorption behavior of NaC and NaDC in water-amino acid mixtures. *Fluid Phase Equilibria* **2015**, *394*, 165-174. DOI: 10.1016/j.fluid.2015.03.012.

(17) Fuguet, E.; Rafols, C.; Roses, M.; Bosch, E. Critical micelle concentration of surfactants in aqueous buffered and unbuffered systems. *Anal. Chim. Acta* **2005**, *548* (1-2), 95-100. DOI: 10.1016/j.aca.2005.05.069.

3. Conclusion and future work

First and above all, the general applicability of LAP-MALDI for high sample throughput was shown. Standards were analysed at 5 samples/s and even for extracts from complex biological samples, analysis speeds of 1 sample per second were achieved. From there, substantial changes to the hardware used in the ionisation source were made. The upgrade to a laser with a higher laser pulse repetition frequency allowed the creation of more ions per time unit and hence the increase of analysis speed (NB: more stringent health and safety regulations had to be met as those lasers are often classified as type 4 lasers). Next, sample plate manipulation was improved by installing a more powerful translational stage, which additionally allowed the movement of larger objects due to an increased range of movement. This was used to replace the manufacturer-specific target plates (1/4 MTP-format) with standardised MTP-format targets which allows a more automated sample preparation. To accommodate both types of target plates, the software for sample movement was adjusted and a new holder was designed and manufactured (see Appendix A.2).

In this work, LAP-MALDI was used with a commercially available QToF instrument. The chosen mass spectrometer proved to be well suited for high-speed analyses. Although ions are not continuously detected in orthogonal ToF instruments, duty cycles have increased significantly with time. The advantage of ToF detection over Fourier-transform instruments is the independence of mass resolution from the speed of analysis (for time dependence of FT see Muller et al.). Besides the influence of the transient time in trapping instruments, the coupling with the ionisation source is more difficult due to the necessity to synchronise the arrival of ions with trapping.[63] Although QToF instruments are in general well suited for fast analyses, the instrument software needed to be adapted to get a more temporally resolved read-out with less dead-time (ISD). Faster electronics and improved data processing were sought to further increase the data quality for high-speed analyses.

Here, an analysis speed of over 40 samples per second was demonstrated. Most other MS-based techniques report speeds lower than 5 samples/s, with the exception of IR-MALDESI with 22 samples/s. ESI and ESI-derived techniques suffer from the rate-limiting sample introduction, while non-contact sampling as found in AMI or MALDI-derived methods is inherently faster. Additionally, lower sample volumes are required and the risk of cross-contamination is reduced. From those non-contact based techniques, LAP-MALDI was shown to offer the highest sample throughput compared to any other mass spectrometric method presented in the literature (see Table 1.3). Further improvements might be possible by increasing the density of sample spots as discussed in section 2.3. The theoretical limitation of the analysis speed is given by the width of each ion signal per desorption/ionisation event (for example measured as full width at half maximum (FWHM)). For LAP-MALDI a FWHM of around 3 ms was reported.[133] In contrast, for ADE 105 ms were described.[120]

Besides analysis speed, the signal stability is important to consider when analysing large sample sets. Here, CVs of < 10 %, for one analyte < 5 % were reported at 9 samples/s (see section 2.3). For higher speeds, higher CVs were obtained. A similar behaviour was described for IR-MALDESI, for which values between 6 and 25 % were obtained at 0.53 and 0.8 samples/s.[63] For slower techniques like the ESI-based RapidFire better CVs of 1.7 %[135] were reported. In a direct comparison between MALDI and ESI screens, higher CVs were reported for the faster MALDI assay.[136] Hence, the stability of the method needs to be carefully evaluated, especially for very high acquisition speeds. Hardware modifications as described below might help to achieve low CVs at high analysis speeds although some applications might still require to lower the speed in order to increase the reproducibility.

When choosing between the available techniques for a mass spectrometry-based screen, factors other than the speed of acquisition, such as ease-of-use, costs of acquisition and operation, versatility and availability need to be considered. Many of the presented ionisation techniques for HTS are commercialised in a vendor-specific way (ESI: Rapid-Fire from Agilent, DESI: DESI-XS from Waters, MALDI: PharmaPulse from Bruker, ADE: ECHO from Sciex). In contrast, IR-MALDESI and LAP-MALDI are not commercialised yet. The operation of the LAP-MALDI source is largely manual and requires skilled workforce as well as special safety precautions due to the open-beam laser. These drawbacks can be addressed in the future through a more automated and re-designed setup as found in the commercial products. The example of MALDI has shown that laser-based methods can be applied in a variety of environments other than research

and the required level of training can be lowered to a cost-effective level by automation (e.g. "sweet-spot hunting" is alleviated by rastering algorithms and intensity checks). In a similar way, LAP-MALDI can be further developed to facilitate its use and enhance reproducibility.

Here, software changes were made to enable the acquisition of several samples in one data file and subsequent data slicing (see sections 2.3 and 2.4). To further facilitate the use of LAP-MALDI, an easier workflow from laser alignment and focussing (see statement about optical setup below) to the actual data acquisition would be desirable. First steps into this direction were taken by integrating the laser control, sample introduction and data acquisition into a one-button control software (see Appendix A.3). This Arduino script can not only control the laser but can also be used within a sample list (to analyse a set of samples). In contrast, the use of Waters Research Enabling Software (WREnS) (see section 2.4) allows labelling of scans with the sample position, which facilitates data processing. A future possibility would be to integrate the Arduino script into the WREnS script. This would allow the use of advanced features like the labelling of scans with the sample position while controlling external components such as the laser. For future experiments, this setup could be used to easily analyse large sample sets or, in conjunction with the features of WREnS, screen for the best analysis conditions by varying the source conditions. Additionally, when using the acquisition from the sample list, each sample set could be analysed in full scan mode first and subsequently, one or multiple fragmentation experiments could be carried out. A similar approach has been demonstrated for the screening of chemical reactions.[56]

HTS is a special application of high-speed analyses as normally no replicates are measured. To improve inter-day reproducibility of LAP-MALDI, in particular for HTS applications, three main points should be addressed. Firstly, the robustness of the optical setup could be improved. Namely, the incidence angle (in respect to the inlet tube and in respect to the x axis) probably has an effect on the generated ion signal (also see[131]) and should be precisely controlled. If choosing a very small angle combined with a short focal length, the use of a lens with a central bore[137] around the inlet tube might be beneficial. To facilitate the laser focussing, a motorised lens mount could be implemented.

Secondly, the use of disposable target plates will eliminate the risk of contamination of individual sample locations. The presence of residual compounds, including salts, can significantly change the obtained mass spectra as shown in section 2.4. Many MALDI manufacturers like Bruker and Shimadzu already offer disposable substrates.

Thirdly, the distance between the target plate and inlet tube as well the positioning of the sample in front of the inlet tube needs to be constant across the whole plate to ensure an equal electric field and laser focus. With the holder designed in this work (see Appendix A.2), a fine angle adjustment is not possible, hence, the CVs of below 10 % presented in section 2.3 were only achieved over a small range of sample locations. To overcome this limitation, a re-design of the holder, for example by incorporating a gimbal-mount, would be beneficial. Also, a spring to fix non-ferromagnetic plates as those from Bruker should be integrated. With the perspective of an automated plate-loading system using robotic translocation, an easier sliding-in of the target plate would be desirable.

The versatility of the different HTS methods in terms of accessible analytes certainly depends on the underlying mechanism of ionisation. In the proof-of-principle work presented here, HTS using LAP-MALDI was shown for complex biological matrices (milk), small molecules, enzymatic assays and peptides. Thanks to the creation of multiply charged ions, the screening of collisionally-induced peptide fragments was shown as well. This is a clear advantage over conventional MALDI for which mainly singly charged ions are created which are inherently more difficult to fragment. The analysis of enzymatic assays using LAP-MALDI is only possible offline, as enzymatic reactions are quenched when mixing with matrix. This "discontinuous" mode of analysis is also true for conventional MALDI and DESI (see Table 1.3). During an initial screen this endpoint evaluation of an enzymatic reaction is sufficient. However, non-interfering techniques, such as IR-MALDESI, ADE and AMI offer the additional possibility to study the enzyme kinetics. Although this is might not be possible by LAP-MALDI, a similar method without need for the matrix[138] could be used.

When studying enzymatic activity, the appearance and disappearance of small molecule substrate or products are monitored. However, for some assays such as binding studies, the monitoring of large molecules or complexes is required. The fast analysis of such large molecular weight analytes has been a main advantage of conventional MALDI over most ambient ionisation techniques. Recently, the fast analysis of proteins and antibodies was shown for ADE (1 sample/s)[139] and IR-MALDESI (22 samples/s).[140] For LAP-MALDI this remains to be shown. The analysis of medium-sized proteins using LAP-MALDI is possible[40] and should be further evaluated in the context of HTS. Especially, the growing interest in biologics[141,142] has led to an increased demand in fast and specific analytical tools to ensure their high quality production[143] and efficient use in treatment.

Most of the ionisation techniques used for HTS do not require an extensive sample preparation as this would limit the throughput. However, compounds present in these assays might interfere with the detection of analyte signal. Although some general guidance on "mass spectrometry-friendly" reagents exist, the susceptibility of different ionisation techniques to various additives will vary as their exact mechanism of ionisation is different. As shown in section 2.4, LAP-MALDI analysis is influenced by many compounds frequently present in biochemical assays. The results obtained from this systematic study will guide future assay development.

One mayor challenge for high-speed analysis is the fast preparation of samples. Ideally, these should be analysed without the need for time-consuming steps. In contrast to ESI, an additional step for mixing with the matrix is necessary. For future applications, an automated sample preparation would be beneficial. The development of LSM without glycerol comes handy in less viscous liquids are easier to handle. For mixing the sample with matrix and spotting it onto target plates, liquid handlers with multiple channels are most suitable. They are very time-efficient as the channels (for example 96 or 384) are used simultaneously. As only less than $1\,\mu$L of sample is needed (see section 2.3) for analysis, devices which can reproducibly deliver small volumes are required (see Appendix A.4). Most systems operate using a relatively narrow volume range which limits the field of application and exhibit lower precision for small volumes which are of interest for LAP-MALDI. For instance the CV for dispensing $0.5\,\mu$L using the CyBio Well Vario is $10\,\%$ (see Appendix A.4). A system specialised on sub-μL liquid handling is the Mosquito from SPTLabTech. A spool with positive displacement tips is used to deliver 8 or 12 samples at a time. So, a 384-MTP can be spotted in $3\,$min. The Mosquito is reported to give $3\,\%$ accuracy even at the lowest volume ($25\,$nL).

In principle, two modes of mixing the sample and matrix exist. Both liquids can be delivered to the target and mixed on target or the liquids can be mixed in larger volumes prior to spotting. The latter is more accurate as larger volumes are used and is required if a direct analysis from MTP is desired. As the required volume of matrix increases, the reagent costs for the matrix would be slightly higher. For example, the analysis of 1 million compounds in 1536-well MTP with a working volume of $10\,\mu$L would require approximately 652 plates and $5\,$L of matrix. The current prices (merck.com, 13.02.2023) for LC-MS water (2.5L, 28£, cat. no. 1.15333), acetonitrile (2.5L, 173£, cat. no. 1.00029) and α-CHCA (5 g, 327£, cat. no. 70990) would mean that for one sample around 0.01 pence needs to be spent for the matrix. For 384-well MTPs with a working volume of $20\,\mu$L around $10\,$L of matrix are required, i.e. 0.02 pence/sample. In contrast,

the costs for one pipette tip (eppendorf.com, cat. number 0030076044, 13.02.2023) are around 11 pence. This highlights on one hand that additional liquid handling steps should be avoided, as even when re-using tips time and reagents for the washing are required. On the other hand it shows that miniaturisation of the sample preparation can significantly reduce the reagent costs.

Due to the number of samples typically encountered in HTS, the direct analysis from MTP in which the assays are prepared is beneficial and has been shown for IR-MALDESI[103] and ADE.[62] For DESI,[144] LAP-MALDI and conventional MALDI[92] an additional transfer to the substrate is necessary. For future applications, a direct analysis from MTP would be desirable. This would reduce the required steps (only mixing, which is possible with normal liquid handling already routinely used in industry), avoid the need for specialised liquid handlers and potentially reduce costs.

In general, requirements for a suitable LAP-MALDI substrate are chemical resistance, low-cost, a non-contaminating composition (polymeric structures), a suitable surface-structure to hold droplets (also see surfactant section in section 2.4) and electrical conductivity. For the use of MTP as substrates the most challenging requirement to fulfil is the conductivity to allow charge separation (see section 1.2 and Appendix A.1). This can be achieved by using coated MTPs or ones produced from electrically-conductive plastic. LazWell™plates normally used for LDTP-APCI have a continuous end-to-end conductive bottom which could facilitate electrical connectivity. In general, these special MTPs are expensive but the decreased costs from reduced liquid handling steps could still outweigh the investment. A possibility to avoid the need for a conductive plate material is to use a floating voltage as for example used in AMI.

To use MTP for LAP-MALDI analysis routinely, some adjustments to the mechanical and optical setup would be necessary. A schematic drawing is given in Appendix Figure A.7. The positioning of the laser optics, namely the last mirror becomes more difficult as only a narrow range of incidence angles α allows the laser beam to irradiate the sample without hitting the inlet tube or the walls of the MTP.

Another challenge arises from the z-positioning of the MTP. The current analysis from stainless-steel substrates uses a distance between target plate and inlet tube of around 3 mm. When using MTPs the distance between the surface of the sample and the inlet tube might vary due to different fill levels. A constant distance could be achieved by adjusting the translational stage in z-axis to ensure optimal laser focussing. Similar challenges are known from MALDI imaging experiments using samples of varying thickness.

To circumvent this, a confocal distance sensor has been mounted in line with the laser beam to determine and adjust the distance of the sample.[145] A similar approach was used by the Spengler group to correct AP-MALDI sample height by laser triangulation using a visible light diode.[146] A low-cost alternative is the determination of the plate position along the z-axis for different fill levels for a set of MTPs as a set calibration. Between the liquid dispensing and the LAP-MALDI analysis an optical fill level determination[147] can be carried out. This method might not be sensitive enough to detect small volume changes between wells but is able to find failed liquid transfers.

When adjusting the z-positioning of the plate, this could mean that the inlet tube protrudes into the cavities of the plate. Firstly, this would result in electrical arcing as the distance between the, supposedly electrically conducting, plate and the inlet tube is reduced. Secondly, conditions of the developing plume probably change dramatically due to the space restrictions and changes in gas flow.

In summary, the current work presents LAP-MALDI as a high-speed ionisation technique for mass spectrometry. Highly competitive acquisition times were obtained and ideas to further develop the technique were given.

Bibliography

(1) Chakraborty, P.; Pradeep, T. *NPG Asia Materials* **2019**, *11*, 48, DOI: `10.1038` `/s41427-019-0149-3`.

(2) Richardson, S. D. *Chemical Reviews* **2001**, *101*, 211–254, DOI: `10.1021/cr990` `090u`.

(3) Arevalo Jr, R.; Ni, Z.; Danell, R. M. *Journal of Mass Spectrometry* **2020**, *55*, e4454, DOI: `10.1002/jms.4454`.

(4) Swiner, D. J.; Jackson, S.; Burris, B. J.; Badu-Tawiah, A. K. *Analytical Chemistry* **2020**, *92*, 183–202, DOI: `10.1021/acs.analchem.9b04901`.

(5) Alberts, B.; Bray, D.; Hopkin, K.; Johnson, A.; Lewis, J.; Raff, M.; Roberts, K.; Walter, P., *Essential Cell Biology*; CRC Press: 2015.

(6) Keller, C.; Maeda, J.; Jayaraman, D.; Chakraborty, S.; Sussman, M. R.; Harris, J. M.; Ane, J. M.; Li, L. *Front Plant Sci* **2018**, *9*, 1238, DOI: `10.3389/fpls.20` `18.01238`.

(7) Feijó Delgado, F.; Cermak, N.; Hecht, V. C.; Son, S.; Li, Y.; Knudsen, S. M.; Olcum, S.; Higgins, J. M.; Chen, J.; Grover, W. H.; Manalis, S. R. *PLoS One* **2013**, *8*, e67590, DOI: `10.1371/journal.pone.0067590`.

(8) Muttenthaler, M.; King, G. F.; Adams, D. J.; Alewood, P. F. *Nature Reviews Drug Discovery* **2021**, *20*, 309–325, DOI: `10.1038/s41573-020-00135-8`.

(9) IUPAC. Compendium of Chemical Terminology, 2nd ed. (the "Gold Book"), Encyclopedia, 1997, DOI: `https://doi.org/10.1351/goldbook`.

(10) Boyd, R.; Somogyi, Á. *Journal of the American Society for Mass Spectrometry* **2010**, *21*, 1275–1278, DOI: `10.1016/j.jasms.2010.04.017`.

(11) Wysocki, V. H.; Tsaprailis, G.; Smith, L. L.; Breci, L. A. *Journal of Mass Spectrometry* **2000**, *35*, 1399–1406, DOI: `10.1002/1096-9888(200012)35:12<1399` `::AID-JMS86>3.0.CO;2-R`.

(12) Vékey, K. *Journal of Mass Spectrometry* **1996**, *31*, 445–463, DOI: `10.1002/(SICI)1096-9888(199605)31:5<445::AID-JMS354>3.0.CO;2-G`.

(13) Kebarle, P.; Verkerk, U. H. *Mass Spectrom Rev* **2009**, *28*, 898–917, DOI: `10.1002/mas.20247`.

(14) Konermann, L.; Ahadi, E.; Rodriguez, A. D.; Vahidi, S. *Anal Chem* **2013**, *85*, 2–9, DOI: `10.1021/ac302789c`.

(15) Aliyari, E.; Konermann, L. *Anal Chem* **2020**, *92*, 10807–10814, DOI: `10.1021/acs.analchem.0c02290`.

(16) Aliyari, E.; Konermann, L. *Analytical Chemistry* **2022**, *94*, 7713–7721, DOI: `10.1021/acs.analchem.2c01355`.

(17) Karas, M.; Bachmann, D.; Hillenkamp, F. *Analytical Chemistry* **1985**, *57*, 2935–2939, DOI: `10.1021/ac00291a042`.

(18) Niehaus, M.; Soltwisch, J. *Sci Rep* **2018**, *8*, 7755, DOI: `10.1038/s41598-018-25946-z`.

(19) Fournier, I.; Brunot, A.; Tabet, J. C.; Bolbach, G. *J Mass Spectrom* **2005**, *40*, 50–9, DOI: `10.1002/jms.772`.

(20) Haglund, R. F. In *Lasers in Materials Science*, Castillejo, M., Ossi, P. M., Zhigilei, L., Eds.; Springer Series in Materials Science; Springer International Publishing: Cham, 2014; Chapter 1, pp 1–28, DOI: `10.1007/978-3-319-02898-9_1`.

(21) Zhigilei, L. V.; Garrison, B. J. *Journal of Applied Physics* **2000**, *88*, 1281–1298, DOI: `10.1063/1.373816`.

(22) Allwood, D. A.; Dreyfus, R. W.; Perera, I. K.; Dyer, P. E. *Rapid Communications in Mass Spectrometry* **1996**, *10*, 1575–1578, DOI: `10.1002/(SICI)1097-0231(199610)10:13<1575::AID-RCM658>3.0.CO;2-C`.

(23) Dreisewerd, K. *Chemical Reviews* **2003**, *103*, 395–426, DOI: `10.1021/cr010375i`.

(24) Chu, K. Y.; Lee, S.; Tsai, M.-T.; Lu, I. C.; Dyakov, Y. A.; Lai, Y. H.; Lee, Y.-T.; Ni, C.-K. *Journal of the American Society for Mass Spectrometry* **2014**, *25*, 310–318, DOI: `10.1007/s13361-013-0792-9`.

(25) Hillenkamp, F.; Peter-Katalinić, J., *MALDI MS : a practical guide to instrumentation, methods, and applications*, Second edition., Wiley Blackwell: Weinheim, 2013.

(26)   Phipps, C., *Laser Ablation and its Applications*; Springer Series in Optical Sciences; Springer US: 2007.

(27)   Rohlfing, A.; Leisner, A.; Hillenkamp, F.; Dreisewerd, K. *Journal of Physical Chemistry C* **2010**, *114*, 5367–5381, DOI: `10.1021/jp905251r`.

(28)   Hellwig, N. Das Laserablationsverhalten von ionischen Flüssigkeiten verschiedener MALDI-Matrices, PhD, 2012.

(29)   Fan, X.; Murray, K. K. *J Phys Chem A* **2010**, *114*, 1492–7, DOI: `10.1021/jp9 077163`.

(30)   Knochenmuss, R. *Annu Rev Anal Chem* **2016**, *9*, 365–85, DOI: `10.1146/annur ev-anchem-071015-041750`.

(31)   Jaskolla, T. W.; Karas, M. *J Am Soc Mass Spectrom* **2011**, *22*, 976–88, DOI: `10.1007/s13361-011-0093-0`.

(32)   Hoteling, A. J.; Nichols, W. F.; Giesen, D. J.; Lenhard, J. R.; Knochenmuss, R. *European Journal of Mass Spectrometry* **2006**, *12*, 345–358, DOI: `10.1255/ejm s.820`.

(33)   Dai, Y.; Whittal, R. M.; Li, L. *Anal Chem* **1996**, *68*, 2494–500, DOI: `10.1021 /ac960238z`.

(34)   Luxembourg, S. L.; McDonnell, L. A.; Duursma, M. C.; Guo, X.; Heeren, R. M. *Anal Chem* **2003**, *75*, 2333–41, DOI: `10.1021/ac026434p`.

(35)   Sze, E. T. P.; Chan, T. W. D.; Wang, G. *Journal of the American Society for Mass Spectrometry* **1998**, *9*, 166–174, DOI: `10.1016/s1044-0305(97)00237-7`.

(36)   Cramer, R.; Corless, S. *Proteomics* **2005**, *5*, 360–70, DOI: `10.1002/pmic.2004 00956`.

(37)   Beaufour, M.; Ginguene, D.; Le Meur, R.; Castaing, B.; Cadene, M. *Journal of the American Society for Mass Spectrometry* **2018**, *29*, 1981–1994, DOI: `10.10 07/s13361-018-2015-x`.

(38)   Towers, M. W.; McKendrick, J. E.; Cramer, R. *J Proteome Res* **2010**, *9*, 1931–40, DOI: `10.1021/pr901089j`.

(39)   Turney, K.; Harrison, W. W. *Rapid Commun Mass Spectrom* **2004**, *18*, 629–35, DOI: `10.1002/rcm.1379`.

(40)   Ryumin, P.; Cramer, R. *Anal Chim Acta* **2018**, *1013*, 43–53, DOI: `10.1016/j.a ca.2018.01.070`.

(41) Schurenberg, M.; Dreisewerd, K.; Hillenkamp, F. *Anal Chem* **1999**, *71*, 221–9, DOI: `10.1021/ac980634c`.

(42) Tanaka, K.; Waki, H.; Ido, Y.; Akita, S.; Yoshida, Y.; Yoshida, T.; Matsuo, T. *Rapid Communications in Mass Spectrometry* **1988**, *2*, 151–153, DOI: `10.1002 /rcm.1290020802`.

(43) Batoy, S. M. A. B.; Akhmetova, E.; Miladinovic, S.; Smeal, J.; Wilkins, C. L. *Applied Spectroscopy Reviews* **2008**, *43*, 485–550, DOI: `10.1080/057049208021 08198`.

(44) Laiko, V. V.; Moyer, S. C.; Cotter, R. J. *Anal Chem* **2000**, *72*, 5239–43, DOI: `10.1021/ac000530d`.

(45) Doroshenko, V. M.; Laiko, V. V.; Taranenko, N. I.; Berkout, V. D.; Lee, H. S. *International Journal of Mass Spectrometry* **2002**, *221*, 39–58, DOI: `10.1016/S1 387-3806(02)00893-X`.

(46) Belov, M. E.; Ellis, S. R.; Dilillo, M.; Paine, M. R. L.; Danielson, W. F.; Anderson, G. A.; de Graaf, E. L.; Eijkel, G. B.; Heeren, R. M. A.; McDonnell, L. A. *Anal Chem* **2017**, *89*, 7493–7501, DOI: `10.1021/acs.analchem.7b01168`.

(47) Moskovets, E.; Misharin, A.; Laiko, V.; Doroshenko, V. *Methods* **2016**, *104*, 21–32, DOI: `10.1016/j.ymeth.2016.02.009`.

(48) Schneider, B. B.; Lock, C.; Covey, T. R. *J Am Soc Mass Spectrom* **2005**, *16*, 176–82, DOI: `10.1016/j.jasms.2004.10.004`.

(49) Cramer, R.; Pirkl, A.; Hillenkamp, F.; Dreisewerd, K. *Angewandte Chemie* **2013**, *125*, 2420–2424, DOI: `10.1002/ange.201208628`.

(50) Spross, J.; Muck, A.; Groger, H. *Anal Bioanal Chem* **2019**, *411*, 6275–6285, DOI: `10.1007/s00216-019-01578-8`.

(51) Koch, A.; Schnapp, A.; Soltwisch, J.; Dreisewerd, K. *International Journal of Mass Spectrometry* **2017**, *416*, 61–70, DOI: `10.1016/j.ijms.2016.11.007`.

(52) Hoffmann, E. d.; Stroobant, V., *Mass spectrometry : principles and applications*, Third edition; John Wiley and Sons, Ltd: 2007.

(53) Sleno, L.; Volmer, D. A. *Journal of Mass Spectrometry* **2004**, *39*, 1091–1112, DOI: `10.1002/jms.703`.

(54) Bayat, P.; Lesage, D.; Cole, R. B. *Mass Spectrometry Reviews* **2020**, *39*, 680–702, DOI: `10.1002/mas.21623`.

(55) DiRico, K. J.; Hua, W.; Liu, C.; Tucker, J. W.; Ratnayake, A. S.; Flanagan, M. E.; Troutman, M. D.; Noe, M. C.; Zhang, H. *ACS Medicinal Chemistry Letters* **2020**, *11*, 1101–1110, DOI: `10.1021/acsmedchemlett.0c00066`.

(56) Wleklinski, M.; Loren, B. P.; Ferreira, C. R.; Jaman, Z.; Avramova, L.; Sobreira, T. J. P.; Thompson, D. H.; Cooks, R. G. *Chem Sci* **2018**, *9*, 1647–1653, DOI: `10.1039/c7sc04606e`.

(57) Sobreira, T. J. P.; Avramova, L.; Szilagyi, B.; Logsdon, D. L.; Loren, B. P.; Jaman, Z.; Hilger, R. T.; Hosler, R. S.; Ferreira, C. R.; Koswara, A.; Thompson, D. H.; Cooks, R. G.; Nagy, Z. K. *Anal Methods* **2020**, *12*, 3654–3669, DOI: `10.1039/d0ay00072h`.

(58) Le, M. T.; Morato, N. M.; Kaerner, A.; Welch, C. J.; Cooks, R. G. *J Am Soc Mass Spectrom* **2021**, *32*, 2261–2273, DOI: `10.1021/jasms.1c00176`.

(59) Hoang, K.; Trimpin, S.; McEwen, C. N.; Pophristic, M. *J Am Soc Mass Spectrom* **2021**, *32*, 124–132, DOI: `10.1021/jasms.0c00298`.

(60) Hasegawa, T.; Imamura, R. M.; Suzuki, T.; Hashiguchi, T.; Nomura, T.; Otsuguro, S.; Maenaka, K.; Sasaki, M.; Orba, Y.; Sawa, H.; Sato, A.; Okabe, T.; Nagano, T.; Kojima, H. *Chem Pharm Bull (Tokyo)* **2022**, *70*, 199–201, DOI: `10.1248/cpb.c21-01003`.

(61) Wen, X.; Liu, C.; Ghislain, L.; Tovar, K.; Shah, V.; Stout, S. J.; Cifelli, S.; Satapati, S.; O'Donnell, G.; Sheth, P. R.; Wildey, M. J.; Datwani, S. S.; Covey, T. R.; Bateman, K. P.; McLaren, D. G. *Anal Chem* **2021**, *93*, 6071–6079, DOI: `10.1021/acs.analchem.0c04312`.

(62) Simon, R. P.; Habe, T. T.; Ries, R.; Winter, M.; Wang, Y.; Fernandez-Montalvan, A.; Bischoff, D.; Runge, F.; Reindl, W.; Luippold, A. H.; Buttner, F. H. *SLAS Discov* **2021**, *26*, 961–973, DOI: `10.1177/24725552211028135`.

(63) Pu, F.; Radosevich, A. J.; Sawicki, J. W.; Chang-Yen, D.; Talaty, N. N.; Gopalakrishnan, S. M.; Williams, J. D.; Elsen, N. L. *Anal Chem* **2021**, *93*, 6792–6800, DOI: `10.1021/acs.analchem.1c00737`.

(64) McLaren, D. G.; Shah, V.; Wisniewski, T.; Ghislain, L.; Liu, C.; Zhang, H.; Saldanha, S. A. *SLAS Discovery* **2021**, *26*, 168–191, DOI: `10.1177/247255522 0980696`.

(65) Dragovich, P. S.; Haap, W.; Mulvihill, M. M.; Plancher, J.-M.; Stepan, A. F. *Journal of Medicinal Chemistry* **2022**, *65*, 3606–3615, DOI: `10.1021/acs.jmed chem.1c02106`.

(66) Brown, D. G.; Boström, J. *Journal of Medicinal Chemistry* **2018**, *61*, 9442–9468, DOI: `10.1021/acs.jmedchem.8b00675`.

(67) Blass, B. E. In *Basic Principles of Drug Discovery and Development*, Blass, B. E., Ed.; Academic Press: Boston, 2015; Chapter 7, pp 307–343, DOI: `10.1016/b97 8-0-12-411508-8.00007-4`.

(68) An, W. F.; Tolliday, N. *Mol Biotechnol* **2010**, *45*, 180–6, DOI: `10.1007/s12033 -010-9251-z`.

(69) Blay, V.; Tolani, B.; Ho, S. P.; Arkin, M. R. *Drug Discovery Today* **2020**, *25*, 1807–1821, DOI: `10.1016/j.drudis.2020.07.024`.

(70) Fox, S.; Farr-Jones, S.; Sopchak, L.; Boggs, A.; Nicely, H. W.; Khoury, R.; Biros, M. *Journal of Biomolecular Screening* **2006**, *11*, 864–869, DOI: `10.1177/10870 57106292473`.

(71) Busby, S. A.; Carbonneau, S.; Concannon, J.; Dumelin, C. E.; Lee, Y.; Numao, S.; Renaud, N.; Smith, T. M.; Auld, D. S. *ACS Chemical Biology* **2020**, *15*, 2636–2648, DOI: `10.1021/acschembio.0c00495`.

(72) Inglese, J.; Johnson, R. L.; Simeonov, A.; Xia, M.; Zheng, W.; Austin, C. P.; Auld, D. S. *Nat Chem Biol* **2007**, *3*, 466–79, DOI: `10.1038/nchembio.2007.17`.

(73) Gribbon, P.; Lyons, R.; Laflin, P.; Bradley, J.; Chambers, C.; Williams, B. S.; Keighley, W.; Sewing, A. *J Biomol Screen* **2005**, *10*, 99–107, DOI: `10.1177/10 87057104271957`.

(74) Rask-Andersen, M.; Almén, M. S.; Schiöth, H. B. *Nature Reviews Drug Discovery* **2011**, *10*, 579–590, DOI: `10.1038/nrd3478`.

(75) Acker, M. G.; Auld, D. S. *Perspectives in Science* **2014**, *1*, 56–73, DOI: `10.101 6/j.pisc.2013.12.001`.

(76) Schuffenhauer, A. et al. *Journal of Medicinal Chemistry* **2020**, *63*, 14425–14447, DOI: `10.1021/acs.jmedchem.0c01332`.

(77) Engels, M. F. M.; Gibbs, A. C.; Jaeger, E. P.; Verbinnen, D.; Lobanov, V. S.; Agrafiotis, D. K. *Journal of Chemical Information and Modeling* **2006**, *46*, 2651–2660, DOI: `10.1021/ci600219n`.

(78) Schamberger, J.; Grimm, M.; Steinmeyer, A.; Hillisch, A. *Drug Discovery Today* **2011**, *16*, 636–641, DOI: `10.1016/j.drudis.2011.04.005`.

(79) Kogej, T.; Blomberg, N.; Greasley, P. J.; Mundt, S.; Vainio, M. J.; Schamberger, J.; Schmidt, G.; Hüser, J. *Drug Discovery Today* **2013**, *18*, 1014–1024, DOI: 10.1016/j.drudis.2012.10.011.

(80) Morgan, P. et al. *Nature Reviews Drug Discovery* **2018**, *17*, 167–181, DOI: 10.1038/nrd.2017.244.

(81) Van Vlijmen, H.; Ortholand, J.-Y.; Li, V. M. J.; de Vlieger, J. S. B. *Drug Discovery Today* **2021**, *26*, 2406–2413, DOI: 10.1016/j.drudis.2021.04.019.

(82) Bakken, G. A.; Bell, A. S.; Boehm, M.; Everett, J. R.; Gonzales, R.; Hepworth, D.; Klug-McLeod, J. L.; Lanfear, J.; Loesel, J.; Mathias, J.; Wood, T. P. *Journal of Chemical Information and Modeling* **2012**, *52*, 2937–2949, DOI: 10.1021/ci300372a.

(83) Ballell, L. et al. *ChemMedChem* **2013**, *8*, 313–321, DOI: 10.1002/cmdc.201200428.

(84) Mayr, L. M.; Bojanic, D. *Curr Opin Pharmacol* **2009**, *9*, 580–8, DOI: 10.1016/j.coph.2009.08.004.

(85) Martis, E.; Radhakrishnan, R.; Badve, R. *Journal of Applied Pharmaceutical Science* **2011**, 02–10.

(86) Sundberg, S. A. *Current Opinion in Biotechnology* **2000**, *11*, 47–53, DOI: 10.1016/S0958-1669(99)00051-8.

(87) Thorne, N.; Auld, D. S.; Inglese, J. *Current Opinion in Chemical Biology* **2010**, *14*, 315–324, DOI: 10.1016/j.cbpa.2010.03.020.

(88) Baell, J. B.; Holloway, G. A. *Journal of Medicinal Chemistry* **2010**, *53*, 2719–2740, DOI: 10.1021/jm901137j.

(89) Zhang, J.-h.; Wu, X.; Sills, M. A. *Journal of Biomolecular Screening* **2005**, *10*, 695–704, DOI: 10.1177/1087057105279149.

(90) Choo, M. Z. Y.; Chai, C. L. L. *ChemMedChem* **2022**, *17*, e202100710, DOI: 10.1002/cmdc.202100710.

(91) Winter, M.; Bretschneider, T.; Kleiner, C.; Ries, R.; Hehn, J. P.; Redemann, N.; Luippold, A. H.; Bischoff, D.; Buttner, F. H. *SLAS Discov* **2018**, *23*, 561–573, DOI: 10.1177/2472555218759267.

(92) Winter, M.; Ries, R.; Kleiner, C.; Bischoff, D.; Luippold, A. H.; Bretschneider, T.; Buttner, F. H. *SLAS Technol* **2019**, *24*, 209–221, DOI: 10.1177/2472630318791981.

(93)   Heap, R. E.; Hope, A. G.; Pearson, L.-A.; Reyskens, K. M. S. E.; McElroy, S. P.; Hastie, C. J.; Porter, D. W.; Arthur, J. S. C.; Gray, D. W.; Trost, M. *SLAS DISCOVERY* **2017**, *22*, 1193–1202, DOI: `10.1177/2472555217717473`.

(94)   Belov, A. M.; Kozole, J.; Bean, M. F.; Machutta, C. A.; Zhang, G.; Gao, E. N.; Ghislain, L.; Datwani, S. S.; Leveridge, M.; Annan, R. S. *Anal Chem* **2020**, *92*, 13847–13854, DOI: `10.1021/acs.analchem.0c02508`.

(95)   Simon, R. P.; Winter, M.; Kleiner, C.; Ries, R.; Schnapp, G.; Heimann, A.; Li, J.; Zuvela-Jelaska, L.; Bretschneider, T.; Luippold, A. H.; Reindl, W.; Bischoff, D.; Büttner, F. H. *SLAS DISCOVERY* **2019**, *25*, 372–383, DOI: `10.1177/2472555 219880185`.

(96)   VanderPorten, E.; Frick, L.; Turincio, R.; Thana, P.; LaMarr, W.; Liu, Y. *Analytical Biochemistry* **2013**, *441*, 115–122, DOI: `10.1016/j.ab.2013.07.003`.

(97)   Roddy, T. P.; Horvath, C. R.; Stout, S. J.; Kenney, K. L.; Ho, P. I.; Zhang, J.-H.; Vickers, C.; Kaushik, V.; Hubbard, B.; Wang, Y. K. *Analytical Chemistry* **2007**, *79*, 8207–8213, DOI: `10.1021/ac062421q`.

(98)   Bretschneider, T.; Ozbal, C.; Holstein, M.; Winter, M.; Buettner, F. H.; Thamm, S.; Bischoff, D.; Luippold, A. H. *SLAS Technology* **2019**, *24*, 386–393, DOI: `10 .1177/2472630318822449`.

(99)   Ding, X.; Liu, K.; Shi, Z. *Mass Spectrometry Reviews* **2021**, *40*, 566–605, DOI: `10.1002/mas.21649`.

(100) Haarhoff, Z.; Wagner, A.; Picard, P.; Drexler, D. M.; Zvyaga, T.; Shou, W. *J Biomol Screen* **2016**, *21*, 165–75, DOI: `10.1177/1087057115607184`.

(101) Sampson, J. S.; Murray, K. K.; Muddiman, D. C. *Journal of the American Society for Mass Spectrometry* **2009**, *20*, 667–673, DOI: `10.1016/j.jasms.2008.12.00 3`.

(102) Caleb Bagley, M.; Garrard, K. P.; Muddiman, D. C. *Mass Spectrometry Reviews* **2021**, DOI: `10.1002/mas.21696`.

(103) Radosevich, A. J.; Pu, F.; Chang-Yen, D.; Sawicki, J. W.; Talaty, N. N.; Elsen, N. L.; Williams, J. D.; Pan, J. Y. *Analytical Chemistry* **2022**, *94*, 4913–4918, DOI: `10.1021/acs.analchem.1c04605`.

(104) De Cesare, V.; Moran, J.; Traynor, R.; Knebel, A.; Ritorto, M. S.; Trost, M.; McLauchlan, H.; Hastie, C. J.; Davies, P. *Nat Protoc* **2020**, *15*, 4034–4057, DOI: `10.1038/s41596-020-00405-0`.

(105) Chandler, J.; Haslam, C.; Hardy, N.; Leveridge, M.; Marshall, P. *SLAS Discov* **2017**, *22*, 1262–1269, DOI: `10.1177/1087057116681726`.

(106) Beeman, K.; Baumgartner, J.; Laubenheimer, M.; Hergesell, K.; Hoffmann, M.; Pehl, U.; Fischer, F.; Pieck, J. C. *SLAS Discovery* **2017**, *22*, 1203–1210, DOI: `10.1177/2472555217727701`.

(107) Haslam, C.; Hellicar, J.; Dunn, A.; Fuetterer, A.; Hardy, N.; Marshall, P.; Paape, R.; Pemberton, M.; Resemannand, A.; Leveridge, M. *J Biomol Screen* **2016**, *21*, 176–86, DOI: `10.1177/1087057115608605`.

(108) Arciniega, C.; Garrard, K. P.; Guymon, J. P.; Manni Sr, J. G.; Apffel, A.; Fjeldsted, J. C.; Muddiman, D. C. *Journal of Mass Spectrometry* **2023**, *58*, e4902, DOI: `https://doi.org/10.1002/jms.4902`.

(109) Morato, N. M.; Holden, D. T.; Cooks, R. G. *Angew Chem Int Ed Engl* **2020**, *59*, 20459–20464, DOI: `10.1002/anie.202009598`.

(110) Kulathunga, S. C.; Morato, N. M.; Zhou, Q.; Cooks, R. G.; Mesecar, A. D. *ChemMedChem* **2022**, *17*, e202200043, DOI: `10.1002/cmdc.202200043`.

(111) Ferguson, C. N.; Benchaar, S. A.; Miao, Z.; Loo, J. A.; Chen, H. *Analytical Chemistry* **2011**, *83*, 6468–6473, DOI: `10.1021/ac201390w`.

(112) Sinclair, I.; Stearns, R.; Pringle, S.; Wingfield, J.; Datwani, S.; Hall, E.; Ghislain, L.; Majlof, L.; Bachman, M. *J Lab Autom* **2016**, *21*, 19–26, DOI: `10.1177/2211068215619124`.

(113) Sinclair, I. et al. *Anal Chem* **2019**, *91*, 3790–3794, DOI: `10.1021/acs.analchem.9b00142`.

(114) Zhang, H.; Liu, C.; Hua, W.; Ghislain, L. P.; Liu, J.; Aschenbrenner, L.; Noell, S.; Dirico, K. J.; Lanyon, L. F.; Steppan, C. M.; West, M.; Arnold, D. W.; Covey, T. R.; Datwani, S. S.; Troutman, M. D. *Analytical Chemistry* **2021**, *93*, 10850–10861, DOI: `10.1021/acs.analchem.1c01137`.

(115) Takáts, Z.; Wiseman Justin, M.; Gologan, B.; Cooks, R. G. *Science* **2004**, *306*, 471–473, DOI: `10.1126/science.1104404`.

(116) Manikandan, M.; Kazibwe, Z.; Hasan, N.; Deenadayalan, A.; Gopal, J.; Pradeep, T.; Chun, S. *TrAC Trends in Analytical Chemistry* **2016**, *78*, 109–119, DOI: `10.1016/j.trac.2016.02.013`.

(117) Shou, W. Z. *Biomedical Chromatography* **2022**, *36*, e5278, DOI: `https://doi.org/10.1002/bmc.5278`.

(118)   Van Berkel, G. J.; Kertesz, V.; Orcutt, M.; Bentley, A.; Glick, J.; Flarakos, J. *Analytical Chemistry* **2017**, *89*, 12578–12586, DOI: `10.1021/acs.analchem.7b 03899`.

(119)   Wagner, A.; Zhang, J.; Liu, C.; Covey, T. R.; Olah, T. V.; Weller, H. B. N.; Shou, W. Z. *Anal Chem* **2020**, *92*, 13525–13531, DOI: `10.1021/acs.analchem .0c03006`.

(120)   Habe, T. T.; Liu, C.; Covey, T. R.; Simon, R. P.; Reindl, W.; Buttner, F. H.; Winter, M.; Bischoff, D.; Luippold, A. H.; Runge, F. *Anal Chem* **2020**, *92*, 12242–12249, DOI: `10.1021/acs.analchem.0c01632`.

(121)   Brown, J.; Morris, M.; Cramer, R. In *ASMS*, Indianapolis, IN, USA, 2017.

(122)   Robinson, K. N.; Steven, R. T.; Race, A. M.; Bunch, J. *Journal of the American Society for Mass Spectrometry* **2019**, *30*, 1284–1293, DOI: `10.1007/s13361-01 9-02193-8`.

(123)   Spraggins, J. M.; Caprioli, R. M. *J Am Soc Mass Spectrom* **2011**, *22*, 1022–31, DOI: `10.1007/s13361-011-0121-0`.

(124)   Muller, M. A.; Kompauer, M.; Strupat, K.; Heiles, S.; Spengler, B. *J Am Soc Mass Spectrom* **2021**, *32*, 465–472, DOI: `10.1021/jasms.0c00368`.

(125)   Steven, R. T.; Dexter, A.; Bunch, J. *Methods* **2016**, *104*, 101–110, DOI: `https: //doi.org/10.1016/j.ymeth.2016.04.010`.

(126)   Fjeldsted, J. Time-of-Flight Mass Spectrometry: Technical Overview, Press Release, 2003.

(127)   Green, M.; Niklewski, W.; Lumley, N.; Pickles, D.; Langridge, D. In *ASMS*, Waters Corp.: Minneapolis, 2022.

(128)   Bae, Y. J.; Shin, Y. S.; Moon, J. H.; Kim, M. S. *Journal of the American Society for Mass Spectrometry* **2012**, *23*, 1326–1335, DOI: `10.1007/s13361-012-0406- y`.

(129)   Page, J. S.; Marginean, I.; Baker, E. S.; Kelly, R. T.; Tang, K.; Smith, R. D. *J Am Soc Mass Spectrom* **2009**, *20*, 2265–72, DOI: `10.1016/j.jasms.2009.08.018`.

(130)   Wei, A. A. J.; Joshi, A.; Chen, Y.; McIndoe, J. S. *International Journal of Mass Spectrometry* **2020**, *450*, 116306, DOI: `https://doi.org/10.1016/j.ijms.20 20.116306`.

(131) Bednařík, A.; Machálková, M.; Moskovets, E.; Coufalíková, K.; Krásenský, P.; Houška, P.; Kroupa, J.; Navrátilová, J.; Šmarda, J.; Preisler, J. *Journal of the American Society for Mass Spectrometry* **2019**, *30*, 289–298, DOI: `10.1007/s13361-018-2078-8`.

(132) Ogrinc Potočnik, N.; Porta, T.; Becker, M.; Heeren, R. M. A.; Ellis, S. R. *Rapid Communications in Mass Spectrometry* **2015**, *29*, 2195–2203, DOI: `https://doi.org/10.1002/rcm.7379`.

(133) Brown, J. Instrumental Development of an Atmospheric Pressure Liquid UV-MALDI Mass Spectrometer Source and Interface for the Analysis of Multiply Protonated Peptide Ions, Thesis, 2020.

(134) Gethings, L. A.; Richardson, K.; Wildgoose, J.; Lennon, S.; Jarvis, S.; Bevan, C. L.; Vissers, J. P. C.; Langridge, J. I. *Rapid Commun Mass Spectrom* **2017**, *31*, 1599–1606, DOI: `10.1002/rcm.7941`.

(135) Katz, A.; LaMarr, W.; Ozba, C.; Rye, P. High-Throughput (Sub-2.5 Second) Direct Injection Analysis by Mass Spectrometry, Press Release, 2021.

(136) Müller, L.; Burton, A. K.; Tayler, C. L.; Rowedder, J. E.; Hutchinson, J. P.; Peace, S.; Quayle, J. M.; Leveridge, M. V.; Annan, R. S.; Trost, M.; Peltier-Heap, R. E.; Dueñas, M. E. *SLAS Discovery* **2023**, *28*, 3–11, DOI: `https://doi.org/10.1016/j.slasd.2022.11.002`.

(137) Guenther, S.; Koestler, M.; Schulz, O.; Spengler, B. *International Journal of Mass Spectrometry* **2010**, *294*, 7–15, DOI: `10.1016/j.ijms.2010.03.014`.

(138) Hale, O. J.; Cramer, R. *Anal Chem* **2019**, *91*, 14192–14197, DOI: `10.1021/acs.analchem.9b03875`.

(139) Zacharias, A. O.; Liu, C.; VanAernum, Z. L.; Covey, T. R.; Bateman, K. P.; Wen, X.; McLaren, D. G. *Journal of the American Society for Mass Spectrometry* **2023**, *34*, 4–9, DOI: `10.1021/jasms.2c00276`.

(140) Pu, F.; Ugrin, S. A.; Radosevich, A. J.; Chang-Yen, D.; Sawicki, J. W.; Talaty, N. N.; Elsen, N. L.; Williams, J. D. *Analytical Chemistry* **2022**, *94*, 13566–13574, DOI: `10.1021/acs.analchem.2c03211`.

(141) Kinch, M. S. *Drug Discovery Today* **2015**, *20*, 393–398, DOI: `https://doi.org/10.1016/j.drudis.2014.09.003`.

(142) Shi, S. *Current Drug Metabolism* **2014**, *15*, 271–290.

(143)   Ratih, R.; Asmari, M.; Abdel-Megied, A. M.; Elbarbry, F.; El Deeb, S. *Microchemical Journal* **2021**, *165*, 106143, DOI: `https://doi.org/10.1016/j.micr oc.2021.106143`.

(144)   Morato, N. M.; Le, M. T.; Holden, D. T.; Graham Cooks, R. *SLAS Technol* **2021**, *26*, 555–571, DOI: `10.1177/24726303211047839`.

(145)   Bartels, B.; Kulkarni, P.; Danz, N.; Böcker, S.; Saluz, H. P.; Svatoš, A. *RSC Advances* **2017**, *7*, 9045–9050, DOI: `10.1039/C6RA26854D`.

(146)   Kompauer, M.; Heiles, S.; Spengler, B. *Nat Methods* **2017**, *14*, 90–96, DOI: `10 .1038/nmeth.4071`.

(147)   Thurow, K.; Stoll, N.; Ritterbusch, K. *Journal of Automated Methods and Management in Chemistry* **2011**, *2011*, 805153, DOI: `10.1155/2011/805153`.

(148)   Cramer, R.; Karas, M.; Jaskolla, T. W. *Anal Chem* **2014**, *86*, 744–51, DOI: `10.1021/ac403228d`.

(149)   Balderas-López, J. A.; Mandelis, A.; Garcia, J. A. *Review of Scientific Instruments* **2000**, *71*, 2933–2937, DOI: `10.1063/1.1150713`.

(150)   Egas, A. P. V.; Talavera-Prieto, N. M. C.; Ferreira, A. G. M.; Santos, J. B.; Santos, M. J.; Almeida, Z. L.; Fonseca, I. M. A. *The Journal of Chemical Thermodynamics* **2021**, *156*, 106367, DOI: `10.1016/j.jct.2020.106367`.

(151)   Wang, L.; Dalglish, G.; Ouyang, Z.; David-Brown, D. G.; Chiriac, C.; Duo, J.; Kozhich, A.; Ji, Q. C.; Peterson, J. E. *SLAS Technology* **2020**, *25*, 463–473, DOI: `https://doi.org/10.1177/2472630320915844`.

A. Appendix

A.1. Estimation of the optical penetration depth

Equation A.1 states how the electric field at the inlet tube E_C can be calculated from the applied potential V_C, the outer radius of the inlet tube r_c and the distance between the target plate and the inlet tube d.[13] The electric field in LAP-MALDI is of the same order of magnitude as in ESI, which is typically $10 \cdot 10^6$ V/m.[13] Thus, charge separation in the liquid sample will likely occur.

$$E_c = \frac{2V_C}{r_c ln(\frac{4d}{r_c})} = \frac{2 * 3\,500\,\text{V}}{1.587\,5 \cdot 10^{-3}\,\text{m} * ln(\frac{4*3\,\text{mm}}{1.587\,5\,\text{mm}})} = 2.2 \cdot 10^6\,\text{Vm}^{-1} \qquad (A.1)$$

The material ejection can be described by analogy with conventional MALDI using equations 1.1 and 1.2. In contrast to conventional solid-state MALDI, the optical penetration depth in LAP-MALDI needs to take into account the dilution of the matrix compound (see Equation A.2). As anticipated the penetration depth is significantly longer as the matrix compound is more diluted. This estimation does not take into account any surface accumulation effects but assumes homogeneous distribution of the compounds in the droplet.

$$A = log_{10}(\frac{I_0}{I}) = \epsilon c l$$

$$I_\delta = I_0 \frac{1}{e}$$

$$\text{from the absorbance measurement we know: } A_c = \epsilon c l$$

$$\text{at the penetration depth: } A_\delta = log_{10}(e) = \epsilon \delta c$$

$$\text{using } \epsilon c \text{ from above: } \delta = \frac{log_{10}(e)l}{A_c}$$

$$\delta = \frac{log_{10}(e)1\,\text{cm}}{0.99} = 0.44\,\text{cm}$$

(A.2)

The measured absorbance can be compared to the calculated value assuming uniform attenuation:

$$A = \sum_{i=1}^{N} A_i = l \sum_{i=1}^{N} \epsilon_i c_i$$

$$\frac{A}{l} = c_{water}\epsilon_{water} + c_{MeCN}\epsilon_{MeCN} + c_{CHCA}\epsilon_{CHCA} + c_{PG}\epsilon_{PG}$$

$$\frac{A}{l} = 17.342M + 5.984M + 0.017M * \left(\frac{(18,300 + 17,100)Lcm^{-1}mol^{-1}}{2}\right) + 5.106M$$

$$(A.3)$$

The pH of the matrix preparation is close to the pkA of α-CHCA. Hence, it can be assumed that the neutral and singly deprotonated species are present at similar proportions (see Figure A.1). At 337 nm, the molar absorption coefficients are $18.300\,\mathrm{Lcm}^{-1mol}$ for the neutral and $17.100\,\mathrm{Lcm}^{-1mol}$ for the singly deprotonated species.[148]

Using α of $9.2 \cdot 10^{-8}\,\mathrm{m}^2/\mathrm{s}$[149] for ethylene glycol and the speed of sound in liquid glycerol of $1\,850\,\mathrm{m\,s}^{-1}$,[150] stress and thermal confinement times can be estimated (see Equations A.4 and A.5).

Thermal and stress confinement times are several orders of magnitude longer than the laser pulse duration. The energy deposited into the liquid sample by the laser radiation is estimated to lead to the spallation-like ejection of material from the sample.

$$\tau_{stress} = \frac{\delta}{C_s} = \frac{0.44 \cdot 10^{-2}\,\mathrm{m}}{1\,850\,\mathrm{m\,s}^{-1}} = 2.4 \cdot 10^{-6}\,\mathrm{s} \tag{A.4}$$

$$\tau_{thermal} = \frac{\delta^2}{\alpha} = \frac{(0.44 \cdot 10^{-2}\,\mathrm{m})^2}{9.2 \cdot 10^{-8}\,\mathrm{m}^2/\mathrm{s}} = 210\,\mathrm{s} \tag{A.5}$$

It can be assumed that large clusters of charge-separated liquid are ejected from the sample. Under atmospheric conditions, evaporation of the solvent and collision of particles with themselves and ambient air will likely lead to the formation of smaller droplets. The ionisation of the analyte within the droplet is thought to occur according to similar processes as in ESI.
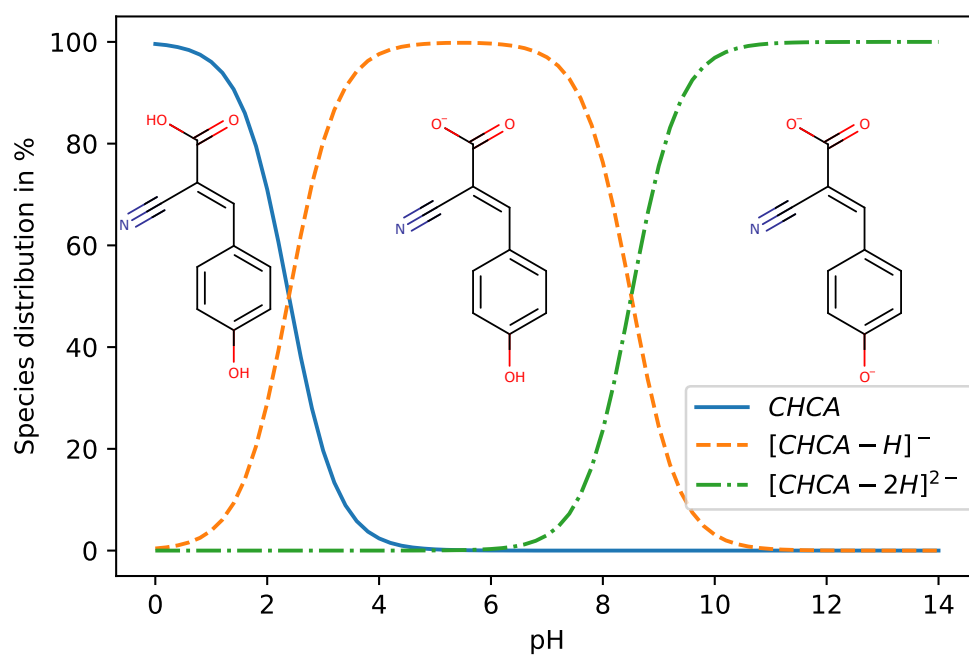
Figure A.1.: Influence of pH on α-CHCA protonation. Calculated with MarvinSketch 22.13. Molecular structures of most common species are overlaid.

A.2. Design of the target plate holder

The existing holder for the sample plates is shown in Figure A.2. With increasing numbers of samples, the wish for a more automated sample preparation grew and the idea of using MTPs was developed.
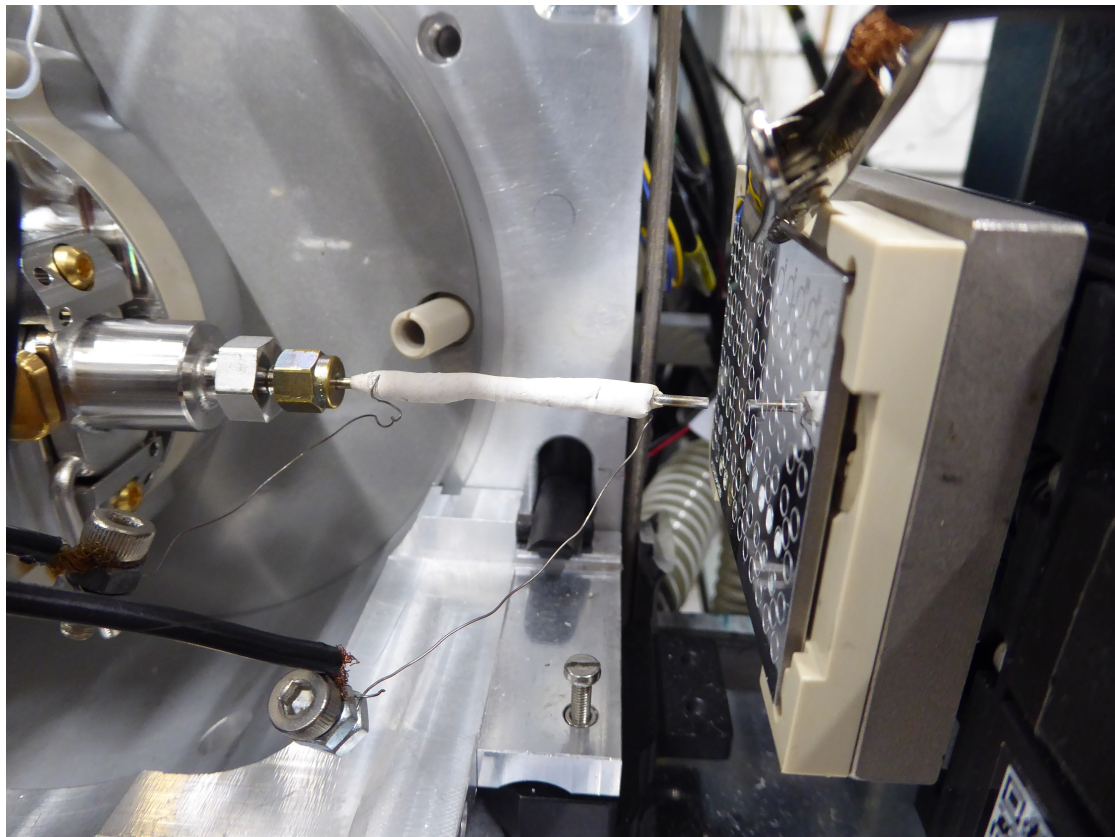

Figure A.2.: Original target plate holder

In conjunction with the new translational stages offering an extended travel range, a CAD design was developed. The printed part is shown in Figure A.3a. With increasing analysis speed and acceleration of the new stages, the high voltage connection proofed unstable. Hence, an aluminium strip was incorporated into the design (see Figure A.3b). The part was equally printed on a 3d-printer and the threads for attaching the strip were subsequently made.

A redesign of version 2 was necessary as its surface was not completely flat. Additionally, standard MTP could not be fitted as there was not enough space in z direction (between
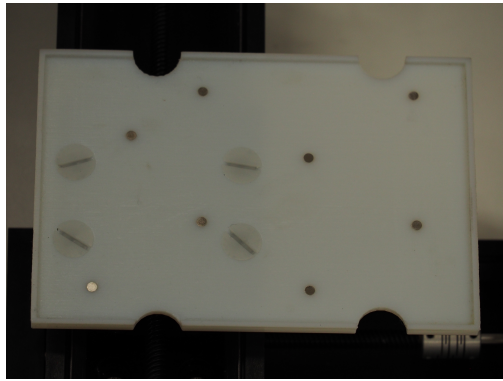
(a) Target holder V1
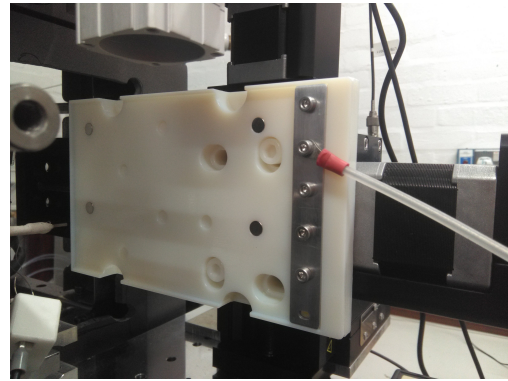
(b) Target holder V2

Figure A.3.: Target holder designs, version 1 und 2.

the translational stage and the inlet tube). The new design is thinner albeit the edges were designed slightly higher, so that thicker target plates from Bruker can be mount more easily. Furthermore, an angle correction was integrated by using set screws at the outer positions to control the distance between the base plate and the plastic holder.
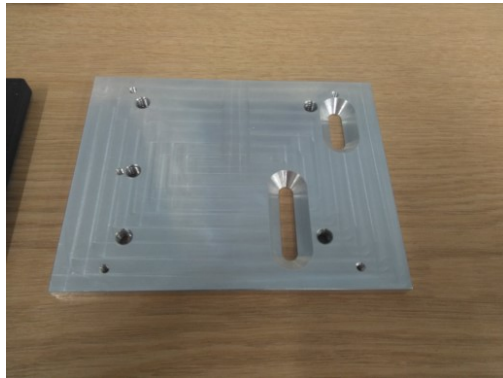
(a) Aluminium baseplate

(b) 3d-printed plate holder

(c) Front view

(d) Back view

Figure A.4.: Third version of the target plate holder. The xy position can be slightly adapted by using the countersunk nylon screws. M3 set screws can be used to tilt the plate.

A.3. Synchronisation

The python code used for automated sample movement used in section 2.3 is presented below. In contrast to code used with the previous translational stages, the new ones allow usage of ascii instead of binary code which facilitates coding. The scripts allows a flexible movement of the translational stage including rastering different plate sizes or repeatably analysing selected samples as used when collecting data on CVs.

Code A.1: Python code for automated sample movement

```python
# -*- coding: utf-8 -*-
"""
Created on Tue Oct 27 09:11:54 2021
@author: Henriette
"""

from zaber_motion import Library, LogOutputMode
from zaber_motion.ascii import Connection,SettingConstants,Stream
from zaber_motion import Units
import time

Library.enable_device_db_store() #downloads device information and makes it
    available for later offline use

def homing(axis):
    #only necessary after being powered off
    axis.home()
    return

def go_to_start(x,y):
    axis_x.move_absolute(x)
    axis_y.move_absolute(y)
    axis_x.move_relative(-2,Units.LENGTH_MILLIMETRES)
    time.sleep(3)

def snake_nostop():
    for x in range(7):
        axis_x.move_relative(23*4.5,Units.LENGTH_MILLIMETRES)
        axis_y.move_relative(-4.5,Units.LENGTH_MILLIMETRES)
        axis_x.move_relative(-23*4.5,Units.LENGTH_MILLIMETRES)
```

```python
        axis_y.move_relative(-4.5,Units.LENGTH_MILLIMETRES)
    axis_x.move_relative(23*4.5,Units.LENGTH_MILLIMETRES)
    axis_y.move_relative(-4.5,Units.LENGTH_MILLIMETRES)
    axis_x.move_relative(-23*4.5,Units.LENGTH_MILLIMETRES)
    axis_x.move_relative(-2,Units.LENGTH_MILLIMETRES)
    return


def snake_extend():
    for x in range(7):
        axis_x.move_relative(23*4.5+4,Units.LENGTH_MILLIMETRES)
        axis_y.move_relative(-4.5,Units.LENGTH_MILLIMETRES)
        axis_x.move_relative(-23*4.5-4,Units.LENGTH_MILLIMETRES)
        axis_y.move_relative(-4.5,Units.LENGTH_MILLIMETRES)
    axis_x.move_relative(23*4.5+4,Units.LENGTH_MILLIMETRES)
    axis_y.move_relative(-4.5,Units.LENGTH_MILLIMETRES)
    axis_x.move_relative(-23*4.5-4,Units.LENGTH_MILLIMETRES)
    return


def big384_plus_labels(x,y):
    axis_x.move_absolute(x)
    axis_y.move_absolute(y)
    axis_x.move_relative(-4.3,Units.LENGTH_MILLIMETRES)
    time.sleep(2)
    for x in range(7):
        axis_x.move_relative(25*4.5,Units.LENGTH_MILLIMETRES)
        axis_y.move_relative(-4.5,Units.LENGTH_MILLIMETRES)
        axis_x.move_relative(-25*4.5,Units.LENGTH_MILLIMETRES)
        axis_y.move_relative(-4.5,Units.LENGTH_MILLIMETRES)
    axis_x.move_relative(25*4.5,Units.LENGTH_MILLIMETRES)
    axis_y.move_relative(-4.5,Units.LENGTH_MILLIMETRES)
    axis_x.move_relative(-25*4.5,Units.LENGTH_MILLIMETRES)
    return


def snake_withstops():
    wait_time = 0.03
    for y in range(8):
        for x in range(24):
            axis_x.move_relative(4.5,Units.LENGTH_MILLIMETRES)
            time.sleep(wait_time)
        axis_y.move_relative(-4.5, Units.LENGTH_MILLIMETRES)
```

```python
        time.sleep(wait_time)
        for x in range(24):
            axis_x.move_relative(-4.5,Units.LENGTH_MILLIMETRES)
            time.sleep(wait_time)
        axis_y.move_relative(-4.5, Units.LENGTH_MILLIMETRES)
        time.sleep(wait_time)
    return


def rows():
    axis_y.move_relative(2*-2.25,Units.LENGTH_MILLIMETRES)
    axis_x.move_relative(24*2.25+2,Units.LENGTH_MILLIMETRES)
    axis_y.move_relative(-2.25,Units.LENGTH_MILLIMETRES)
    axis_x.move_relative(-24*2.25-2,Units.LENGTH_MILLIMETRES)
    axis_y.move_relative(-2.25,Units.LENGTH_MILLIMETRES)
    return


def rows_loop():
    axis_y.move_relative(6*-2.25,Units.LENGTH_MILLIMETRES)
    for x in range(300):
        axis_x.move_relative(24*2.25+3,Units.LENGTH_MILLIMETRES)
        axis_y.move_relative(-2.25,Units.LENGTH_MILLIMETRES)
        axis_x.move_relative(-24*2.25-3,Units.LENGTH_MILLIMETRES)
        axis_y.move_relative(2.25,Units.LENGTH_MILLIMETRES)
    return


def rows_96():
    axis_y.move_relative(-6*4.5,Units.LENGTH_MILLIMETRES)
    axis_x.move_relative(12*4.5+2,Units.LENGTH_MILLIMETRES)
    #axis_y.move_relative(-4.5,Units.LENGTH_MILLIMETRES)
    #axis_x.move_relative(-12*4.5-2,Units.LENGTH_MILLIMETRES)
    #axis_y.move_relative(-2.25,Units.LENGTH_MILLIMETRES)
    return


def velocity(axis, speed):
    axis.settings.set("maxspeed", speed, Units.VELOCITY_MILLIMETRES_PER_SECOND)
    return


def acceleration(device):
    device.settings.set("accel", 1,
        Units.ACCELERATION_MILLIMETRES_PER_SECOND_SQUARED)
```

```python
    return

def stream(device):
    device.stream.setup_store(1,1)
    return

def circle():
    axis_y.move_relative(-4*4.5,Units.LENGTH_MILLIMETRES)
    #axis_x.move_relative(2*4.5,Units.LENGTH_MILLIMETRES)
    for x in range(24):
        axis_x.move_relative(8*4.5,Units.LENGTH_MILLIMETRES)
        axis_y.move_relative(-4.5,Units.LENGTH_MILLIMETRES)
        axis_x.move_relative(-8*4.5,Units.LENGTH_MILLIMETRES)
        axis_y.move_relative(4.5,Units.LENGTH_MILLIMETRES)

    return

def circle_extended():
    #axis_y.move_relative(-4*4.5,Units.LENGTH_MILLIMETRES)
    #axis_x.move_relative(2*4.5,Units.LENGTH_MILLIMETRES)
    for x in range(6):
        axis_x.move_relative(10*4.5,Units.LENGTH_MILLIMETRES)
        axis_y.move_relative(-4.5,Units.LENGTH_MILLIMETRES)
        axis_x.move_relative(-10*4.5,Units.LENGTH_MILLIMETRES)
        axis_y.move_relative(-4.5,Units.LENGTH_MILLIMETRES)
        axis_x.move_relative(10*4.5,Units.LENGTH_MILLIMETRES)
        axis_y.move_relative(-4.5,Units.LENGTH_MILLIMETRES)
        axis_x.move_relative(-10*4.5,Units.LENGTH_MILLIMETRES)
        axis_y.move_relative(3*4.5,Units.LENGTH_MILLIMETRES)
    return

with Connection.open_serial_port("COM4") as connection:
    device_list = connection.detect_devices()
    #print("Found {} devices".format(len(device_list)))
    device_x = device_list[0]
    axis_x = device_x.get_axis(1)
    device_y = device_list[1]
    axis_y = device_y.get_axis(1)
    velocity(axis_x,50)
    velocity(axis_y,50)
```

```
go_to_start(133322,59260)
circle_extended()
#rows_96()
#snake_extend()
#big384_plus_labels(8866,140539)
#Homing is only necessary after power cut
#Library.set_log_output(LogOutputMode.FILE, "motion_library_log.txt")
```

To facilitate automatic sample measurement, different components of the setup, namely sample movement, laser emission and mass spectrometric data acquisition, were merged into one control software. The Synapt G2-Si mass spectrometer has a simple interface for "contact closure". Normally used for interfacing liquid chromatography devices, the instrument was configured to await a TTL signal to start the acquisition. In a similar way, the Flare NX laser can be run in the so-called "gated mode", which means that the laser is firing with the set PRF as long as the event input voltage is applied.

To generate the required 5 V TTL signal, an Arduino micro-controller was used. The manufacturer of the translational stages offers the possibility of an add-on (so-called "shield") to provide an interface between the Arduino and the stages. A picture of the device is shown in Figure A.5. Thanks to the provision of libraries and minimal working examples from Zaber, a script was written to control the three devices (see code A.2). The code is loaded to the Arduino micro-controller and executed. When the experiment is prepared (sample plate is loaded, laser is turned on, etc.), the script can be started by pressing "s" on the keyboard of the acquisition computer. Similarly, the script can be stopped by pressing "e". A delay between the start of the different components was introduced to account for the time needed to start of the data acquisition or move to the first sample.
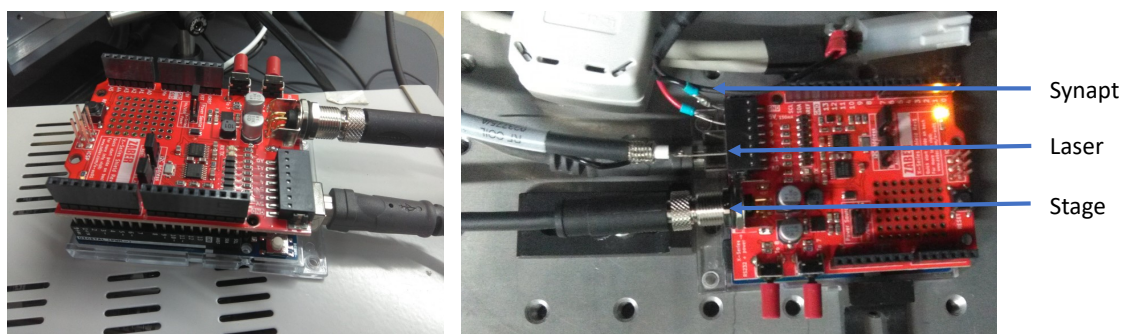

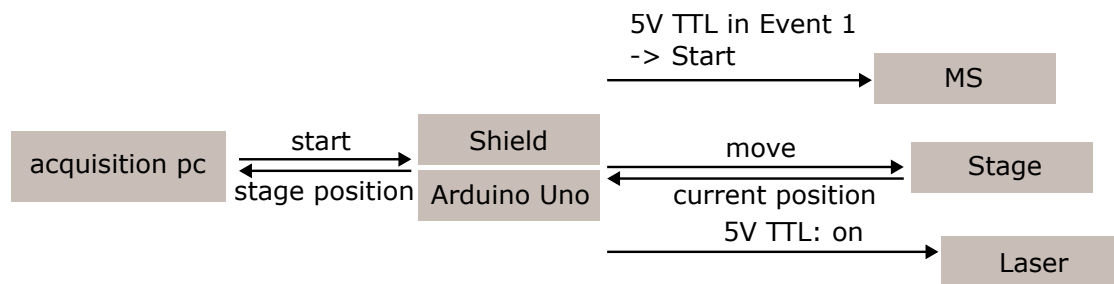**Figure A.5.:** Arduino Uno microcontroller with Zaber shield X-AS01.

Figure A.6.: Scheme of controlling the mass spectrometer, laser and translational stages with the Arduino Uno microcontroller and Zaber shield.

Code A.2: Arduino code to control translational stage, start the laser and mass spectrometer

```
/*
Read serial port and start/stop experiment (synapt data acquisition, laser
    firing, stage movement)
*/
#include <ZaberAscii.h>

int laser = 3; // the pin the laser is connected to
int synapt = 6; // the pin the Synapt is connected to

// Specify the device number and axis number for the X and Y axes of the scan.
const int X_DEVICE_ADDRESS = 1;
const int Y_DEVICE_ADDRESS = 2;
const int X_AXIS_NUMBER = 1;
const int Y_AXIS_NUMBER = 1;

// unit conversion: microstep size to micrometers (for X-LSQ-B)
const float X_MICROSTEP_SIZE = 0.49609375;
const float Y_MICROSTEP_SIZE = 0.49609375;

// how many microsteps make up a millimeter,
#define X_uSTEPS(mm) (long int)((mm) * 1000.0 / X_MICROSTEP_SIZE)
#define Y_uSTEPS(mm) (long int)((mm) * 1000.0 / Y_MICROSTEP_SIZE)

//convert microsteps to mm ?
#define ToMm(steps) (float) ((steps) * X_MICROSTEP_SIZE / 1000)

// convert speed from mm/s?
#define SPEED_UNIT(mm_s) (long) (((mm_s) * 1.6384) / (X_MICROSTEP_SIZE / 1000))
```

```cpp
//convert acceleration from mm/s2?
#define ACCEL_UNIT(mm_s2) (int) ((mm_s2) * 1.6384 / (10000 * (X_MICROSTEP_SIZE
    / 1000)))

// Startposition in microsteps
const unsigned long X_FIRST_POINT = 9891;
const unsigned long Y_FIRST_POINT = 142486;

//Initialise Timing
unsigned long synaptMillis;
const unsigned long laserDelay = 1000; //delay between synapt trigger and
    laser trigger
const unsigned long stageDelay = 1100; //delay between synapt trigger and
    stage start
bool triggerLaser = false; //will be changed to true when start signal is
    received
bool triggerStage = false; //will be changed to true when start signal is
    received

// for serial port reading
char rx_byte; //initialise character received by serial

// initialise bools for encoder loop
bool stageXBusy = true;
bool stageYBusy = true;

// Helper to report errors.
bool check_error(ZaberAscii::reply reply)
{
  if (reply.isRejected)
  {
    Serial.println("Error: device " + String(reply.deviceNumber) + " rejected a
        command.");
    return true;
  }

  return false;
}


ZaberShield shield(ZABERSHIELD_ADDRESS_AA);
```

```cpp
ZaberAscii za(shield);

//set paramters of Zaber stage (speed, acceleration)
void Zaber_Settings() {
  za.send(X_DEVICE_ADDRESS, X_AXIS_NUMBER," set maxspeed", SPEED_UNIT(100));
  za.receive();
  za.send(Y_DEVICE_ADDRESS, Y_AXIS_NUMBER,"set maxspeed", SPEED_UNIT(100));
  za.receive();
  za.send(X_DEVICE_ADDRESS, X_AXIS_NUMBER,"set accel", ACCEL_UNIT(1000));
  za.receive();
  za.send(Y_DEVICE_ADDRESS, Y_AXIS_NUMBER,"set accel", ACCEL_UNIT(1000));
  za.receive();
  Serial.println("Stage parameters set");
}


void Zaber_StartPosition(){
  za.send(X_DEVICE_ADDRESS, X_AXIS_NUMBER,"move abs",X_FIRST_POINT);
  za.receive();
  za.send(Y_DEVICE_ADDRESS, Y_AXIS_NUMBER,"move abs",Y_FIRST_POINT);
  za.receive();
  za.pollUntilIdle(X_DEVICE_ADDRESS);
  za.pollUntilIdle(Y_DEVICE_ADDRESS);
  Serial.println("Stage in start position");
}

void Zaber_EncoderPos(){
  while (stageXBusy == true || stageYBusy == true){
    za.send(1,1, "get encoder.pos");
    ZaberAscii::reply reply = za.receive();
    if (!reply.isReply){
      Serial.println("*** Received a non-reply message from device " +
          String(reply.deviceNumber) + ".");
    }
    else if (reply.isRejected){
      Serial.println("*** A command was rejected by device " +
          String(reply.deviceNumber) + ".");
    }
    else{
      Serial.println( String(reply.deviceNumber) + ", " +
          String(reply.responseData));
```

```
    }
    if (!reply.isBusy) {
      stageXBusy = false;
    }
    za.send(2, 1, "get encoder.pos");
    ZaberAscii::reply answer = za.receive();
    if (!answer.isReply){
      Serial.println("*** Received a non-reply message from device " +
          String(answer.deviceNumber) + ".");
    }
    else if (answer.isRejected){
      Serial.println("*** A command was rejected by device " +
          String(answer.deviceNumber) + ".");
    }
    else{
      Serial.println( String(answer.deviceNumber) + ", " +
          String(answer.responseData));
    }
    if (!answer.isBusy){
      stageYBusy = false;
    }
  }
  stageXBusy = true;
  stageYBusy = true;
}


void Zaber_MoveSnake(){
    for (int i = 0; i <= 7; i++) {
        za.send(X_DEVICE_ADDRESS, X_AXIS_NUMBER, "move rel", X_uSTEPS(23*4.5));
        za.receive();
        Zaber_EncoderPos();
        za.pollUntilIdle(X_DEVICE_ADDRESS);
        za.send(Y_DEVICE_ADDRESS, Y_AXIS_NUMBER, "move rel", Y_uSTEPS(-4.5));
        za.receive();
        Zaber_EncoderPos();
        za.pollUntilIdle(Y_DEVICE_ADDRESS);
        za.send(X_DEVICE_ADDRESS, X_AXIS_NUMBER, "move rel", X_uSTEPS(-23*4.5));
        za.receive();
        Zaber_EncoderPos();
        za.pollUntilIdle(X_DEVICE_ADDRESS);
```

```
        za.send(Y_DEVICE_ADDRESS, Y_AXIS_NUMBER, "move rel", Y_uSTEPS(-4.5));
        za.receive();
        Zaber_EncoderPos();
        za.pollUntilIdle(Y_DEVICE_ADDRESS);
    }
}

void Zaber_GetPosition(){
  za.send(X_DEVICE_ADDRESS, X_AXIS_NUMBER, "get pos");
  ZaberAscii::reply reply = za.receive();
  long x = reply.responseData;
  Serial.println("X Position: (" + String(x) + ") " );
  za.send(Y_DEVICE_ADDRESS, Y_AXIS_NUMBER, "get pos");
  long y = reply.responseData;
  Serial.println("Y Position: (" + String(y) + ") " );
}

void stopAll(){
  digitalWrite(laser, LOW);
  digitalWrite(synapt, HIGH);
  za.send(X_DEVICE_ADDRESS,X_AXIS_NUMBER,"stop"); //maybe try estop, but could
      cause damage
  za.send(Y_DEVICE_ADDRESS,Y_AXIS_NUMBER,"stop");
}

void startTimed(){
  digitalWrite(synapt, HIGH);
  pinMode(synapt, OUTPUT);
  synaptMillis = millis();
  digitalWrite(synapt, LOW); //synapt acquisition trigger
  Serial.println("Synapt triggered");
  triggerLaser = true;
  triggerStage = true;
  Zaber_Settings(); //start stage setup
  Zaber_StartPosition();
}

void setup(){
  shield.begin(115200);
  Serial.begin(115200);
```

```
}

void loop() {
  if (Serial.available()) {
    rx_byte = Serial.read();
    if (rx_byte == 115) {
      Serial.println("Start");//character s is interpreted in ASCII as 115
      startTimed();
      }
    else if (rx_byte == 101) { //character e is interpreted in ASCII as 101
      Serial.println("Stop");
      stopAll();
      }
    else{
      Serial.println("Invalid input");
      }
    }
  unsigned long currentMillis = millis();
  if (triggerLaser == true){
    if (synaptMillis - currentMillis > laserDelay) {
      digitalWrite(laser, HIGH);
      Serial.println("Laser triggered");
      triggerLaser = false;
    }
  }
  if (triggerStage == true){
    if (synaptMillis - currentMillis > stageDelay) {
      //start stage movement
      Serial.println("Stage rastering starts");
      Zaber_MoveSnake();
      triggerStage = false;
    }
  }
}
```

A.4. Liquid handling devices for small volume dispensing

Several types of liquid handlers exist: most use exchangeable tips which can be rinsed or discarded, while some systems use continuous channels to dispense the liquid (for example from the company M2-Automation GmbH, Berlin, Germany). Those devices have reduced the costs for consumables but require more time due to the washing steps and have an increased risk of cross-contamination. Hence, liquid handlers without tips are more suited for repeated dispensing of the same liquid. A third option besides tips and channels is the use of pins. Those small features are dipped into the solution which covers the pins externally, although slotted versions are available for higher volumes. When in contact with a surface or liquid, a defined volume is dispensed. This volume depends for example on the type of liquid, the depth of immersion and the speed of movement. CVs of 3 % to 5 % are reported by V&P Scientific Inc. and costs are approximately $ 4000. Those pin tools can be operated manually or combined with a robotic arm. So, they can be a first step when analysing larger sample sets before investing into more elaborate robotic solutions. The pins are available as re-usable or disposable versions, so the risk of cross-contamination can be adjusted depending on the application. A completely non-contact liquid dispensing technology is the acoustic transfer of liquids in the nL range. This technology is widely used in drug screening procedures to deliver DMSO-based compound libraries.[151] In contrast, the Andrew+ system is not designed for high-throughput applications but provides an automated but versatile platform. The robotic arm can accommodate pipettes of different volume ranges and numbers of channels. It is more useful for earlier stages of the sample preparation.

Table A.1.: Summary of selected commercially available liquid handlers suitable for LAP-MALDI sample preparation.

| Model	Company	Price in GBP	Channels per head	Price per tip in GBP	Volume range in µL	Deck positions	Benefits	Drawbacks
Mosquito LV	SPT Labtech	90,0000	8 or 12	0.035 (8-head) or 0.062 (12-head)	25 nL - 1.2µL	5	very fast, small footprint, easy to install, positive displacement	narrow volume range
Mosquito HV	SPT Labtech	90,000	8 or 12	0.054 (8 head), 0.062 (12 head)	0.5-5µL	5	very fast, small footprint, easy to install, positive displacement	narrow volume range
Apricot S3 CyBio Well Vario	SPT Labtech Analytic Jena	70,000+pc	96, 384, 1536	96 or 384 0.13	0.5-125µL 0.5-25µL (CV 10% for 0.5µL)	3 10		
Andrew +	Waters Corp.	25,000-40,000	1 or 8	0.059	0.2µL-5 mL	11 (incl. tip rack)	good accuracy over large volume range, flexible (SPE, magnetic pull-down, shaking, cooling/heating, standard pipette tips	slow, max. 384-well MTP
VP 407FP12	V& P Scientific	3315 (ex. tax)	96 (384 available)	0	fixed	0	Manual and robotic use, no tips	Contamination possible, volume depends on liquid and handling

A.5. Direct analysis from MTP
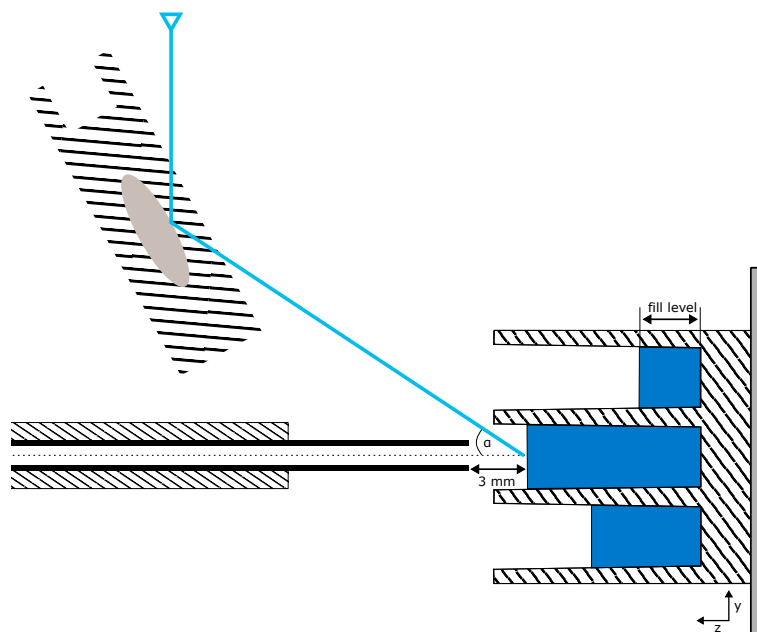
Figure A.7.: Possible setup for the direct LAP-MALDI analysis from a MTP using a 384-well flat bottom plate from Greiner (catalogue number 781101). The inlet tube's outer diameter is 1/16" (inner diameter 0.04"). The laser beam is reflected by a 7 mm mirror hold by a fixed mirror mount (MFM7/M from Thorlabs) before reaching the sample.